UNIVERSIDADE DE LISBOA
FACULDADE DE CIÊNCIAS
DEPARTAMENTO DE FÍSICA

ANALYSIS OF THE EXTRATROPICAL STRATOSPHERE-TROPOSPHERE CIRCULATION COUPLING USING A 3D NORMAL MODE APPROACH

Margarida da Conceição Rasteiro Magano Lopes Rodrigues Liberato

DOUTORAMENTO EM FÍSICA

(Meteorologia)

2008

UNIVERSIDADE DE LISBOA
FACULDADE DE CIÊNCIAS
DEPARTAMENTO DE FÍSICA

ANALYSIS OF THE EXTRATROPICAL STRATOSPHERE-TROPOSPHERE CIRCULATION COUPLING USING A 3D NORMAL MODE APPROACH

Margarida da Conceição Rasteiro Magano Lopes Rodrigues Liberato

DOUTORAMENTO EM FÍSICA

(Meteorologia)

Tese orientada pelo Professor Doutor Carlos da Camara,
Professor Associado do Departamento de Física da
Faculdade de Ciências da Universidade de Lisboa
e pelo Professor Doutor José Manuel Castanheira,
Professor Auxiliar do Departamento de Física da
Universidade de Aveiro

2008

ACKNOWLEDGEMENTS

First of all, I would like to thank my supervisors. I am especially indebted to Prof. José Manuel Castanheira for introducing me to the 3D Normal Modes enchanted, though physically based, world. I am grateful for his guidance, his enthusiasm, his neverending persistence, confidence and patience as well as for all his suggestions for further research. Without his constructive support and encouragement, friendship and advice this thesis would not have been finished. I am especially grateful to Prof. Carlos da Camara for suggesting this research theme and for being my supervisor, for his advice and support as well as for his friendship.

I am also extremely thankful to my friend and PhD colleague, Célia Gouveia for her unconditional friendship and endless patience and support, share of information, valuable suggestions and fruitful scientific discussions, which helped overcoming difficulties and broadened my scientific interests and research. I am also thankful to Dr. Ricardo Trigo for his friendship and support, words of motivation, suggestions, share of information as well as enthusiastic and varied conversations, some science-related, many not, contributing to make each visit to FCUL a gratifying experience.

I am thankful to the University of Trás-os-Montes e Alto Douro, where I have been teaching since 1998, for granting a three-year leave for full time scientific research, and for allowing my participation at all the International Scientific Conferences and Symposiums where I have presented scientific results. A word of recognition and acknowledgment is also due to my colleagues at the Physics Department for support that eased the last several years and made work a more enjoyable experience.

Finally, a very special thought towards my family and close friends, for the love they have always demonstrated, for their neverending patience, support and encouragement. To my husband, José António, who provided more love and support than anyone could deserve, and to my daughters, Catarina and Helena, I dedicate this work.

The Portuguese Foundation of Science and Technology (FCT) partially supported this research (Grant SFRH / BD / 32640 / 2006).

ABSTRACT

The annular nature of the leading patterns of the Northern Hemisphere winter extratropical circulation variability is analysed by means of a Principal Component Analysis (PCA) of tropospheric geopotential height fields followed by lagged correlations of relevant Principal Components with the stratospheric polar vortex strength as well as with a proxy of midlatitude tropospheric zonal mean zonal momentum anomalies.

Results suggest that two processes, occurring with a time scale separation of about two weeks, contribute for the Northern Annular Mode (NAM) spatial structure. Polar vortex anomalies appear to be associated with midlatitude tropospheric zonal momentum anomalies leading the vortex. Zonal mean zonal wind anomalies of the same sign lagging the vortex are then observed in the troposphere at high latitudes. Tropospheric variability patterns which seem to respond to the polar vortex variability have a hemispheric scale. A dipolar structure may be observed only over the Atlantic basin that resembles the North Atlantic Oscillation pattern (NAO), but with the node line shifted northward.

The association between zonal symmetric components of the tropospheric and stratospheric circulations is further confirmed by a PCA on the barotopic component of the Northern winter atmospheric circulation. Results show that a zonally symmetric component of the middle and lower tropospheric circulation variability exists at high latitudes. At the middle latitudes obtained results suggest that the zonally symmetric component, as identified in other works, is artificially overemphasized by the usage of PCA on single isobaric tropospheric levels.

The 3-Dimensional normal mode expansion of the atmospheric general circulation was also used to relate the variability of the stratospheric polar vortex to the energy variability of the forcing planetary waves. Positive (negative) anomalies of the energy

associated with the first two baroclinic modes of planetary Rossby waves with zonal wavenumber 1 are followed by downward progression of negative (positive) anomalies of the vortex strength. The analysis of the correlations between individual Rossby modes and the vortex strength further contributed to confirm the result from linear theory that the waves which force the vortex are those associated with the largest zonal and meridional scales.

Keywords: stratospheric polar vortex; wave-mean flow interaction; Northern Annular Mode; Artic Oscillation; North Atlantic Oscillation; 3D normal mode; planetary or Rossby waves; Stratospheric Sudden Warming and Stratospheric Final Warming.

RESUMO

Nas últimas décadas assistiu-se a um interesse crescente pelo estudo da interacção entre a troposfera e a estratosfera extratropicais. A atenção dedicada a este tema justifica-se, em boa parte, pela relação existente entre a variabilidade estratosférica e os modos anulares na troposfera. Cada vez mais se tem maior evidência de que os processos dinâmicos na estratosfera desempenham um papel significativo na variabilidade climática da troposfera através de uma larga gama de escalas temporais. Com efeito, as relações estatísticas entre a intensidade do vórtice polar e a circulação troposférica estendem-se até à superfície, podendo tornar-se úteis para a previsão do tempo à escala mensal [Baldwin e Dunkerton 2001], bem como para uma melhor compreensão da variabilidade climática.

O acoplamento dinâmico estratosfera-troposfera tem influência na variabilidade climática da circulação troposférica [Perlwitz e Graf 1995; Thompson e Wallace 1998; Castanheira e Graf 2003], tendo Perlwitz e Graf [1995] mostrado que anomalias da circulação estratosférica exercem influência sobre os regimes de circulação da troposfera e posteriormente sugerido que a reflexão de ondas planetárias desempenhava papel importante [Perlwitz e Graf 2001a]. Outros autores [Hines 1974; Geller e Alpert 1980; Schmitz e Grieger 1980; Perlwitz e Harnik 2003] têm igualmente sugerido a reflexão descendente da energia das ondas pela estratosfera de volta à troposfera como constituindo um mecanismo pelo qual a estratosfera pode afectar a troposfera.

Nas latitudes elevadas do Hemisfério Norte, a variabilidade da estratosfera é dominada por intensificações e desacelerações "esporádicas" do vórtice polar, que ocorrem com escalas temporais da ordem de semanas a meses durante o Inverno [Holton e Mass 1976; Yoden 1990; Scott e Haynes 1998]. O forçamento troposférico da variabilidade estratosférica é então explicado pela propagação vertical de ondas, que transferem momento e energia para a estratosfera. Contudo, os mecanismos

dinâmicos pelos quais a troposfera reage a variações da estratosfera não estão ainda bem compreendidos. Muitos estudos recentes do acoplamento dinâmico entre a estratosfera e a troposfera enfatizam a dinâmica do escoamento médio zonal relacionada com os Modos Anulares [Baldwin e Dunkerton 1999; 2001; Kuroda e Kodera 1999; Kodera et al. 2000; Christiansen 2001; Ambaum e Hoskins 2002; Black 2002; Polvani e Kushner 2002; Plumb e Semeniuk 2003]. Acresce que as observações, em particular, mostram que anomalias elevadas na intensidade do vórtice polar estratosférico descem à baixa estratosfera, sendo seguidas por regimes meteorológicos troposféricos anómalos semelhantes ao Modo Anular do Hemisfério Norte (NAM) [Baldwin e Dunkerton 1999; 2001; Thompson et al. 2002].

O fenómeno de aquecimento súbito estratosférico (SSWs - Sudden Stratospheric Warmings) domina a variabilidade da circulação estratosférica durante o Inverno do Hemisfério Norte, tendo-se que os SSWs envolvem interacções entre o escoamento zonal da estratosfera polar e as ondas planetárias de propagação ascendente, principalmente com números de onda zonal 1 e 2 [Andrews et al. 1987]. Durante um SSW as temperaturas estratosféricas polares aumentam e o escoamento médio zonal enfraquece dramaticamente num curto intervalo de tempo. Com este enfraquecimento do escoamento zonal, a circulação estratosférica torna-se extremamente assimétrica e o vórtice estratosférico polar é afastado do pólo. Nos casos mais dramáticos, as temperaturas podem subir cerca de 50 K, e o escoamento estratosférico circumpolar pode reverter em apenas alguns dias [Limpasuvan et al. 2004].

Nesta conformidade, procede-se ao estudo da natureza anular dos principais padrões de variabilidade da circulação extratropical durante o Inverno do Hemisfério Norte e apresentam-se resultados que evidenciam a separação entre as componentes anular e não anular da variabilidade da circulação atmosférica do Hemisfério Norte. Efectua-se uma Análise em Componentes Principais dos campos troposféricos da altura do geopotencial, procedendo-se, em seguida, a um estudo das correlações desfasadas das Componentes Principais relevantes com a intensidade do vórtice polar estratosférico e com um *proxy* das anomalias das médias zonais do vento zonal nas latitudes médias

da troposfera. Os dados utilizados consistem em reanálises do European Centre for Medium-Range Weather Forecasts (ECMWF ERA-40) [Uppala et al. 2005]

Os resultados sugerem que os processos, que contribuem para a estrutura espacial do NAM, ocorrem em duas fases distintas, separadas por cerca de duas semanas. Anomalias das médias zonais do vento zonal nas latitudes médias da troposfera precedem, em cerca de uma semana, anomalias, de igual sinal, na intensidade do vórtice polar. Posteriormente às anomalias do vórtice polar, observam-se anomalias, de igual sinal, no vento médio zonal, na troposfera em latitudes elevadas. Estes resultados sugerem, pois, que o padrão dominante da variabilidade troposférica (o NAM), abundantemente referido na literatura, representa variabilidade associada a uma mistura de processos desfasados no tempo. Os padrões de variabilidade troposféria, que surgem como resposta à variabilidade do jacto polar boreal, apresentam uma escala hemisférica embora contenham uma estrutura dipolar, localizada apenas sobre a bacia Atlântica. Embora esse dipolo se assemelhe ao padrão da NAO, a linha nodal surge deslocada para Norte.

A natureza dinâmica da AO e da NAO é ainda investigada através de uma nova abordagem que combina os métodos tradicionais multivariados, como a Análise em Componentes Principais, com um procedimento de filtragem dinâmica baseado na análise tridimensional de modos normais da circulação global da atmosfera, cuja utilização se justifica na medida em que proporciona uma filtragem dos dados determinada pela própria natureza termohidrodinâmica do escoamento atmosférico. Com efeito, para além da decomposição da análise de Fourier em número de onda zonal, o esquema de modos normais permite ainda uma separação nas escalas espaciais meridional e vertical e, sobretudo, assegura uma decomposição do campo da circulação nas suas componentes rotacional e divergente. Os dados utilizados consistem em reanálises do National Centers for Environmental Prediction–National Center for Atmospheric Research (NCEP-NCAR; Kalnay et al. 1996; Kistler et al. 2001). Analisam-se as variabilidades anular e não anular da circulação extratropical durante o Inverno do Hemisfério Norte, tendo-se que os resultados obtidos mostram

que metade da variabilidade mensal da circulação barotrópica, com simetria zonal, do Hemisfério Norte, representada pela primeira EOF, é estatisticamente distinta da variabilidade remanescente. A correlação dos índices NAM da baixa estratosfera com as séries temporais diárias das anomalias da circulação projectadas sobre a primeira EOF é elevada ($r > 0.7$), evidenciando o facto de que a variabilidade anular se estende desde a estratosfera até à troposfera.

A realização de uma Análise em Componentes Principais à variabilidade residual do campo da altura do geopotencial aos 500-hPa – definida como a variabilidade remanescente após subtracção do campo da altura do geopotencial aos 500-hPa projectado sobre o índice NAM da baixa estratosfera – revela também um padrão com uma componente zonalmente simétrica nas latitudes médias. Contudo, esta componente zonalmente simétrica surge na segunda EOF da variabilidade residual e corresponde a dois dipolos independentes sobre os oceanos Pacífico e Atlântico. Estes resultados evidenciam a existência, nas latitudes elevadas, de uma componente zonalmente simétrica da variabilidade da circulação da baixa e média troposferas. Nas latitudes médias, a componente zonalmente simétrica da variabilidade da circulação – a existir – é, pois, artificialmente enfatizada pela utilização da Análise em Componentes Principais em níveis isobáricos troposféricos únicos.

O acoplamento dinâmico estratosfera-troposfera foi também estudado através da análise da energia associada às ondas planetárias. A expansão em modos normais tridimensionais da circulação geral da atmosfera proporciona a separação da energia total (cinética + potencial disponível) da atmosfera entre energia associada a ondas planetárias ou de Rossby e a ondas gravítico-inerciais, com estruturas verticais barotrópica ou baroclínicas. A análise, aqui efectuada, distingue-se das análises tradicionais, pois o forçamento estratosférico é diagnosticado em termos das anomalias da energia total associada a ondas tridimensionais, em vez das anomalias dos fluxos de calor e de momento associados a componentes de Fourier obtidas através de uma decomposição unidimensional da circulação atmosférica.

No contexto da dinâmica da interacção entre as ondas e o escoamento médio e através do estudo das correlações desfasadas entre a intensidade do jacto polar e a energia das ondas, investigou-se a forma como o vórtice polar oscila em função da energia total das ondas de Rossby. Foi também analisada a forma como ambas as escalas, zonal e meridional, dos modos de Rossby interagem com a intensidade do vórtice. Os resultados indicam que um aumento da energia total é acompanhado por um aumento da propagação de ondas de número de onda zonal 1 para a estratosfera, que desaceleram o jacto. A análise da correlação entre os modos de Rossby individuais e a intensidade do vórtice confirmam ainda os resultados da teoria linear que indicam que as ondas que forçam o vórtice polar são as associadas com as maiores escalas zonal e meridional.

Finalmente, efectuaram-se análises de compósitos aos dois tipos de fenómenos de aquecimento súbito estratosférico, nomeadamente aos episódios ditos de deslocamento e de separação, tendo os respectivos compósitos revelado que se encontram associados a mecanismos dinâmicos distintos. Mostra-se que os fenómenos de aquecimento súbito estratosférico do tipo deslocamento são forçados por anomalias positivas da energia, associadas com os dois primeiros modos baroclínicos das ondas planetárias de Rossby com número de onda zonal 1. Por outro lado, os fenómenos de aquecimento súbito estratosférico do tipo separação são forçados por anomalias positivas da energia, associadas com as ondas planetárias de Rossby com número de onda zonal 2, surgindo o modo barotrópico como a componente mais importante. De referir, finalmente, que no que respeita aos fenómenos de aquecimento final estratosférico, os resultados obtidos sugerem que o mecanismo dinâmico é semelhante ao dos fenómenos de aquecimento súbito estratosférico do tipo deslocamento.

Palavras Chave: vórtice polar estratosférico; interacção entre ondas e escoamento médio; modo anular; NAO e AO; modos normais 3D; ondas planetárias ou de Rossby; aquecimento súbito estratosférico.

TABLE OF CONTENTS

LIST OF FIGURES

LIST OF TABLES

LIST OF ACRONYMS

AM	Annular Mode
AO	Artic Oscillation
CPCA	Combined Principal Component Analysis
CCA	Canonical Correlation Analysis
ECMWF	European Centre for Medium-Range Weather Forecasts
EP	Eliassen–Palm
EOF	Empirical Orthogonal Function
NAM	Northern Hemisphere Annular Mode
NAO	North Atlantic Oscillation
NCEP	National Centers for Environmental Prediction
NCAR	National Center for Atmospheric Research
NH	Northern Hemisphere
NPO	North Pacific Oscillation
NPO/WP	North Pacific Oscillation/West Pacific
PAM	Polar Annular Mode
PC	Principal Component
PCA	Principal Component Analysis
PNA	Pacific/North American
PV	Potential Vorticity
QBO	Quasi-Biennial Oscillation
RPCA	Rotated Principal Component Analysis

SAM	Southern Annular Mode
SAT	Surface Air Temperature
SFW	Stratospheric Final Warming
SH	Southern Hemisphere
SLP	Sea Level Pressure
SO	Southern Oscillation
SSW	Stratospheric Sudden Warming
SVD	Singular Value Decomposition
SVR	Strong Vortex Regime
U_{50} (65)	50-hPa zonal mean zonal wind at 65ºN
U_{500} (45-55)	500-hPa zonal mean zonal wind averaged in the 45–55ºN latitudinal band
U_{00}	wind speed of the barotropic circulation
U500	500-hPa zonal mean zonal wind
$U500_R$	500-hPa zonal mean zonal wind regressed on the 70-hPa NAM
VI	Vortex Intensification
WKBJ	Wentzel–Kramers–Brillouin–Jeffries
WMO	World Meteorological Organization
WVR	Weak Vortex Regime
Z_{00}	geopotential height of the barotropic circulation
Z1000	1000-hPa geopotential height
Z500	500-hPa geopotential height
$Z500_R$	500-hPa geopotential height regressed on the 70-hPa NAM

1. INTRODUCTION

In the last decade an increasing number of observational and model studies strongly suggests that deviations in the stratospheric mean state associated to natural variability and external forcing may have a significant effect on tropospheric climate through the dynamical linkage between the two atmospheric layers.

The primary mechanism of dynamical troposphere-stratosphere coupling is the upward propagation of planetary or Rossby waves from the troposphere into the stratosphere. These waves whose origin lies upon the rotation and sphericity of the Earth [Rossby 1939] are generated in the troposphere by orography and heat sources. The stratospheric mean flow is then modified when Rossby waves grow enough to break and be absorbed. The subsequent circulation in both the stratosphere and troposphere may be in turn influenced through downward propagation of wave-induced stratospheric anomalies.

Changes in the tropospheric circulation may therefore have a substantial effect on the circulation of the stratosphere. Since wave propagation is on the whole from the tropospheric source up into the stratospheric sink, an effect of the stratosphere on the troposphere is not as straightforward. The stratospheric basic state, however, has a direct effect on the propagation characteristics of the waves [*e.g.*, Charney and Drazin 1961; Matsuno 1970]. As a result, zonal mean flow anomalies in the stratosphere will modify the waves and accordingly their interaction with the mean flow.

An interesting aspect of the dynamics of troposphere- stratosphere coupling is the one linked to annular modes (AMs) which are dominant variability patterns that arise in the Northern and Southern extratropics throughout the troposphere and the stratosphere. The strong coupling, presented by AMs, between troposphere and stratosphere, is considered by some authors as being intrinsic to the dynamics of the zonally symmetric polar vortex. AMs also exhibit a meridional seesaw between the polar region and the midlatitudes. Most prominent among AMs is the Northern

Annular Mode (NAM) or Arctic Oscillation (AO) which is highly correlated with the North Atlantic Oscillation (NAO) pattern. According to Wallace [2000], and despite being highly correlated, there is a clear distinction between the AO and NAO paradigms which is essential to the understanding of the physical mechanisms associated to Northern Hemisphere (NH) variability.

The aim of the present thesis is to further investigate the physical nature of both AO and NAO by means of a novel approach that combines traditional multivariate methods, such as Principal Component Analysis (PCA) with a dynamical filtering procedure based on 3-D normal modes of atmospheric variability.

We begin by discussing the annular nature of the leading isobaric empirical orthogonal functions (EOFs) of the NH winter extratropical circulation variability. It will be shown that the NAM spatial structure may result from the contribution of processes occurring at two different times, separated by about 2 weeks, namely i) midlatitude tropospheric zonal mean zonal wind anomalies occurring before stratospheric anomalies (polar vortex anomalies) and ii) zonal mean zonal wind anomalies of the same sign that are observed in the troposphere at high latitudes, after polar vortex anomalies. It is worth emphasizing that the separation of the two processes is of particular importance in studies of the tropospheric response to changes originated in the stratosphere, *e.g.* changes in stratospheric chemical composition and related climate changes. It is suggested that, whereas the NAM indices represent zonally symmetric zonal wind anomalies which spread from mid to high latitudes, the annularity of tropospheric response to stratospheric anomalies is confined to high latitudes. Moreover, even though tropospheric variability patterns, which appear to respond to polar vortex variability, have a hemispheric scale, a dipolar structure only appears over the Atlantic basin. This dipole resembles the NAO pattern, but its node line is shifted northward. The midlatitude zonal mean zonal wind anomalies tend in turn to occur before vortex anomalies and do not seem to take part on the downward progression of vortex anomalies.

Using a 3D normal modes dynamical filtering approach we investigate differences between the meridional profile of EOF1 of the barotropic zonally symmetric circulation and the zonally symmetric components of the annular modes defined at single isobaric tropospheric levels (EOF1). Results allow us to conclude that a large fraction of the midlatitude zonally symmetric variability, as represented by the leading EOF at single isobaric tropospheric levels, is not linearly associated with stratospheric variability.

The dynamic troposphere-stratosphere coupling and the specific problem of the variability of the stratospheric polar vortex are also studied from the point of view of planetary wave energetics. Performed analysis relies on 3D normal mode expansion and it may be noted that the adopted procedure mainly departs from traditional ones in respect to the wave forcing, which is here assessed in terms of total energy amounts associated with Rossby waves. Within the context of wave-mean flow interaction, we further investigate how the polar night jet oscillates with total energy of Rossby waves through lagged correlations between the vortex strength and the wave energy. We also pay attention to the way both the zonal and the meridional scales of Rossby modes interact with the vortex strength. Recently, a set of observational studies [Limpasuvan et al. 2004; 2005; McDaniel and Black 2005; Black et al. 2006; Nakagawa and Yamazaki 2006; Charlton and Polvani 2007] has focused on the daily evolution of strong vortex anomalies, polar vortex intensification, the life cycle of stratospheric sudden warming (SSW) events and the evolution of stratospheric final warming (SFW) events. Accordingly, an analysis of displacement- and split-type SSW events and of SFW events is also performed that reveals the distinct wave dynamics involved in the two types.

In Chapter 2 there is a brief discussion of some relevant aspects of the atmospheric circulation, namely the zonal mean circulation, planetary waves and stratospheric vortex dynamics. Chapter 3 introduces data and methods, with special emphasis on the three-dimensional (3D) normal mode expansion scheme of the atmospheric general circulation. Main results are presented and discussed in chapters four and five;

the annular nature of the leading patterns of the NH winter extratropical circulation variability is revisited in chapter 4 and evidence is presented of the separation of both components of annular and non-annular variability of the NH atmospheric circulation. The annular versus non-annular variability of the northern winter extratropical circulation is also reassessed, based on reanalysis data which were dynamically filtered by 3D normal modes. Results in this chapter have been included in Castanheira et al. [2007] and Castanheira et al. [2008]. Chapter 5 presents an analysis, relying on the 3D normal mode expansion, which is performed on the energetics of planetary wave forcing associated with the variability of the wintertime stratospheric polar vortex [Liberato et al. 2007]. Concluding remarks are included in the last chapter.

2. THEORETICAL BACKGROUND

2.1. Waves in the atmosphere

Atmospheric waves may be classified according to their physical properties and their restoring mechanisms; buoyancy or internal gravity waves owe their existence to stratification; inertio-gravity waves result from a combination of stratification and Coriolis effects; planetary or Rossby waves are due to the beta-effect or, more generally, to the northward gradient of potential vorticity.

Atmospheric waves may be also classified into free waves and forced waves, the latter as opposed to the former having to be continuously maintained by an excitation mechanism of given phase speed and wavenumber.

Some waves may propagate in all directions, whereas others may be trapped or evanescent in some directions. Most planetary (or Rossby) waves in the stratosphere and mesosphere appear to propagate upward from forcing regions in the troposphere, but under certain circumstances horizontally propagating planetary waves may be trapped in the vertical.

Atmospheric waves may be further separated into stationary waves, *i.e* those waves whose phase surfaces are fixed with respect to the earth, and travelling waves, *i.e.* those whose surfaces of constant phase move. It may be noted that information is carried by both types since it propagates with the wave train (with group velocity) and not with individual components (with phase speed). Another distinction may be made between waves whose amplitudes are time-varying and steady waves, *i.e.* those whose amplitudes are independent of time, denoted as steady waves.

2.2. Zonal mean dynamical structure of the atmosphere

The circulation of the middle atmosphere varies strongly in height, latitude, and

longitude. However, the most systematic variations are found in latitude and height.. Figure 2.1 shows a height-latitude cross-section of longitudinal average of zonal wind. Differences are well apparent between the winter hemisphere, where the flow is dominated by an eastward "polar vortex" and the summer hemisphere, where the flow is westward.

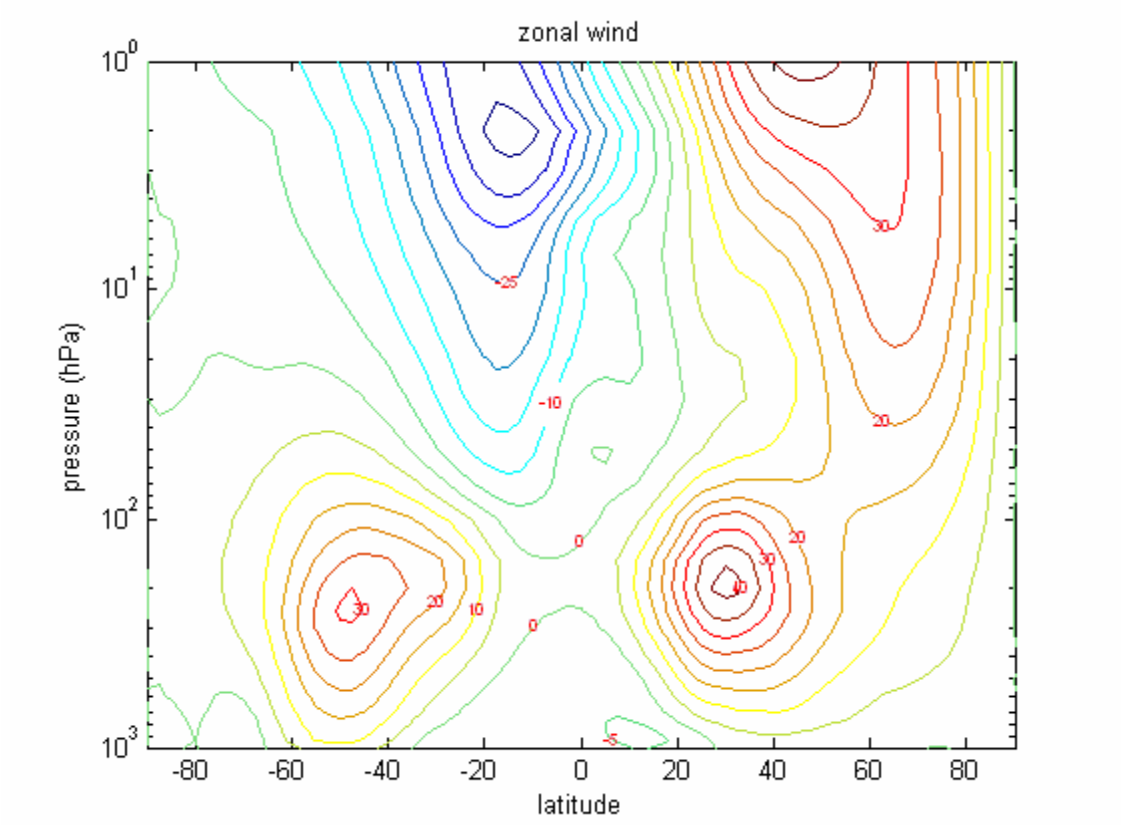

Figure 2.1 – Longitudinally averaged zonal component of wind in troposphere and stratosphere for December to March (Northern Hemisphere winter). Negative regions correspond to westward winds (contour: 5 m/s). The winter hemisphere has strong eastward jets in the stratosphere (the "polar vortex") while the summer hemisphere has strong westward winds. The field is based on monthly mean zonal wind from ECMWF (ERA-40) Reanalysis covering the period 1958-2002.

The development of the theory of wave mean-flow interaction in the 1960s and 1970s was stimulated by some of the questions posed by the observed state of the middle atmosphere. In particular it has long been known that an explanation of the longitudinally averaged state requires systematic effects of the deviations of the actual circulation from the mean to be taken into account. Such deviations are usually termed waves or eddies. The essence of the theory of wave mean-flow interaction is that there is long-range momentum transport between the location where the waves are generated and the location where the waves break or dissipate. This theory has been providing a useful quantitative framework for understanding the circulation of the middle atmosphere and is discussed in detail *e.g.* in Andrews et al. [1987] and references therein.

In the wave mean-flow description the flow is conveniently split into a longitudinal average (or zonal mean part), defined as

$$\overline{A}(\phi,z,t)=(2\pi)^{-1}\int_0^{2\pi}A(\lambda,\phi,z,t)\,d\lambda \tag{2.1}$$

and disturbance (or wave part), given by

$$A'(\lambda,\phi,z,t)\equiv A-\overline{A} \tag{2.2}$$

Using this separation, the quasi-geostrophic equations in the β-plane take the form [Equations 3.5.5 Andrews et al. 1987]

$$\frac{\partial\overline{u}}{\partial t}-f_0\overline{v}^*=\mathcal{G} \tag{2.3}$$

$$\frac{\partial\overline{\theta}}{\partial t}+\overline{w}^*\frac{\partial\theta_0}{\partial z}-\overline{Q}=0 \tag{2.4}$$

$$\frac{\partial\overline{v}^*}{\partial y}+\frac{1}{\rho_0}\frac{\partial}{\partial z}(\rho_0\overline{w}^*)=0 \tag{2.5}$$

$$f_0\frac{\partial\overline{u}}{\partial z}+\frac{R}{H}e^{-\kappa z/H}\frac{\partial\overline{\theta}}{\partial y}=0 \tag{2.6}$$

where (u, v, w) are the velocity components; Ω is the angular speed of rotation of the earth; $f_0 = 2\Omega \sin \phi_0$ is the Coriolis parameter; (x, y, z) are the eastward, northward and vertical log-pressure coordinates, with $z = -H \ln\left(p / p_S\right)$ (p being the pressure and p_S a standard reference pressure), $H \equiv RT_0 / g_0$ is a mean scale height (T_0 being a constant reference temperature); t is the time; Φ is the geopotential; θ is the potential temperature; $\theta_0(z) = T_0(z) e^{\kappa z / H}$, where $T_0(z)$ is a reference temperature, with $\kappa = R / c_p$ (R being the gas constant for dry air and c_p the isobaric specific heat capacity); Q is the net diabatic heating rate, and $(\bar{v}^*, \bar{w}^*)$ is the residual mean meridional circulation, given by [Equations 3.5.4 Andrews et al. 1987]

$$\begin{aligned} \bar{v}^* &\equiv \bar{v}_a - \frac{1}{\rho_0} \frac{\partial}{\partial z} \frac{\rho_0 \overline{v'\theta'}}{\partial \theta_0 / \partial z} \\ \bar{w}^* &\equiv \bar{w}_a + \frac{\partial}{\partial y} \frac{\overline{v'\theta'}}{\partial \theta_0 / \partial z} \end{aligned} \tag{2.7}$$

where v_a and w_a are the meridional and vertical ageostrophic velocities.

The set of equations (2.3) – (2.6) are the so-called transformed Eulerian equations. This formulation of the zonal mean equation takes into account the near cancellation of eddy and the ageostrophic mean meridional flow processes.

It may be noted that term $\mathcal{G}$ of equation (2.3) is the zonal force, which contains the effect of the large scale Rossby waves and the drag effect of unresolved eddies (such as gravity waves), *i.e.*

$$\mathcal{G} = \nabla \cdot \vec{F} + \bar{X}, \tag{2.8}$$

where the first term, which accounts for the large scale effect, is the divergence of the Eliassen-Palm flux (EP flux)

$$\vec{F} \equiv \left(0, -\rho_0 \overline{v'u'}, \rho_0 f_0 \overline{v'\theta'} \left(\frac{\partial \theta_0}{\partial z} \right)^{-1} \right) \tag{2.9}$$

and $\bar{X}$ represents the force due to unresolved eddies.

2.3. Planetary or Rossby waves and stratospheric vortex dynamics

According to Haynes [2005], on the large scale and on timescales greater than a day, the extratropical stratosphere is well described as a "balanced" system in which potential vorticity (PV) is a single time-evolving scalar field materially conserved in adiabatic, frictionless motion, and from which all other dynamical fields may be instantaneously determined through a PV "inversion" [McIntyre 2003a,b and references therein]. Considering small amplitude deviations with respect to a background flow, a linearized form of the PV conservation equation may be obtained, which allows for a set of solutions usually described as a Rossby waves.

The dynamics of Rossby waves involves adiabatic horizontal advection (*i.e.* advection along θ-surfaces) of PV, which has a strong pole-to-pole gradient, with resulting changes in temperature and pressure fields and vertical displacement of fluid parcels. The balance assumption excludes other waves, such as inertio-gravity waves and acoustic waves.

Planetary-scale Rossby waves (also known as planetary waves) are an essential feature of the dynamics of the troposphere and stratosphere, as they are excited and continually maintained in the troposphere, mainly by flow over topography and by latent heat release, and then propagate from the troposphere up into the stratosphere and the mesosphere.

In the context of Rossby waves, the zonal force $\mathcal{G}$ has to represent the propagation, breaking, and vortex interaction behaviour and therefore has to be a complicated nonlinear (and, as yet, undetermined) function of the mean flow and of wave sources.

The first major study of stratospheric planetary waves was performed by Charney and Drazin [1961], using quasi-geostrophic theory on a β-plane. In the frame of this theory the geostrophic wind is given by

$$\left(u_g, v_g\right) \equiv \left(-\frac{\partial \psi}{\partial y}, \frac{\partial \psi}{\partial x}\right) \tag{2.10}$$

where

$$\psi \equiv \frac{1}{f_0}\left(\Phi - \Phi_0\right) \tag{2.11}$$

is the geostrophic stream function and $\Phi_0(z)$ is a suitable reference geopotential profile; note that the definition of ψ involves f_0 and not $f = f_0 + \beta y$.

Following the linearization performed for the full quasi-geostrophic set of equations [Equations 3.2.9 of Andrews et al. 1987] the linearized version of the quasi-geostrophic potential vorticity equation may be written as

$$\left(\frac{\partial}{\partial t} + \bar{u}\frac{\partial}{\partial x}\right) q' + v' \frac{\partial \bar{q}}{\partial y} = Z' \tag{2.12}$$

where q' is the disturbance quasi-geostrophic potential vorticity

$$q' \equiv \frac{\partial^2 \psi'}{\partial x^2} + \frac{\partial^2 \psi'}{\partial y^2} + \rho_0^{-1} \frac{\partial}{\partial z}\left(\rho_0 \varepsilon \frac{\partial \psi'}{\partial z}\right) \tag{2.13}$$

$v' = \dfrac{\partial \psi'}{\partial x}$ is the northward geostrophic wind, $\dfrac{\partial \bar{q}}{\partial y}$ is the basic northward quasi-geostrophic potential vorticity gradient

$$\frac{\partial \bar{q}}{\partial y} \equiv \beta - \frac{\partial^2 \bar{u}}{\partial y^2} - \rho_0^{-1} \frac{\partial}{\partial z}\left(\rho_0 \varepsilon \frac{\partial \bar{u}}{\partial z}\right) \tag{2.14}$$

and Z' denotes the nonconservative terms.

Considering a basic zonal flow $\overline{u} = \overline{u}(y,z)$, taking $\varepsilon = \left(\frac{f_0}{N}\right)^2$ as constant (where N is the "buoyancy frequency"), setting the nonconservative terms to zero ($Z' = 0$) and assuming a stationary wave solution of zonal wavenumber $k = \frac{s}{a\cos\phi}$

$$\psi' = e^{z/2H}\,\mathrm{Re}\left[\Psi(y,z)e^{ik(x-ct)}\right] \tag{2.15}$$

we obtain

$$\frac{\partial^2\Psi}{\partial y^2} + \varepsilon\frac{\partial^2\Psi}{\partial z^2} + n_k^2\Psi = 0 \tag{2.16}$$

where n_k^2 is the squared refractive index [Dickinson 1968], for zonal wavenumber k and phase speed c, given by.

$$n_k^2(y,z) = \frac{1}{(\overline{u}-c)}\frac{\partial\overline{q}}{\partial y} - k^2 - \frac{\varepsilon}{4H^2} \tag{2.17}$$

It is expected that waves propagate in regions where $n_k^2 > 0$ and that they become evanescent in regions where $n_k^2 < 0$.

Vertically propagating stationary planetary waves in the stratosphere were studied in detail by Matsuno [1970], based on the hypothesis of stationary waves in the NH winter stratosphere being forced from the troposphere. Matsuno [1970] used a linearized quasi-geostrophic potential vorticity equation in spherical coordinates, and considered a stationary wave solution of zonal wavenumber, s.

The vertical propagation of stationary Rossby waves from the troposphere into the stratosphere depends on zonal wind and the horizontal wavenumber [Charney and Drazin 1961]. The Charney-Drazin classic result shows that waves propagate upward only through flow that is weakly eastward relative to phase speed (with maximum relative flow speed from propagation decreasing as length scale decreases) and only if the scale of the waves is sufficiently large. On the basis of this very simple model,

wavenumber 1 ($s = 1$) propagates in westerlies weaker than about 28 $m\ s^{-1}$, wavenumber 2 propagates in westerlies weaker than about 16 m s^{-1}. Given that the dominant forcing of stratospheric Rossby waves is geographically stationary, Charney-Drazin criterion for vertical propagation of stationary Rossby waves makes evident the role of Rossby waves (and vortex dynamics) in shaping the winter stratospheric circulation and the dynamics of the longitudinal mean flow. It further provides a basic explanation of why the winter stratosphere (with eastward flow around the pole; see Figure 2.1) is much more disturbed than the summer stratosphere (with westward flow around the pole) and why the disturbances in the winter stratosphere tend to have much larger scales than is typical of the troposphere below [Haynes 2005].

Dynamical mechanisms operating in stratospheric flows, namely reversible displacements and distortions of the polar vortex may be studied through the time evolution of the PV field. McIntyre and Palmer [1983; 1984] used PV maps and associated reversible displacements and distortions of the polar vortex with upward propagating Rossby waves. They also analysed the nonlinear stirring of the PV field outside the vortex, calling this region outside the vortex the stratospheric "surf zone", and identified it with the breaking of upward propagating Rossby waves.

The two-dimensional vorticity equation became a simple and computationally inexpensive proxy for three-dimensional balanced systems, and a number of numerical studies of two-dimensional stratosphere-like flows gave important insights into the dynamics of the stratospheric polar vortex and surf zone. This method was first used by Juckes and McIntyre [1987] who showed material coherence of the vortex (*i.e.* the high PV core of the vortex), which, even for quite large-amplitude forcing, experienced reversible deformation but with almost no transport of fluid between interior and exterior. They also explained the strong stirring effect of the disturbed flow outside the vortex, which tended to pull filaments of material out of the edge of the vortex and mix them into the exterior flow.

When the wave forcing is strong enough, the main vortex may be significantly displaced from the pole, strongly deformed in shape, or even split into two, and these events are known as "sudden stratospheric warmings". They are noticeable as very rapid increases in temperature, due to adiabatic warming through descent. In the Northern Hemisphere SSWs occur in mid-winter in about half of winters, on average, and there is also often a sudden-warming-like event at the end of winter - the "final warming". These disturbances to the vortex are generally stronger in the Northern Hemisphere than in the Southern Hemisphere, as expected from the distinction of topography and proportion of ocean versus land.

In the winter stratosphere, Rossby waves are primary responsible for driving the Brewer-Dobson circulation [Holton et al. 1995], for formation of the "surf zone" through irreversible isentropic mixing related to Rossby wave breaking [McIntyre and Palmer 1984] and for sudden stratospheric warmings [Matsuno 1971; Holton 1976; Labitzke 1982; McIntyre 1982]. An increased number of studies show that stratospheric response to upward propagating Rossby waves has a tendency to propagate downward. Observational and model studies in the last decade suggest that variations in the stratospheric mean state caused by natural variability and external forcing might have a significant effect on the tropospheric circulation and climate through the dynamical link between the two atmospheric layers [e. g. Kodera 1993; Graf et al. 1994; 1995; Perlwitz and Graf 1995; Shindell et al. 1999a,b; Hartmann et al. 2000; Robock 2000; Christiansen 2001; Baldwin and Dunkerton 2001; Plumb and Semeniuk 2003; Polvani and Waugh 2004; Perlwitz and Harnik 2004]. There is now evidence of downward dynamical links between the stratosphere and troposphere which may determine, for example, the effect on surface weather and climate of stratospheric aerosol changes due to volcanic eruptions and may imply a strong role for the stratosphere in determining future changes in the tropospheric climate due to increases in carbon dioxide and other greenhouse gases.

3. DATA AND METHODS

In this chapter we introduce the three-dimensional (3D) normal mode expansion scheme of the atmospheric general circulation. Former applications of this methodology are presented with the aim of showing its significance in the study of global circulation variability. A short description of the 3D normal modes of the linearized primitive equations is also given. In addition to this method, we discuss the applications of PCA on the NH extratropical circulation and refer to some of the physical/dynamical aspects involved as well as to the problems of the EOF technique which are due to statistical uncertainties as well as to those that are inherent to the method itself. In the last part of the chapter we refer to the global reanalysis data used and describe the data preparation performed for this research. Indices representing the strength of the stratospheric polar vortex are described and we present data series of SSW and SFW events that will be analysed. A reference to climatology and anomalies is performed and we present the bootstrap technique that allows estimating the statistical significance of anomalies.

3.1. Three-dimensional Normal Mode Decomposition

The use of the 3D normal mode decomposition in the study of global circulation variability has been discussed in several works [*e.g.*, Castanheira 2000; Castanheira et al. 2002; Tanaka and Tokinaga 2002; Tanaka et al. 2004]. The orthogonal projection of the atmospheric circulation field onto 3D normal mode functions, as originally presented by Kasahara and Puri [1981], allows partitioning the circulation field into gravity and rotational components, a feature that makes of normal modes an important tool, both in objective data analysis and in model initialization [Daley 1991]. The problem involves solving a linearized system of primitive equations with the aim of building up an orthogonal base of functions, and is therefore a problem of free oscillations [Castanheira et al. 1999].

Global energetics analysis using 3D normal mode functions [Kasahara and Puri 1981; Tanaka 1985; Tanaka and Kung 1988; Castanheira et al. 1999] lays the grounds for a unified frame encompassing the three, 1-dimensional spectral energetics, respectively, in the zonal, meridional and vertical domains. Castanheira et al. [1999] stress that this method further allows the separation of the atmospheric circulation between planetary (Rossby) and inertio-gravity waves. It also allows each zonal wave to be decomposed into a number of meridional scales. Moreover, the 3D normal mode scheme identifies the contribution of each wave for the global total energy.

In another study Castanheira et al. [2002] give more evidence of the importance of using 3D normal mode decomposition in the study of atmospheric circulation. These authors point out that the search for recurrent atmospheric circulation patterns is usually performed by means of statistical analysis of gridded field variables [*e.g.*, Wallace and Gutzler 1981; Preisendorfer 1988; Kushnir and Wallace 1989; Bretherton et al. 1992]. However, in order to obtain statistically stable solutions, the number of degrees of freedom must be kept small. This means that one must consider a limited region of the atmosphere, i. e. limited horizontal areas as well as a small

number of vertical levels. Besides, the uncovered patterns are based on a purely statistical approach and their physical significance is usually tested, a posteriori, by the fraction of explained variability, by the significance level of the computed statistics, or by retrieving similar patterns from different subsets of the data [*e.g.*, North et al. 1982; Livezey and Chen 1983; Kushnir and Wallace 1989]. Castanheira et al. [2002] also mention another type of approach that consists on a prefiltering of data by means of a Fourier analysis allowing isolating the most relevant zonal wavenumbers or by means of a spherical harmonic analysis aiming to select both the most important zonal wavenumbers and meridional scales [*e.g.*, Schubert 1986; Nakamura et al. 1987]. The physical reason for using spherical harmonics comes from the fact that they are eigensolutions of the nondivergent barotropic vorticity equation over the sphere, with the same dispersion relationship of the Rossby–Haurwitz waves. It may be noted that spherical harmonics also appear as asymptotic forms of wave solutions of the linearized shallow water equations [Longuet-Higgins 1968]. The search for circulation patterns by means of an analysis performed in the phase spaces of either Fourier or spherical harmonics coefficients does bring some a priori meaning to the uncovered patterns due to the fact that the obtained statistics are computed on the amplitudes of functions that are believed to represent spatial structures of physical entities. However, the nondivergent barotropic vorticity equation does not account for the vertical stratification of the atmosphere and is certainly not an adequate approach for the intertropical circulation.

The linearization of the atmospheric primitive equations around a basic state at rest may be viewed as an oversimplification in the sense that it disregards the nonlinearity of the real atmosphere and does not account for a climatological wind. However, in spite of these important limitations, a set of linearized primitive equations does grasp much more of the physics of the real atmosphere than does the nondivergent barotropic vorticity equation. On the other hand, the normal modes — free oscillations — of the linearized system are vector functions defined over the whole atmosphere and represent, simultaneously, the horizontal wind and mass fields. This

allows for the possibility of a dynamically consistent filtering of the atmospheric circulation [Daley 1991].

In our study the motivation for the use of this method lies on the assumption that the more physically based the entities are, from which statistics are derived, the more physical meaning may be assigned to the uncovered patterns.

The following section presents the method described by Castanheira et al. [2002] and Liberato et al. [2007] for the use of 3D atmospheric normal modes in the study of global atmospheric circulation variability.

3.1.1. 3D Normal Mode Decomposition Scheme

A short description of the 3D normal modes of the linearized primitive equations is given in this section.

A hydrostatic and adiabatic atmosphere may freely oscillate around a reference state at rest. For such an atmosphere, the primitive equations, linearized with respect to a basic state at rest having a pressure-dependent temperature distribution $T_0(p)$, may be written in the following form

$$\begin{aligned} &\frac{\partial u}{\partial t} - 2\Omega v \sin\theta + \frac{1}{a\cos\theta}\frac{\partial \phi}{\partial \lambda} = 0 \\ &\frac{\partial v}{\partial t} + 2\Omega u \sin\theta + \frac{1}{a}\frac{\partial \phi}{\partial \theta} = 0 \\ &\frac{\partial}{\partial p}\left[\frac{1}{S_0}\frac{\partial}{\partial p}\left(\frac{\partial \phi}{\partial t}\right)\right] - \vec{\nabla}\cdot\vec{V} = 0 \end{aligned} \tag{3.1}$$

where (λ, θ, p) are the longitude, latitude and pressure coordinates; ϕ, the perturbed geopotential field, is the deviation from the basic state geopotential profile $\Phi_0(p)$; and

$$S_0 = \frac{R}{p}\left(\frac{kT_0}{p} - \frac{\mathrm{d}T_0}{\mathrm{d}p}\right) \tag{3.2}$$

is the static stability parameter of the reference state. The remaining symbols in

Equations 3.1 and 3.2 are the horizontal wind components (u, v), the earth's radius a, the angular speed of earth's rotation Ω, the specific gas constant R, and the ratio k of specific gas constant to specific heat at constant pressure.

As model boundary conditions, it is assumed that $\omega = dp/dt$ vanishes as p → 0 and that the linearized geometric vertical velocity $w = dz/dt$ vanishes at a constant pressure, p_s, near the earth's surface.

As described in *e.g.* Tanaka [1985] and references therein, the vertical and horizontal structures of each mode of oscillation may be separated by means of the technique of separation of variables. The horizontal structure is identical to that of a free oscillation mode of an incompressible, homogeneous, hydrostatic and inviscid fluid over a rotating sphere. The free oscillations – normal modes – of the linearized primitive equations (Equation 3.1) may be written in the form

$$\begin{bmatrix} u \\ v \\ \phi \end{bmatrix}_{msl,\alpha} = \exp\left(-i2\Omega\nu t\right) G_m\left(p\right) \exp\left(is\lambda\right) \overline{\overline{C}}_m \cdot \begin{bmatrix} U\left(\theta\right) \\ iV\left(\theta\right) \\ Z\left(\theta\right) \end{bmatrix}_{msl,\alpha} \tag{3.3}$$

where $\overline{\overline{C}}_m = diag\left(\sqrt{gh_m}, \sqrt{gh_m}, gh_m\right)$ is a diagonal matrix of scaling factors, with g the earth's gravity and h_m the equivalent height. $G_m(p)$ are the separable vertical structures and m is a vertical index. The horizontal structures are given by the product of a zonal wave with wavenumber s and a vector $\left[U\left(\theta\right), iV\left(\theta\right), Z\left(\theta\right)\right]^T_{msl,\alpha}$ which defines the meridional profiles of the wave. Because the meridional index l is associated with the number of zeros of the meridional profiles, it may be regarded as an index of the meridional scale of the motion. The index α = 1, 2, 3 refers to westward travelling inertio-gravity waves, Rossby planetary waves and eastward travelling inertio-gravity waves, respectively. ν is a dimensionless frequency.

The normal modes form a complete orthogonal basis that allows the expansion of the horizontal wind and the geopotential fields [Daley 1991; Castanheira 2000;

Castanheira et al. 2002; Tanaka 2003].

$$\begin{bmatrix} u \\ v \\ \phi \end{bmatrix} = \sum_{m=0}^{\infty} \sum_{s=-\infty}^{\infty} \sum_{l=0}^{\infty} \sum_{\alpha=1}^{3} w_{msl}^{\alpha}(t) G_m(p) \exp(is\lambda) \overline{\overline{C}}_m \cdot \begin{bmatrix} U(\theta) \\ iV(\theta) \\ Z(\theta) \end{bmatrix}_{msl,\alpha} \tag{3.4}$$

The expansion coefficients are obtained by means of a vertical projection onto the vertical structure functions, $G_m(p)$,

$$(\hat{u}, \hat{v}, \hat{\phi})_m^T = \frac{1}{p_s} \int_0^{p_s} (u, v, \phi)^T G_m(p) dp \tag{3.5}$$

followed by an horizontal projection onto the horizontal structures, $\vec{H}_{msl}^{\alpha}(\lambda, \theta) = \exp(is\lambda)\left[U(\theta), iV(\theta), Z(\theta)\right]_{msl,\alpha}^T$

$$w_{msl}^{\alpha} = \frac{1}{2\pi} \int_0^{2\pi} \int_{-\pi/2}^{\pi/2} (\vec{H}_{msl}^{\alpha})^* \left(\overline{\overline{C}}_m\right)^{-1} \cdot (\hat{u}, \hat{v}, \hat{\phi})_m^T \cos\theta \, d\theta \, d\lambda \tag{3.6}$$

It may be noted that it has been assumed that the vertical structures, $G_m(p)$, and the horizontal structures, $\vec{H}_{msl}^{\alpha}(\lambda, \theta)$ have unitary norms. The superscript T denotes the transpose, and ( )* denotes the complex conjugate of the transpose.

It may be shown that the squared expansion coefficients are proportional to the Total (*i.e.* Kinetic + Available Potential) energy per unit area associated with the respective modes [Castanheira et al. 1999, and references therein]

$$E_{msl}^{\alpha}(t) = \frac{p_s h_m}{c_s} \left| w_{msl}^{\alpha}(t) \right|^2 \tag{3.7}$$

For $s = 0$, one has $c_0 = 4$ and in such case E_{m0l}^{α} represents the total energy associated with a zonal symmetric α mode with vertical and meridional indices (m,l), respectively. For $s \geq 1$, E_{msl}^{α} represents the total energy of the complex conjugate pair of modes (α, msl) and $(\alpha, m(-s)l)$ and therefore $c_s = 2$.

3.2. Principal Component Analysis

Since their introduction in meteorology [Obukhov 1947; Lorenz 1956; Kutzbach 1967] empirical orthogonal function (EOF) or principal component analysis (PCA) have become customary as a convenient means of representing climatological fields. PCA is a multivariate statistical technique whose aim is to extract spatio-temporal information when dealing with datasets formed by a large number of variables that are not statistically independent. This technique allows computing an optimal new system of uncorrelated variables, referred to as principal components (PCs). Each PC is expressed as a linear combination of the original variables, the coefficients of the linear combination being referred to as the EOF of the corresponding PC. Since PCs are uncorrelated, the total variance of the original dataset may be expressed as the sum of the variances of each PC. PCs are usually ranked in terms of decreasing explained variance and the dimensionality of the dataset may be often reduced by retaining a relatively low number of PCs that explain a sufficiently high part of the total variance. PCA is one of the most important methods in multivariate statistics. If the structure of the data is inherently linear (e. g., if the underlying distribution is Gaussian), then PCA is an optimal feature extraction algorithm; however, if the data contain a nonlinear lower-dimensional structure, it will not be detectable by PCA.

PCA is a well-studied subject and standard references exist describing the method and its implementation [Preisendorfer 1988; Wilks 1995; 2005; von Storch and Zwiers 1999; 2002]. Among the wide range of applications, reduction of data dimensionality for data interpretation and forecasting [*e.g.* Wallace and Gutzler 1981; Barnston and Livezey 1987; Miller et al. 1997] is worth being mentioned in the context of the global circulation of the atmosphere.

PCA is a purely statistical procedure, in the sense that it is entirely based on computing the eigenvectors and eigenvalues of the covariance (or correlation) matrix of the data. However, the first EOF/PC pairs often reflect physically meaningful

patterns, which are associated to physical mechanisms whose signatures in the dataset are captured by PCA. When such is the case, besides reducing data dimensionality, PCA leads to a better characterization and understanding of the original dataset.

EOFs are defined as the eigenvectors of the spatial cross-covariance matrix of the data to be analyzed [*e.g.*, Jolliffe 1986]. In the context of our research, we will consider covariances of time series at different grid points. The eigenvectors are linear combinations of the individual station or grid point data and are uncorrelated with each other. Weights of the linear combination for the various stations or grid points may be represented as contour maps, and their patterns are of great interest [North et al. 1982].

EOFs are optimal in explaining total variance with any specified number of spatial patterns. The first EOF explains most of the temporal variance in the dataset among all possible spatial fields. The subsequent EOFs are mutually orthogonal (in space and time) and successively explain less variance. However, the interpretation of EOFs as physical/dynamical modes of variability has always to be made with much care [Ambaum et al. 2001]. North [1984] or Mo and Ghil [1987] are two examples where connection between the results of PCA, which are statistical in nature, and the underlying dynamics of the system under consideration has been successfully performed.

By construction EOFs are constrained by their mutual orthogonality. Accordingly, if a dataset is a linear superposition of two patterns that are not orthogonal, the EOF analysis will not yield these patterns. At the same time, EOFs present a strong tendency to reach the simplest possible spatial structure inside the domain. This tendency leads to strong dependence of EOFs on the shape of the spatial domain [*e.g.*, Richman 1986].

Ambaum et al. [2001] also refer that EOF analysis is nonlocal in the sense that the loading values at two different spatial points in an EOF do not simply depend on the time series at those two points but depend on the whole dataset, a feature that may

lead to locally counterintuitive results. This contrasts with the one-point correlation analyses used to define teleconnections [Wallace and Gutzler 1981], for which the patterns may be interpreted locally. Ambaum et al. [2001] stress this point by noting that two same-signed points in an EOF do not necessarily have correlated time series. These authors state that the nonlocal nature of EOFs demands a careful interpretation of the pattern structure of any particular EOF.

EOFs also have statistical uncertainties that must be carefully evaluated. North et al. [1982] presented a rule of thumb that allows assessing whether a given EOF is likely to be subject to large sampling fluctuations. The rule is simply based on the assumption that if the sampling error of a particular eigenvalue, λ, is comparable to or larger than the spacing between λ and a neighbouring eigenvalue, then the sampling errors for the EOF associated with that particular eigenvalue will be comparable to the size of the neighbouring EOF. If such is the case, then if a group of true eigenvalues, λ_i, lie within one or two $\delta\lambda$ of each other, then they form an "effectively degenerate multiplet", and sample eigenvectors are a random mixture of the true eigenvectors.

For instance, North et al. [1982] state that Wallace and Gutzler [1981] provide another example of the variability of EOF patterns from one sample to another on their investigation for the NH wintertime geopotential height field. The rule of thumb described here indicates that the first two pairs of EOFs derived from the record available to those authors are likely to be mixed by sampling fluctuations, which was borne out in their analysis of a similar but independent record.

3.2.1. PCA on filtered transformed space

PCA may be also applied to data that were previously filtered either by means of a Fourier analysis allowing isolating the most relevant zonal wavenumbers or by means of a spherical harmonic analysis aiming to select both the most important zonal wavenumbers and meridional scales. This methodology was presented by Castanheira et al. [2002] who, by using also 3D normal mode decomposition, also uncovered

horizontal patterns of atmospheric circulation variability by means of a PCA performed on the time series of the projection coefficients. A set of selected coefficients were ordered in a column vector

$$\left[w_1^{'}(t), w_2^{'}(t), ..., w_\beta^{'}(t), ..., w_q^{'}(t) \right]^T \tag{3.8}$$

where β stands for a quartet of indices (m*sl*,α) and *q* is the number of modes that were retained in the analysis. Next the complex variance–covariance matrix was computed

$$S_{\beta\beta'} = \frac{1}{N-1} \sum_{t=1}^{N} w_\beta^{'}(t) w_{\beta'}^{'*}(t) \tag{3.9}$$

and then the eigenvalue and eigenvector problem was solved

$$\sum_{\beta'} S_{\beta\beta'} e_k(\beta') = \lambda_k e_k(\beta) \tag{3.10}$$

All eigenvalues are real because the variance–covariance matrix S is Hermitian.

Finally, replacing the w_{msl}^{α} coefficients in the expansion in Equation 3.4 by the respective components $e_k(\beta)$ of the eigenvector $\hat{e}_k$ allows retrieving the atmospheric circulation pattern associated with a global variance λ_k.

It is worth stressing that the 3D structures of the free oscillations of an adiabatic and hydrostatic atmosphere around a basic state at rest are used as a physical filtering for atmospheric data. Moreover, the filtering procedure allows considering simultaneously the three primitive variables (*u*, *v*, φ) over the whole atmosphere. Accordingly, the computed statistics do not simply rely on the information provided by a single variable of circulation, such as the 500-hPa geopotential field.

Using the above-described method, Castanheira et al. [2002] isolated two classical patterns in the barotropic (*m = 0*) component of the circulation, one resembling the Pacific/North America (PNA) pattern, the other similar to the North Atlantic Oscillation (NAO) pattern. Associating the barotropic and the second baroclinic components, a coupling in variability was retrieved between the strength of the winter

stratospheric polar vortex and the tropospheric circulation over the North Atlantic. The authors stressed that those modes had only been recovered by means of statistical analysis and that this was the first study that showed their existence in physically filtered fields. Moreover the obtained results make clear that the observed winter pattern of NAO is not a simple atmospheric mode of variability, but results instead from mean flow wave interaction that modulates tropospheric planetary Rossby waves.

3.2.2. On the physical meaning of EOFs

In recent years the EOF technique has been largely used to identify potential physical modes. Whereas North et al. [1982] and Richman [1986] have discussed the problem of statistical uncertainty in the estimation of the EOFs, Dommenget and Latif [2002] concentrate on problems of the EOF technique which are not due to statistical uncertainties but are more inherent to the method itself. Their discussion is mostly focused on the differences among spatial patterns, but taking into account that each pattern is related to a specific time series. Patterns that do show large differences in the spatial structures will, in general, have large differences in the corresponding time series as well.

In a simple low-dimensional example Dommenget and Latif [2002] consider three modes of variability. According to the authors, the three modes may be interpreted as the ‘‘real physical modes’’ of the domain. From a mathematical point of view all representations of this simple low-dimensional example are equally valid, but from a physical point of view the authors have been looking for the representation which most clearly points toward the real physical modes of the problem.

By construction the EOF analysis maximizes the explained variance in the leading EOFs. This will generally lead to the fact that only a few EOF patterns are needed to explain a large amount of variability. In this artificial example the two leading EOFs explain more than 95% of the total variance. However, since Dommenget and Latif’s

[2002] artificial example has three modes, these authors conclude that this indicates that the EOF analysis will, in general, underestimate the complexity of the problem.

Their main conclusions may be summarized as follows.

- Teleconnection patterns as derived from the orthogonal analysis may not necessarily be interpreted as teleconnections that are associated with a potential physical process.
- The centers of action as derived from the EOF methods do not need to be the centers of action of the real physical modes.
- The PCs of the dominant patterns are often a superposition of many different modes that are uncorrelated in time and that are often modes of remote regions that have no influence on the region in which the pattern of the considered PC has its centre of action.

North [1984] had already demonstrated that individual EOF modes correspond to individual physical modes only in the very limited class of linear dynamical systems, for which the linear operator commutes with its adjoint. By studying the mean and covariance structure of an idealized zonal jet that fluctuates in strength, position, and width, Monahan and Fyfe [2006] obtained analytic results demonstrating that in general individual EOF modes may not be interpreted in terms of individual physical processes.

In fact, EOF analysis may produce zonally symmetric leading patterns even when , in particular, the dynamics is not zonally coherent on hemispheric length scales [Ambaum et al. 2001; Gerber and Vallis 2005]. As shown by these authors, performing a PCA on a variability field dominated by independent dipolar structures, like the NAO or the North Pacific Oscillation/West Pacific pattern (NPO/WP), one may obtain leading EOF patterns with a high degree of zonal symmetry.

3.3. Data and Data Preparation

3.3.1. Projection onto 3D normal modes

Data were obtained from the global reanalysis dataset of the National Centers for Environmental Prediction–National Center for Atmospheric Research (NCEP-NCAR; Kalnay et al. 1996; Kistler et al. 2001). We have used November-April daily means of the horizontal wind components (*u, v*) and of the geopotential height, available at 17 standard pressure levels from 1000-to 10-hPa, with a horizontal grid resolution of 2.5° latitude × 2.5° longitude, covering the period 1958–2005. Each period from November to April is identified by the year to which January belongs.

We have projected the data onto the normal modes of the NCEP–NCAR reference atmosphere, which allows partitioning the atmospheric circulation into one barotropic and several baroclinic components. Figure 3.1 shows the first five vertical structure functions of the NCEP–NCAR atmosphere, which were obtained numerically using a Galerkin method [Castanheira et al. 1999] between 0 and the mean surface pressure, p_s. However, since the NCEP–NCAR data only extend up to the 10-hPa level, the vertical structures are not represented above that upper level. The number of nodes (zeros) of a given vertical structure function is equal to the corresponding vertical index *m*. Since the projection [Equation 3.5] onto the barotropic vertical structure, $G_0(p)$, is nearly a vertical average of the atmospheric circulation, it may be regarded as representing the tropospheric circulation [Castanheira et al. 2002]. It is worth noting that all baroclinic modes *m = 2, 3*, and *4* have a zero above 10-hPa, which is not represented in Figure 3.1.

The first and the second baroclinic structures, $G_1(p)$ and $G_2(p)$, respectively, have their nodes in the stratosphere, while the third and the higher vertical baroclinic structure functions have one or more nodes in the troposphere. This feature together

with the large amplitude presented by $G_1(p)$ and $G_2(p)$ in the stratosphere make these vertical structure functions especially sensitive to the stratospheric circulation features.

Projections onto the vertical structure functions were then followed by projections onto the horizontal normal modes [Equation 3.6], allowing to obtain the complex wave amplitudes, *i.e.*, the coefficients w_{msl}^{α}. Finally the total energy associated with each planetary Rossby or gravity wave characterized by a given vertical structure *m* and a given wavenumber *s* was obtained by summing the energy as given in Equation 3.7 for all meridional indices *l*.

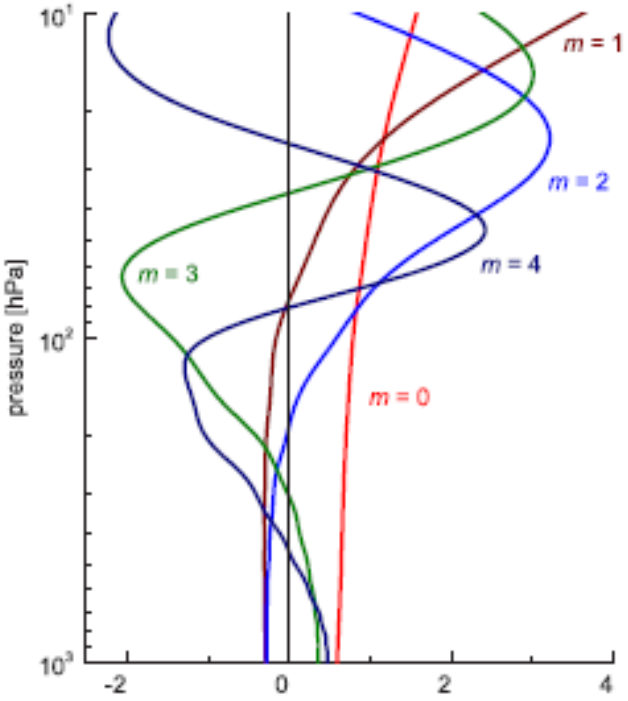

Figure 3.1 – Vertical structure functions of the barotropic *m = 0* and the first four baroclinic modes (*m = 1,…,4*) of the NCEP–NCAR atmosphere. It is worth noting that the NCEP–NCAR database only extends up to the 10-hPa level.

3.3.2. PCA

We have also used the 1000- and 500-hPa geopotential height fields and the zonal wind data as obtained from the European Centre for Medium-Range Weather Forecasts (ECMWF) ReAnalysis (ERA-40) datasets [Uppala et al. 2005]. We have computed daily means, with a 2.5° latitude × 2.5° longitude horizontal grid resolution, for 45 winters (November to March) from 1958 to 2002. A PCA was then performed on the NH extratropical circulation north of 30ºN at 1000- and 500-hPa isobaric levels. Vertical connection between the obtained patterns and the vortex strength was finally assessed by means of lagged correlations between the respective PCs and the U_{50} (65) index described bellow.

3.3.3. Stratospheric Polar Vortex Strength Indices

In our study the strength of the polar vortex is represented by means of the stratospheric Northern Hemisphere annular mode (NAM) time series as computed by Baldwin and Dunkerton [2001] (NAM indices, covering the period 1958-2006, were kindly made available by M. Baldwin).

The strength of the stratospheric polar vortex is also represented by the 50-hPa zonal mean zonal wind at 65ºN, here denoted as the U_{50} (65) index. Considering the 15-day running means, the correlation between the NAM index at 50-hPa and the U_{50} (65) index is 0.96. Hence, the much simpler zonal mean wind is nearly identical with the 50-hPa NAM index.

3.3.4. Midwinter Sudden Warming Events

Following the World Meteorological Organization (WMO) definition, a major midwinter stratospheric warming event occurs when the zonal mean zonal wind at 60°N and 10-hPa becomes easterly, and the gradient of 10-hPa zonal mean

temperature becomes positive between 60° and 90°N. Charlton and Polvani [2007] adhered to this more widely used WMO definition of SSW events (easterly winds at 10-hPa and 60°N) and examined both the NCEP–NCAR and the 40-yr ECMWF ReAnalysis (ERA-40) datasets in the extended winter (November–March). These authors developed a more sophisticated algorithm, based on the sign of the zonal mean zonal wind, to automatically extract SSW events from large datasets and distinguish between different types of SSW events.

Charlton and Polvani [2007] distinguish between different types of SSW events, based on the synoptic structure in the middle stratosphere. Following O'Neill [2003], one type of SSW events, the so-called vortex displacement, is characterized by a clear shift of the polar vortex off the pole, and its subsequent distortion into a "comma shape" during the extrusion of a vortex filament; an example is given in Figure 3.2a. The other type of SSW events, the so-called vortex split, is easily recognizable in that the polar vortex breaks up into two pieces of comparable size (Figure 3.2b). While these two types of SSW events are often associated with large amplitudes of longitudinal wavenumbers 1 and 2, respectively, a simple Fourier decomposition is not sufficient to identify them [Waugh 1997, their appendix].

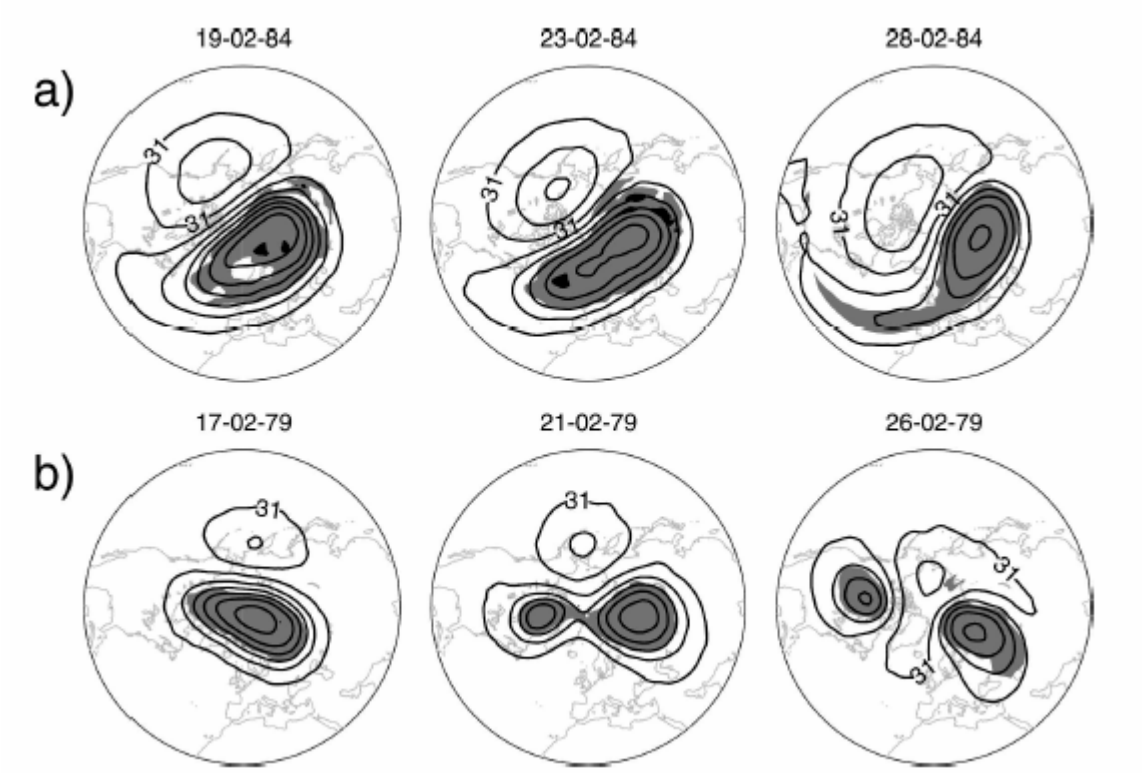

Figure 3.2 – Polar stereographic plot of geopotential height (contours) on the 10-hPa pressure surface. Contour interval is 0.4 km, and shading shows potential vorticity greater than 4.0×10^{-6} K kg^{-1} m^2 s^{-1}. (a) A vortex displacement type warming that occurred in February 1984. (b) A vortex splitting type warming that occurred in February 1979 (Figure 1 from Charlton and Polvani [2007]).

Table 3.1 shows the list of SSW events that were used in the present work as identified in the NCEP–NCAR reanalysis dataset by means of the algorithm developed by Charlton and Polvani [2007]. Since we have restricted the computation of daily energies to the periods from 1 November to 30 April, and due to the fact that we will have to compute composites starting 35 days before and ending 35 days after the central date of each SSW event, we have excluded from the analysis all events with central dates before 6 December (*i.e.*, one vortex split and two vortex

displacements). However, composites computed for shorter time intervals and including the three excluded SSW events led to results identical to the ones that will be presented.

Table 3.1 – List of SSW events that were considered in this work. SSW events were identified in the NCEP–NCAR dataset based on the algorithm developed by Charlton and Polvani [2007]. Letters D and S in the second column identify displacement- and split-type SSW events, respectively. Here ΔT refers to area-weighted means of the polar cap temperature anomaly at the 10-hPa level, during periods from 5 days before up to 5 days after the central dates of each event.

Central date	Type	ΔT (K)	Central date	Type	ΔT (K)
30 Jan 1958	S	7.8	29 Feb 1980	D	11.5
16 Jan 1960	D	5.9	24 Feb 1984	D	11.1
23 Mar 1965	S	4.4	2 Jan 1985	S	13.0
8 Dec 1965	D	6.7	23 Jan 1987	D	10.2
24 Feb 1966	S	3.1	8 Dec 1987	S	14.1
8 Jan 1968	S	12.0	14 Mar 1988	D	11.7
13 Mar 1969	D	4.3	22 Feb 1989	S	12.8
2 Jan 1970	D	6.8	15 Dec 1998	D	12.7
17 Jan 1971	S	9.6	25 Feb 1999	S	11.0
20 Mar 1971	D	-2.9	20 Mar 2000	D	5.3
2 Feb 1973	S	6.6	11 Feb 2001	D	6.3
22 Feb 1979	S	3.7	2 Jan 2002	D	12.9

3.3.5. Stratospheric Final Warming Events

Concurrently, Black et al. [2006] studied the evolution of SFW events. In the stratosphere each winter season concludes with a rather abrupt transition from circumpolar westerly winds to easterlies. This annual breakdown of the polar vortex is known as the stratospheric final warming (SFW). Their observational study on the relationship between SFW events and the Northern extratropical circulation found that SFW events strongly organize the large-scale circulation of the stratosphere and troposphere. SFW events were defined as the final time during which the zonal mean zonal wind at 70°N drops below 0 without returning to a specified positive threshold value until the subsequent autumn. The criterion was applied to 5-day averages at 10- and 50-hPa zonal mean zonal winds with thresholds of 10 and 5 m s^{-1}, respectively.

We will compute composites of daily energies from 40 days before to 20 days after the central dates of each SFW event identified at the 50-hPa level. Event dates were kindly made available by R. X. Black and are based on the NCEP–NCAR reanalysis dataset covering the 47-yr period 1958–2004. The list of SFW events includes the 22 earliest events and the 22 latest events but our composite analysis will restrict to 19 earliest events (*i.e.* those events with central dates earlier than 20 days before 30 April). If central dates were chosen up to 10 days before 30 April and composites were built up from 40 days before to 10 days after the central dates of each SFW event, then a set of 30 events would be retained. However, we have verified that similar features were obtained with both samples during the common period (*i.e.* from 40 days before to 10 days after the central dates).

3.3.6. Climatology and Anomalies

For every variable, we have removed the respective seasonal cycle, which was estimated by computing at each day the respective interannual mean and then by smoothing the obtained time series of daily interannual means with a 31-day running average. Daily values of the energy for the total circulation (*i.e.* climatology + anomaly field) were computed before the seasonal cycle was removed. Similarly, daily anomalies of the other fields were obtained by subtracting the seasonal cycle from the original daily means. A 15-day running mean was applied to the anomalies, in order to filter out shorter time scales.

On the other hand since we intend to analyze composites of the daily energy during stratospheric events, there is the need to remove the interannual components, which for each extended winter was estimated by the respective winter average. Accordingly all anomalies used in our work represent intraseasonal fluctuations (*i.e.* departures from the respective winter averages).

3.3.7. Statistical Significance of Anomalies

Statistical significance of anomalies in the energy composites was assessed by means of resampling tests, also known as rerandomization or Monte-Carlo tests. This approach to non-parametrical testing is based on the construction of artificial datasets of the same size as the actual data from a given real dataset, which are obtained by resampling the observations [*e.g.* Wilks 2005]. In single-sample situations a very useful technique is the so-called "bootstrap", which operates by construction of the artificial data sets using sampling with replacement from the original data. Conceptually, the sampling process is equivalent, in this case, to writing each of the n data values (say, n periods of daily energies of 60 consecutive days) on n separate slips of paper and putting all of them in a hat. To construct one bootstrap sample, the

slips of paper are drawn one by one from the hat, with replacement, being this process repeated a large number of times (typically n_B=1,000 to 10,000 random periods). A particular time series of the original dataset may be drawn several times, or not at all, in a given bootstrap sample.

Bootstrap is used here to estimate confidence intervals around observed values of a test statistic. This procedure may be applied to any test statistic, since bootstrap method does not depend on the analytical form of its sampling distribution. Confidence regions are easily approached using the percentile method, which is a straightforward procedure. To form a (1–α)% confidence interval, one simply finds the values of the parameter estimates defining the largest and the smallest $n_B \times \alpha/2$ of the n_B random samples. This method was also used on the subsequent studies, varying the number of elements on the bootstrap estimate.

4. BRIDGING THE ANNULAR MODE AND NORTH ATLANTIC OSCILLATION PARADIGMS

In this chapter the annular nature of the leading patterns of the NH winter extratropical circulation variability is revisited, and evidence is presented of the separation of both components of annular and non-annular variability of the NH atmospheric circulation. The analysis relies on a PCA of tropospheric geopotential height fields and lagged correlations with the stratospheric polar vortex strength and with a proxy of midlatitude tropospheric zonal mean zonal momentum anomalies.

Results suggest that two processes, occurring at different times, contribute to the NAM spatial structure. Polar vortex anomalies appear to be associated to midlatitude tropospheric zonal mean zonal wind anomalies occurring before stratospheric anomalies. Following polar vortex anomalies, zonal mean zonal wind anomalies of the same sign are observed in the troposphere at high latitudes. The separation timescale between the two signals is about 2 weeks. It is suggested that the leading tropospheric variability patterns found in the literature represent variability associated with both processes. The tropospheric variability patterns which appear to respond to the polar vortex variability have a hemispheric scale but show a dipolar structure only over the Atlantic basin. The dipole resembles the NAO pattern, but with the node line shifted northward. These results have been published in Castanheira et al. [2007].

The annular versus non-annular variability of the northern winter extratropical circulation is reassessed on the second part of this chapter, based on reanalysis data which were dynamically filtered by 3D normal modes. Results show that one half of the monthly variability of the barotropic zonally symmetric circulation of the NH is statistically distinct from the remaining variability, and being explained by its leading EOF alone. The daily time series of the circulation anomalies projected onto the leading EOF is highly correlated ($r \geq 0.7$) to the lower stratosphere NAM indices,

showing that annular variability extends from the stratosphere deep into the troposphere.

A PCA of the residual variability of the 500-hPa geopotential height field (defined as the departures from the 500-hPa geopotential height regressed onto the lower stratosphere NAM index), also reveals a pattern with a zonally symmetric component at midlatitudes. However, this zonally symmetric component appears as the second EOF of the residual variability and is the imprint of two independent dipoles over the Pacific and Atlantic oceans.

These results, accepted for publication in Castanheira et al. [2008], show that a zonally symmetric component of the middle and lower tropospheric circulation variability exists at high latitudes. At the middle latitudes, obtained results suggest that the zonally symmetric component, that has been identified in other works, is artificially overemphasized by the usage of PCA on single isobaric tropospheric levels.

4.1. Extratropical Atmospheric Circulation Variability

In this section a review of the state of the art of the extratropical winter variability is performed following the paper by Wallace and Gutzler [1981]. Section 4.1.1 describes wintertime extratropical variability of the horizontal circulation in the troposphere and stratosphere, and vertical coupling is described in the following section. The discussion and relation between NAO and NAM paradigms is reviewed in Section 4.1.3 and finally the timescale of teleconnection patterns is discussed in section 4.1.4.

4.1.1. Space-time variability of horizontal circulation

Sir Gilbert Walker pioneered early attempts to understand and identify low-frequency circulation modes. He was the first to use statistical regression methods to search for significant teleconnection patterns (though he did not actually use the term

'teleconnections'). He introduced the use of correlation to study teleconnections and the use of multiple regression to deal with the problem of long-range forecasting. His pioneering work culminated in the landmark paper of Walker and Bliss [1932], where three dominant teleconnection patterns were identified: the Southern Oscillation (SO), the North Atlantic Oscillation (NAO), and the North Pacific Oscillation (NPO).

The usefulness of Walker's empirical methods was widely recognised and a large number of researchers have applied them to larger and higher quality data sets. Van Loon and Rogers [1978] and Rogers [1981] confirmed many of Walker's results regarding NAO and NPO.

Wallace and Gutzler [1981] were the first to provide a comprehensive and extensive summary of teleconnection patterns in the monthly averaged sea level pressure (SLP) and upper-level geopotential height fields during the NH winter season. They used correlations and PCA, which they applied to a 15-year record of winter-time monthly averaged 500-hPa geopotential height fields. Wallace and Gutzler [1981] constructed one-point correlation maps and introduced the concept of teleconnectivity, which helps summarising one-point correlation maps of individual teleconnection patterns in just one map. Wallace and Gutzler [1981] defined "teleconnections" as significant simultaneous correlations between geopotential heights on a given pressure surface at widely separated points on earth and "teleconnectivity" as the strongest negative correlation on each one-point correlation map, plotted at the base grid point. They further proposed the use of "teleconnectivity" to contrast the strength of teleconnection patterns for different base points.

These authors identified in the existing literature at least four recurrent spatial patterns indicative of standing oscillations in planetary waves (*i.e.* standing wave structures with geographically distinct and fixed nodes and antinodes) during NH winter, with timescales on the order of months or longer. These four patterns are the following: NAO and NPO, both identified by Walker and Bliss [1932], a zonally symmetric seesaw between sea level pressures in polar and temperate latitudes, first noted by

Lorenz [1951], and the Pacific/North American (PNA) pattern, as labelled by Wallace and Gutzler [1981].

4.1.1.1. NH winter season teleconnection patterns

Both the NAO and the PNA patterns are strongly evident in Wallace and Gutzler's [1981] study and were considered by these authors as teleconnection patterns at middle and high latitudes of the NH winter season. Wallace and Gutzler [1981] described NAO as being associated with fluctuations in the strength of the climatological mean jet stream over the western Atlantic. The PNA pattern included in turn a north-south seesaw in the central Pacific somewhat reminiscent of the NPO as mentioned by Walker and Bliss [1932] and Bjerknes [1969], together with centres of action over western Canada and the south-eastern United States.

Figure 4.1 shows the teleconnectivity maps for SLP and 500-hPa geopotential height. Figure 4.1a confirms the SLP patterns associated with the NAO and NPO as described by Walker and Bliss [1932]. The dipole shaped pattern in the eastern North Pacific may be considered as a reflection of another major teleconnection, the PNA.

In addition to these two main teleconnection patterns, both characterized by north-south seesaws or standing oscillations in the sea level pressure field with a node located near 50ºN latitude, Wallace and Gutzler [1981] stated that the leading eigenvector of the correlation matrix of the sea level pressure field is dominated by a planetary scale, zonally symmetric seesaw between sea level pressures in the polar cap region and lower latitudes. These authors noted also that a similar pattern of pressure anomalies has been observed in connection with two stratospheric phenomena, sudden warmings and the quasi-biennial oscillation (QBO).

Whilst the sea level pressure statistics presented by Wallace and Gutzler [1981] were dominated by negative correlations between the polar region and temperate latitudes, most of them with only one or two well-defined centres of action at the earth's surface, the 500-hPa statistics were dominated by patterns of a more regional scale, which display a nearly equivalent barotropic structure with amplitudes increasing with

height. According to these authors, their structure at these levels resembles that of forced stationary waves on a sphere, because at mid-tropospheric levels they are wavelike in appearance and characterized by multiple centres of action. That is, the horizontal scale and spatial orientation of the patterns resemble the steady, linear response of a spherical atmosphere to thermal and/or orographic forcing [Hoskins and Karoly, 1981].

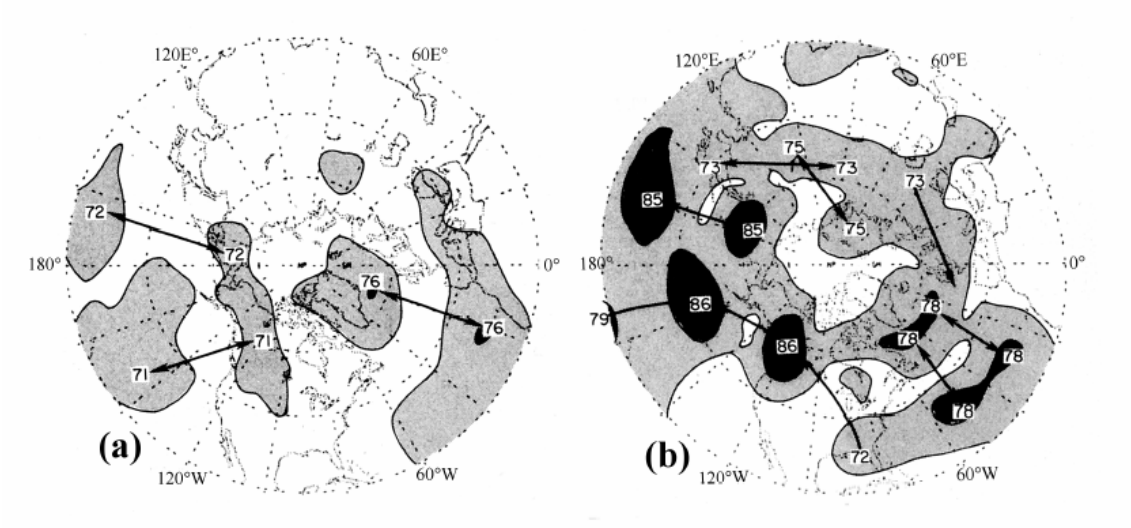

Figure 4.1 – Strongest negative correlation ρ_i on each one-point correlation map, plotted at the base grid point (originally referred to as "teleconnectivity") for (a) SLP and (b) 500-hPa height. Correlation fields were computed over 45 winter months from 1962-1963 to 1976-1977. Negative signs have been omitted and correlation coefficients multiplied by 100. Regions where $\rho_i < 60$ are unshaded; $60 \le \rho_i < 75$ stippled lightly; $75 \le \rho_i$ stippled heavily. Arrows connect centres of strongest teleconnectivity with the grid point, which exhibits strongest negative correlation on their respective one-point correlation maps (Figure 7 from Wallace and Gutzler [1981]).

Another important result stressed by Wallace and Gutzler [1981] is that there are some notable differences between their eigenvector patterns and their teleconnection patterns. According to these authors, the latter tend in general to be somewhat more localized, with fewer strong centres of action, explaining a larger fraction of the local variance of 500-hPa height in the vicinity of those centres of action. So, the main advantages of the teleconnection patterns are their somewhat more localized spatial structure which facilitates their dynamical interpretation, their greater efficiency at explaining the local variance of the 500-hPa height field, and the simplicity with which their pattern indices can be computed.

Wallace and Gutzler's [1981] review study was followed by a large number of studies of low-frequency atmospheric variability (*i.e.* variability of the planetary waves on time scales of several weeks upward to several years), which have produced a diverse and occasionally confusing set of teleconnection patterns, dynamical modes and oscillations [Barnston and Livezey 1987; Trenberth and Hurrell 1994; Wallace et al. 1995; Mantua et al. 1997; Thompson and Wallace 1998; 2000; Honda and Nakamura 2001]. Barnston and Livezey [1987] list in their Appendix B some of the patterns of variability identified prior to that time, and they present similar winter results based on a high resolution 35-year period of record. These authors have identified some less obvious patterns and provide further details on the better-known ones. Barnston and Livezey [1987] stress that the NAO is the only pattern found for every month of the year, which systematically contracts northward in summer and expands southward in winter, being both the strongest winter and the strongest summer patterns (Figures 4.2 and 4.3). Using twice-daily data these authors replicated their own results using monthly, 3-month and 10-day means of 700-hPa height, stressing in their work that results using 10-day means point the way to use a larger sample without noticeably obscuring the low-frequency signal.

It may be noted that the patterns that have emerged in all these studies have been conditioned not only by the different analysis techniques used but also by the spatial domain of the analysis, the way in which seasonality is treated, and the time interval

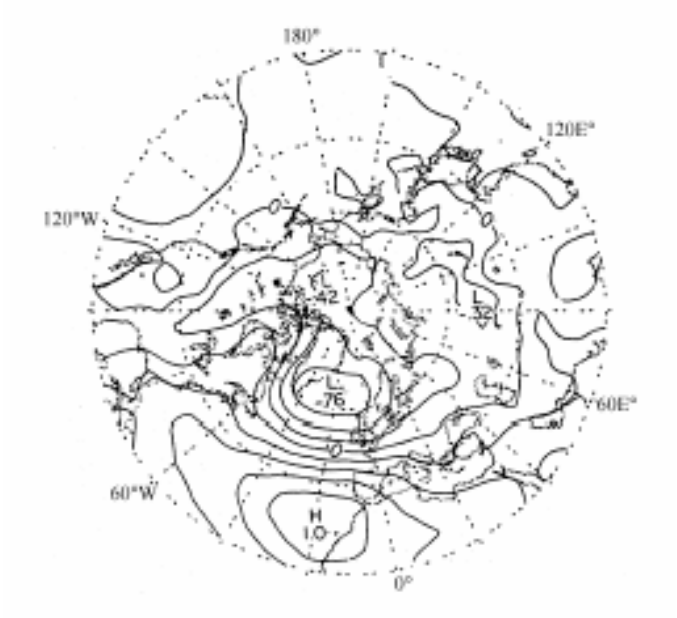

Figure 4.2 – One-point correlation map showing correlation coefficients between SLP at the grid point 30°N, 20°W, and SLP at every grid point. Based on same 45-month data set as Figure 4.1. Contour interval is 0.2 (Figure 8b from Wallace and Gutzler [1981]).

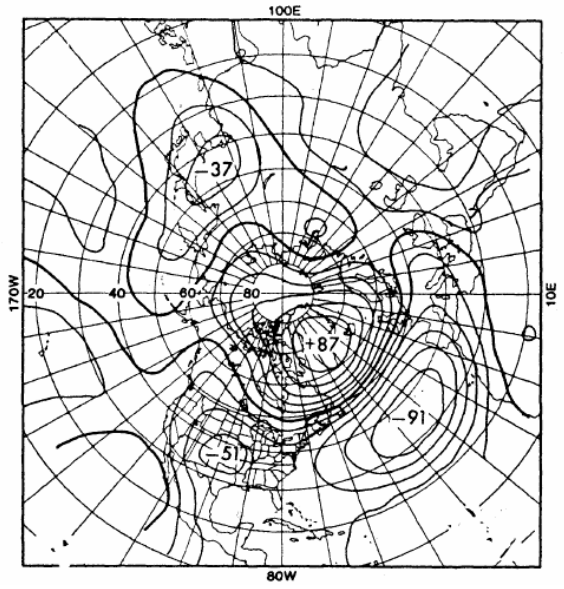

Figure 4.3 – The NAO in January as depicted in the RPCA of Barnston and Livezey [1987].

over which the data are averaged before the analysis is performed. Barnston and Livezey [1987] have applied rotated principal component analysis (RPCA), repeatedly to different sets of years and to the full 35-year record, concluding that the RPCA method provides both a physically meaningful and a statistically stable result, with the simplicity of teleconnection patterns but with superior pattern choice to that of the teleconnection method. Using Monte Carlo simulations Richman [1986] has addressed the issue of statistical stability of unrotated and rotated principal components and has confirmed that the latter are much less vulnerable to sampling error than the former.

Quadrelli and Wallace [2004a,b] attempted to simplify the climate dynamics literature by placing all these patterns in a common framework that would allow for systematic intercomparison of the spatial patterns and their associated time series. They suggested that most NH extratropical wintertime patterns that have been identified in monthly mean SLP and geopotential height data project strongly upon the two-dimensional phase space defined by the first two EOFs of the monthly mean SLP field – defined on the basis of winter (December through March) monthly data, in the period 1958-99. In a similar manner, the time-varying indices of these patterns may be reproduced by a linear combination of the first two PCs of the SLP field. Quadrelli and Wallace [2004a] also demonstrated that the leading EOFs (PCs) of the geopotential height field at levels throughout the troposphere project strongly onto the phase subspace defined by the first two EOFs (PCs) of the SLP field, and that the same is true for SLP EOFs and PCs derived from seasonal-mean data, and for the spatial pattern of SLP trends over the NH. Patterns they have obtained are reproduced in Figure 4.4.

Following the authors, the leading SLP EOF corresponds to the NAM, in agreement with the works of Thompson and Wallace [1998] which is very similar to the NAO [Hurrell 1995]. The second EOF resembles the PNA pattern, agreeing with Wallace and Thompson [2002] who previously suggested that the second EOF pattern is the surface manifestation of an extended PNA, a prominent linear wave pattern found by

Simmons et al. [1983].

On other words, Quadrelli and Wallace [2004a] showed that the NH wintertime geopotential height, temperature and precipitation fields on time scales of months and longer may be represented in terms of the two leading patterns of SLP north of 20ºN. These results may contribute to laying the grounds to the belief that the first two EOFs represent teleconnection patterns [Wallace and Thompson 2002].

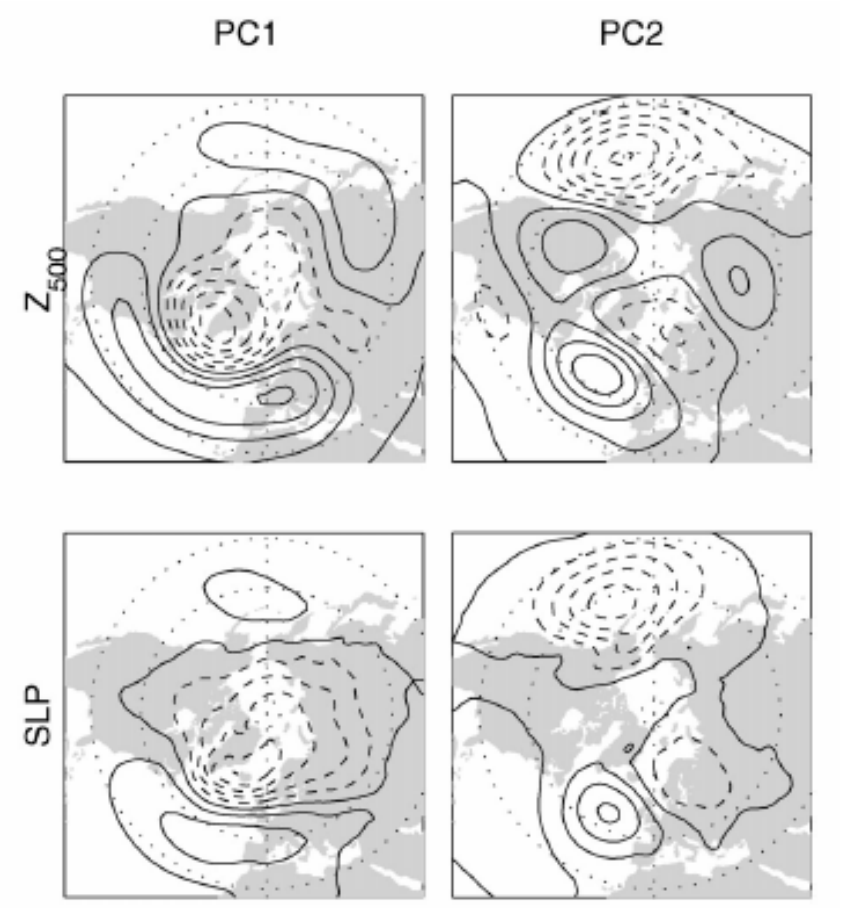

Figure 4.4 – Monthly mean 500-hPa height and SLP fields regressed on standardized PC1 and PC2 of monthly mean DJFM SLP anomalies poleward of 20ºN, based on data for the period 1958–99. Contour interval 1.5 hPa for SLP and 15 m for 500-hPa height; negative contours are dashed. The latitude circles plotted correspond to 30º and 45ºN (Figure 1 from Quadrelli and Wallace [2004b]).

4.1.1.2. AO and Annular Modes

The annular modes (AM) are dominant variability patterns that arise in the Northern and Southern extratropics throughout the troposphere and stratosphere. These AM describe a meridional seesaw between the polar region and midlatitudes. Most prominent among these is the Northern AM (NAM) or Arctic Oscillation which has been introduced by Thompson and Wallace [1998] as the leading EOF of the surface pressure.

Following the earlier studies of Lorenz [1951] and Kutzbach [1970], Thompson and Wallace [1998; 2000] and Thompson et al. [2000] have given evidence to the importance of the pattern of variability they refer to as the Arctic Oscillation (AO). This pattern, known today indistinctly as AO or NAM, is highly correlated with the NAO pattern. According to Wallace [2000], although the two patterns are highly correlated, there is a clear distinction that could play a guiding role in how we attempt to understand physical mechanisms in the NH variability.

Usually defined as the first EOF of the mean sea level pressure field in the NH, the AO is a robust result from EOF analysis of that field on timescales from weeks to decades in any season [Kutzbach 1970; Thompson and Wallace 1998]. This is now a conventional definition of the ‘‘annular mode’’ [Thompson and Wallace 2000], although the correspondence of EOFs to the dynamical modes of climate generally cannot be made precise [North 1984].

On the other hand, Thompson and Wallace [1998] stated that the leading EOF of the wintertime sea-level pressure field resembles the NAO in many aspects, but its primary centre of action covers more of the Arctic, giving it a more zonally symmetric appearance. Coupled to strong fluctuations at the 50-hPa level at the intraseasonal, interannual, and interdecadal time scales, this “Arctic Oscillation” may be interpreted as the surface signature of modulations in the strength of the polar vortex aloft. It is proposed by Thompson and Wallace [1998] that the zonally asymmetric surface air temperature and mid-tropospheric circulation anomalies

observed in association with the AO may be secondary baroclinic features induced by land-sea contrasts.

A characteristic of the AM is its vertical extension into the stratosphere and its downward propagation [Baldwin and Dunkerton, 1999]. This latter issue will be analised in detail in the next section.

According to Baldwin and Dunkerton [2001], variations in the strength of the polar vortex are well characterized by "annular modes," which are hemispheric-scale patterns characterized by synchronous fluctuations in pressure of one sign over the polar caps and of opposite sign at lower latitudes. They used daily November to April data to independently define the annular mode indices at each of 26 pressure levels from 1000- to 0.316-hPa, during the period 1958-1999. At each pressure level the annular mode is the first EOF of 90-day low-pass filtered geopotential anomalies north of 20°N. Daily values of the annular mode, spanning the entire 42-year data record, were calculated for each pressure level by projecting daily geopotential anomalies onto the leading EOF patterns.

In this paper the authors stated that, in the stratosphere, annular mode values are a measure of the strength of the polar vortex, while the near-surface annular mode is called the "Arctic Oscillation" (AO) [Thompson and Wallace 1998], which is recognized as the NAO [Hurrell 1995; Wallace 2000] over the Atlantic sector.

According to Baldwin and Dunkerton [2001] their observations suggest that large circulation anomalies in the lower stratosphere are related to substantial shifts in the AO/NAO and that these stratospheric signals may be used as a predictive tool. Their results further suggest the possibility that other changes in the stratosphere (*e.g.*, from volcanic aerosols, solar irradiance or greenhouse gases) could in turn be related to surface weather if they affect the likelihood or timing of extreme circulation events in the polar lower stratosphere.

However, while in the stratosphere the NAM is simply interpreted as representing the variability of polar vortex strength, the interpretation in the troposphere is much more

difficult due to the entangled sources of tropospheric variability. This will be subject to further investigation and discussion in this thesis.

Thompson and Wallace [2000] show that the structures of the NH and SH annular modes are remarkably similar, not only in the zonally averaged geopotential height and zonal wind fields, but also in the mean meridional circulations. The authors note that they both exist year-round in the troposphere, though they amplify with height upward into the stratosphere during those seasons in which the strength of the zonal flow is conducive to strong planetary wave-mean flow interactions, namely midwinter in the NH and late spring in the SH, which they defined as "active seasons".

The Southern Hemisphere (SH) counterpart of the NAM, referred to as Antarctic Oscillation [Gong and Wang 1999] or Southern Annular Mode (SAM), is a large-scale pattern of climate variability characterized by fluctuations in the strength of the SH circumpolar flow. Stratospheric AM is "active" only in certain months, comprising the boreal winter (January to March) for the NAM and the SH late spring (November) for the SAM. The stratospheric circulation is most variable during winter, when the cold, cyclonic polar vortex varies in strength and is disturbed by planetary-scale Rossby waves. These waves originate mainly in the troposphere and transport westward angular momentum upward, where they interact with the stratospheric flow. In particular, the SAM is "inactive" during austral winter [Thompson and Wallace 2000].

Thompson et al. [2005] examined the temporal evolution of the tropospheric circulation following large-amplitude variations in the strength of the SH stratospheric polar vortex in data from 1979 to 2001 as well as following the SH sudden stratospheric warming of 2002. In both cases, anomalies in the strength of the SH stratospheric polar vortex precede similarly signed anomalies in the tropospheric circulation that persist for more than 2 months. These SH tropospheric circulation anomalies reflect a bias in the polarity of the SAM. Consistent with the climate impacts of the SAM, variations in the stratospheric polar vortex are also followed by

coherent changes in surface temperatures throughout much of Antarctica.

Results presented in Thompson et al. [2005] are remarkably similar to those observed in association with anomalies in the NH stratospheric polar vortex, as documented in Baldwin and Dunkerton [2001]. Thus, results provide independent verification for the observed relationships between long-lived anomalies in the NH stratosphere and the surface climate. One notable difference between the two hemispheres is the enhanced persistence of the SH anomalies. In the NH, major stratospheric events are followed by anomalies in the lower stratosphere and troposphere that persist for up to circa 60 days; in the SH such events are followed by anomalies in the lowermost stratosphere and troposphere that persist for up to circa 90 days. The enhanced persistence of anomalies in the SH stratosphere is consistent with the relative dearth of dynamical forcing there.

Thompson et al. [2005] results add to a growing body of evidence that suggests that stratospheric variability plays an important role in driving climate variability at Earth's surface on a range of time scales.

4.1.2. Vertical Coupling

There are several techniques that may be used to isolate important coupled modes of variability between time series of two fields, and several approaches have been applied to geophysical data. The work of Kutzbach [1967] was decisive in the use of PCA in climate research by revealing that two or more field variables may be combined in the same PCA to document the relationships between fields. Bretherton et al. [1992] reviewed several methods for finding correlated patterns between two fields.

By comparing methods (CPCA, CCA and SVD) applied to a simple but geophysically relevant model these authors introduced a conceptual framework for comparing methods that isolate important coupled modes of variability between time series of two fields. They compare the quantitative performance of the methods in isolating a

coupled signal as they vary parameters such as the spatial localization of the coupled signal, the number of sampling times, the number of grid points in each field, and the ratio of the coupled signal amplitude to uncoupled variability. In a companion paper, Wallace et al. [1992] have compared the performance of CPCA, CCA and SVD applied to a geophysical problem, the interannual coupling between wintertime Pacific SST anomalies and the anomalies in the atmospheric 500-hPa geopotential height field over the North Pacific, illustrating that SVD clearly isolates the two most important extratropical modes of variability in the studied case.

In the works of Perlwitz and Graf [1995] and of Thompson and Wallace [1998] the statistical analysis was repeated for different tropospheric levels allowing studying the vertical structure of the mode. Thompson and Wallace [1998] refer to growing evidence indicating that the stratospheric polar vortex is implicated in some of the interannual variability of climate at the earth's surface. Baldwin et al. [1994], Perlwitz and Graf [1995], Cheng and Dunkerton [1995] and Kitoh et al. [1996] have documented the existence of coupling between the strength of the nearly zonally symmetric polar night jet at the 50-hPa level and a more wavelike pattern reminiscent of the NAO at the 500-hPa level.

On the other hand, Hurrell [1995] has shown that the NAO modulates wintertime surface air temperature (SAT) over much of Eurasia: negative SLP anomalies over Iceland and enhanced westerlies across the North Atlantic at 50ºN (*i.e.* the positive polarity of the NAO) are associated with positive SAT anomalies extending from Great Britain and Scandinavia far into Siberia. Hurrell [1996] went on to demonstrate that the upward trend in the NAO during the past 30 years accounts for much of the warming in SAT averaged over the domain poleward of 20ºN. Kodera and Yamazaki [1994], Graf et al. [1995], and Kodera and Koide [1997] have suggested the possibility of a dynamical linkage between the recent wintertime warming over Eurasia and a strengthening of the polar night jet, Robock and Mao [1992], Graf et al. [1994] and Kodera [1994] have invoked similar linkages to explain the observed positive SAT anomalies over Eurasia during the winters following major volcanic

eruptions.

Additionally, Thompson and Wallace [1998] stated that their results confirm the existence of deep vertical coupling in the wintertime polar vortex and its relation to SAT anomalies over Eurasia and the Northwest Atlantic during an extended (November-April) winter season. Whereas the studies of Baldwin et al. [1994], Perlwitz and Graf [1995], Cheng and Dunkerton [1995] and Kitoh et al. [1996] have represented the tropospheric circulation in terms of the 500- or 850-hPa height fields, Thompson and Wallace [1998] have emphasized the SLP field. These authors have shown that fluctuations in the intensity of the stratospheric circulation are linked to the leading EOF of SLP, a robust, quasi-zonally symmetric mode of variability that has received much less attention than the more wavelike teleconnection patterns that dominate the leading EOFs of the mid-tropospheric geopotential height field. This deep vertical coupling conspicuously prevails through a wide range of frequencies and is simulated in modelling studies of Kitoh et al. [1996], Kodera et al. [1996] and Volodin and Galin [1998].

In their work Thompson and Wallace [1998] hypothesize that strong coupling between troposphere and stratosphere is intrinsic to the dynamics of the zonally symmetric polar vortex; *i.e.*, that under certain conditions, dynamical processes at stratospheric levels may affect the strength of the polar vortex all the way down to the Earth's surface through the combined effects of an induced, thermally indirect mean meridional circulation analogous to the Ferrell cell and induced changes in the poleward eddy fluxes of zonal momentum at intermediate levels.

They further speculate that the tropospheric signature of these induced fluctuations would be zonally symmetric were it not for the existence of land-sea contrasts. A stronger zonal flow should advect more mild marine air into the interior of the continents, cold continental air over the western oceans, and increase the frequency of Atlantic cyclones tracking through the Kara Sea [Rogers and Thompson 1995], thereby inducing a pattern of SAT anomalies much like that described.

Thompson and Wallace's [1998] work prompted Baldwin and Dunkerton [2001] to look higher in the atmosphere for AO connections. They found downward links as well as upward ones. A switch from a strong stratospheric vortex to a weak one would move down through the stratosphere, entering the troposphere and reaching the surface as a weakening and diversion of the AO's westerly winds. Because it may take a few weeks for a switch to get from the vortex to the AO, predicting a switch a week or two ahead looked possible.

Circulation regimes in the stratosphere tend to persist for several weeks or more, but the stratospheric circulation is generally regarded as having little influence on surface weather patterns. Baldwin and Dunkerton [2001] have taken a more detailed look at 42 years of vortex and AO wintertime behaviour and found that the connection may be a persistent one. Once a major switch reaches the lower stratosphere, the vortex remains unusually weak or strong for an average of 60 days, which should let forecasters predict extremes in the underlying AO and the accompanying likelihood of weather extremes out as far as a month or two.

Stratospheric and tropospheric annular mode variations are sometimes independent of each other, but (on average) strong anomalies just above the tropopause appear to favor tropospheric anomalies of the same sign. Opposing anomalies are possible, but anomalies of the same sign dominate the average.

Using daily data (stratospheric weather maps) to identify large stratospheric circulation anomalies, Baldwin and Dunkerton [2001] then examined time averages and variability of the near-surface circulation during 60-day periods after the onset of these anomalies. This methodology makes it clear that large stratospheric anomalies precede tropospheric mean-flow anomalies and may therefore be useful for tropospheric weather prediction. From the observed time delay they speculated that the stratospheric anomalies might also have a causal role in creating the subsequent tropospheric anomalies. However, in a later work, Polvani and Waugh [2004] showed that strong (weak) vortex events are preceded by weak (strong) eddy heat anomalies

at 100-hPa. Furthermore, they demonstrated that anomalously strong (weak) integrated eddy heat flux at 100-hPa are followed by anomalously large (small) surface values of the AO index up to 60 days following each event.

4.1.3. NAO and NAM paradigms

As a consequence of the referred studies the identity of the NAO has become a subject of a debate. An alternative teleconnection, termed the AO, also known as NAM, has been suggested by Thomson and Wallace [2000], who argued that the AO shows a closer link with Eurasian SAT than the NAO. These authors found that the AO resembles the NAO but its primary centre covers more of the Arctic. The AO exhibits a distinct signature in the geopotential height and temperature fields marked by a zonally symmetric, equivalent barotropic structure. Thompson and Wallace [1998] also linked the recent climatic trends (warming of the lower troposphere over Eurasia) with the AO and the strengthening of the westerlies at subpolar latitudes with weakening of the jet stream at low latitudes.

Today, there is a strong difference in opinions among the meteorological community on which teleconnection pattern, NAO or AO, deserves more physical meaning. Ambaum et al. [2001] concluded that NAO is more physically relevant and robust for NH variability than AO, whereas Wallace [2000] had suggested that NAO and AO were two paradigms of the same phenomenon, arguing that these could not be equally valid and proposing some methods of distinguishing between them. On a recent work, Quadrelli and Wallace [2004a] agree that the proposed coordinate axes (referred above on section 4.1.1.1) could be alternatively chosen to correspond with NAO and PNA patterns, as suggested by Ambaum et al. [2001].

Wallace [2000] started a discussion about the importance of the distinction between NAO and AO. This author argued that the two patterns may represent two different paradigms of the NH variability, namely the ‘‘regional paradigm’’ (associated with the NAO) and the ‘‘annular paradigm’’ (associated with the AO). Wallace [2000]

concludes that it is important to come to a consensus as to which of them is more appropriate.

Consequently Ambaum et al. [2001] examined and compared the definition and interpretation of the AO with those of the NAO. It is shown by these authors that the NAO reflects the correlations between the surface pressure variability at its centres of action, whereas this is not the case for the AO. These authors show that NAO pattern may be identified in a physically consistent way by applying PCA to various fields in the Euro-Atlantic region. A similar identification is found in the Pacific region for the PNA pattern, but these authors claim that no such identification is found for the AO. Ambaum et al.'s [2001] results suggest that the NAO paradigm may be more physically relevant and robust for NH variability than is the AO paradigm. However, they consider that this does not disqualify many of the physical mechanisms associated with annular modes for explaining the existence of the NAO.

Because of the overlap of the NAO and AO patterns in the Atlantic sector, the time series of the two patterns are highly correlated. Wallace [2000] notes that the original definition of the NAO by Walker and Bliss [1932] is more like the modern definition of the AO than like the currently accepted definitions of the NAO. The NAO points to a mechanism local to the Atlantic region, whereas the more zonal structure of the AO led Thompson and Wallace [2000] to suggest that the AO may be a representation of a fundamentally zonally symmetric mode – an ''annular mode'' – modified by zonally asymmetric forcings, such as topography.

According to Ambaum et al. [2001], although the NAO and AO time series are highly correlated, the differences of the patterns suggest different underlying basic physical mechanisms. Moreover, these authors also showed that the AO may be an artefact of EOF analysis. Considering the three mean sea level pressure centres of action in the AO (Azores 42ºN, 15ºW; Iceland 67ºN, 9ºW; Pacific 44ºN, 168ºW) they showed that although the coupling between the Atlantic and Pacific regions is weak, as expressed by their covariances in the covariance matrix for this three-component system, the

dominant EOF for this system has strong loadings in both regions. Ambaum et al. [2001] argue that the AO is mainly a reflection of similar behaviour in the Pacific and Atlantic basins, namely, the tendency in both ocean basins for anticorrelation between geostrophic winds near 35º and 55ºN. These authors further state that the teleconnections (*i.e.* covariance structures) in a dataset between the three centres of action do not match the AO pattern. Through one-point correlation maps for both the Pacific and Icelandic centres of action in the AO, they suggest that the Pacific centre of action is related to PNA variability [Wallace and Gutzler 1981, and references therein], whereas the Atlantic centres are related to NAO variability.

Ambaum et al. [2001] also noted that the lack of correlation between the Pacific and Atlantic regions had also been observed in the strengths of the zonal jets by Ting et al. [2000] and by Barnett [1985], who hypothesized that on longer timescales the signatures of the Southern Oscillation and the NAO may be joined in the first EOF of sea level pressure.

This issue also had the attention of Deser [2000] who analyzed the teleconnectivity of the three centres of the surface NAM (the Arctic Oscillation pattern). The author concluded that the correlation between the Pacific and Azores centres of action is not significant and that the AO therefore cannot be viewed as reflecting such a teleconnection. Deser [2000] suggested that the AO reflects independent teleconnectivity between the variability over each ocean basin and the variability over the polar cap. These results also support the NAO paradigm as well as Ambaum et al.'s [2001] conclusions: winter extratropical tropospheric circulation variability is dominated by a regional meridional seasaw over the Atlantic basin (the NAO) and a wave train pattern over the Pacific/North American sector (the PNA).

Castanheira and Graf [2003] have also addressed this issue. Their analysis showed that stratospheric circulation controls the correlation between the North Atlantic and the North Pacific pressure patterns at least in a statistical sense. A teleconnection between SLP over the North Pacific and the North Atlantic is found during what they

defined as the strong vortex regime (SVR), but not when the polar vortex is weak (WVR) or just does not exceed the limit of $20ms^{-1}$ at 50-hPa near the polar circle.

Another significant result of their analysis concerns the pattern structure of the NAO. According to Castanheira and Graf [2003] if the analysis takes into consideration that a strong and a weak polar vortex represent two different regimes of the atmospheric circulation, the NAO pattern appears as a strict meridional dipole. This result matches with the findings of Castanheira et al. [2002] that an NAO-like strictly meridional dipole over the North Atlantic is an eigensolution of the equations of motion linearized around a layered atmosphere at rest. However, some differences in the correlation/regression patterns are observed between the two stratospheric vortex regimes. The teleconnection over the North Atlantic appears to be stronger during the SVR and the Azores High extends farther over North Africa.

On Castanheira and Graf's [2003] results the difference between the mean SLP fields of the two vortex regimes (Figure 4.5) shows a spatial structure close to that of the first EOF of SLP when computed over the whole extratropical NH [Thompson and Wallace 1998], the AO pattern. This pattern was interpreted by Monahan et al. [2001], as a transitional mode between two hemispheric variability regimes. The characteristic SW to NE tilt of the isobars over the Euro-Atlantic region, found in these patterns, is also obtained when the SLP EOF is computed only over the Euro-Atlantic region in winter [Glowienka-Hense 1990]. The same result may be obtained from three-dimensional linear studies of the coupled lower stratospheric and tropospheric circulation variability [Perlwitz and Graf 1995; 2001b; Kodera et al. 1999; Deser 2000; Castanheira et al. 2002]. In all these studies the NAO patterns over the Euro-Atlantic region are oriented in the same way in winter: SW-NE.

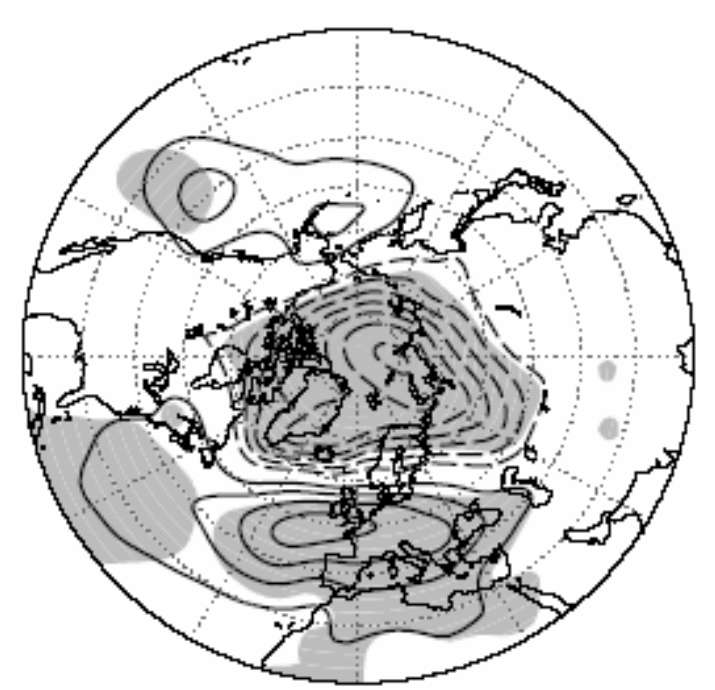

Figure 4.5 – Difference between the mean SLP in the two vortex regimes (SVR-WVR). Contour interval is 0.75 mb. Negative contours are dashed and the zero contour line has been suppressed. The shading indicates where the mean difference is significant at least at the 95% confidence level (Figure 8 from Castanheira and Graf [2003]).

4.1.4. The Timescale of teleconnection patterns

Feldstein [2000] questioned the use of monthly or seasonally averaged data on the study of the properties of low-frequency anomalies, such as the NAO and PNA teleconnection patterns [*e.g.*, Wallace and Gutzler 1981; Barnston and Livezey 1987], arguing that such time averaging could obscure some of the underlying dynamical processes. This should be the case if the timescale of these anomalies would be much shorter than two months. According to the investigation of persistent anomalies performed by Dole [1986], the timescale for a number of low-frequency anomalies

may be much less than one month, where it was found that they decay with an "integral timescale" [Leith 1973] on the order of 15 days.

Feldstein [2000] identified the anomalies through the application of RPCA to daily unfiltered 300-hPa geopotential height field and examined the timescale of these low-frequency anomalies by applying spectral analysis to each PC time series. This author showed that several of the prominent low-frequency anomalies are well described as a red noise (or first-order) autoregressive process. Feldstein [2000] showed that, for all dominant atmospheric low-frequency anomalies, the e-folding timescale has a value between 6 and 10 days, much less than two months. Thus, the key finding of this study is that the temporal evolution of the NAO and the PNA patterns may be interpreted as being a stochastic process, and that all of the above teleconnections are fundamentally short timescale processes.

Feldstein [2000] pointed out that the shortness of these timescales has important implications since the calculation of monthly and seasonally averaged anomalies represents a temporal averaging over many shorter timescale fluctuations. When one intends to increase the signal-to-noise ratio in the data such time averaging is beneficial, but such is not the case when the goal is to improve our understanding of the fundamental dynamics of the excitation, maintenance and decay of teleconnection patterns.

Furthermore, for those low-frequency anomalies that are well described as a Markov process, Feldstein [2000] investigated whether the interannual variability of these anomalies could be interpreted as arising from climate noise [*e.g.*, Leith 1973; Madden 1976; Dole 1986; Feldstein and Robinson 1994], studying whether the variance associated with interannual fluctuations of anomalies, such as NAO or PNA, arises from statistical sampling fluctuations associated with the much shorter 6-10 day fluctuations of that anomaly, as expected in any Markov process. Feldstein [2000] concluded, at the 95% confidence level, that although climate noise contributes toward both NAO and PNA interannual variability, some amount of external forcing,

such as interannual variations in SST [*e.g.*, Horel and Wallace 1981; Mo and Livezey 1986], is also playing a key role.

Some recent studies suggest it may be possible that the AO and NAO are the statistics of stochastic variability constrained by mass and momentum conservation of fluid motion, and not dynamical oscillations [*e.g.*, Gerber and Vallis 2005; Wittman et al. 2005]. In such case there is no intrinsic distinction between the AO and NAO besides the domain on which the analysis is applied. On the other hand, if they are dynamical oscillations, their distinction must remain on the dynamical mechanisms which control their variability. This will be subject of our study.

4.2. Principal Component Analysis

As described in section 4.1.3, the annular variability mode extends from the stratosphere down to the surface [Thompson and Wallace 1998; Baldwin and Dunkerton 1999]. The suggested mechanism underlying the NAM paradigm is the eddy-mean flow interaction [*e.g.*, Eichelberger and Holton 2002]. In the stratosphere, geopotential height anomalies are dominated by a zonal symmetric component and the downward propagation may be interpreted as zonal mean flow-wave interaction. This is not the case in the troposphere where the geopotential height anomalies reveal wavy structures of zonal wavenumbers $s = 1$ and $s = 2$. Thompson and Wallace [1998; 2000] suggested that the zonal symmetry is modified, in the troposphere, due to the topographic and heating field asymmetries and in response to zonal wind fluctuations. The variability due to the response to surface forcing is superimposed to the annular variability.

This study discusses the annular nature of the leading isobaric EOFs of the NH winter extratropical circulation variability. It will be shown that two processes occurring at different times may constitute the NAM spatial structure.

4.2.1. Extratropical tropospheric circulation variability

The leading EOFs of the geopotential height daily fields at 1000- and 500-hPa are very similar to the ones found in the literature, based in monthly time scales and longer. For the sake of comparison, the first three leading patterns are shown in Figures 4.6 and 4.7, for the 1000- and 500-hPa, respectively. It may be noted that the sampling errors of the eigenvalues according to North's Rule of Thumb [North et al. 1982] (as discussed in chapter 3, section 3.2) were calculated taking into consideration the time series autocorrelation. Only the first EOF is well separated in both fields.

As discussed in section 3.2.2, although statistically distinct, the first EOFs are not necessarily physical modes. It is also worth noting that, for the leading EOF structures, it makes no difference chosing the spatial domain to be the NH extratropical circulation north of 30º N, as done here, or including lower latitudes from 20º N as in the works of Thompson and Wallace [1998; 2000] and others.

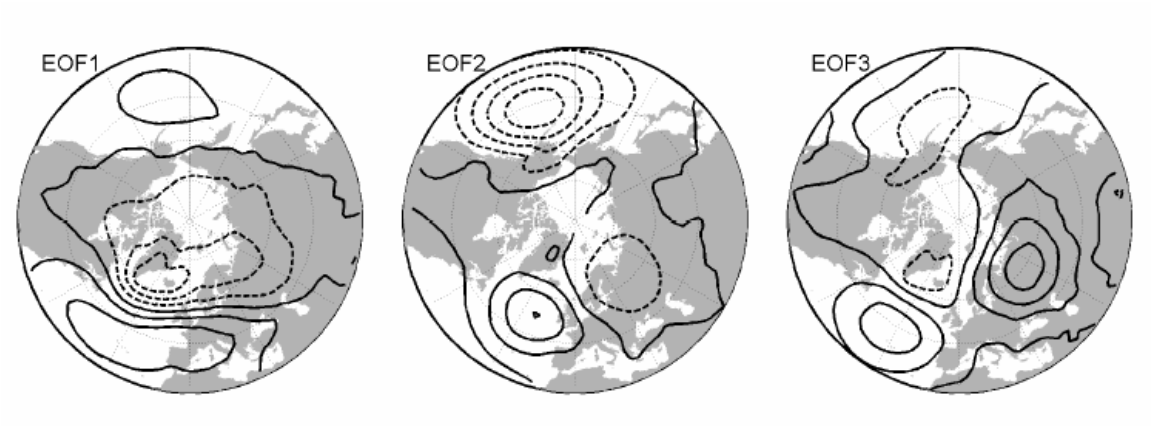

Figure 4.6 – Regression patterns (EOFs) of the 1000-hPa geopotential height on standardized PCs of 15-days running mean climatological anomalies, north of 30ºN. EOFs 1, 2 and 3 explain 19.0%, 11.8% and 10.3% of the climatological variability, respectively. Contour interval is 10 gpm, and negative contours are dashed.

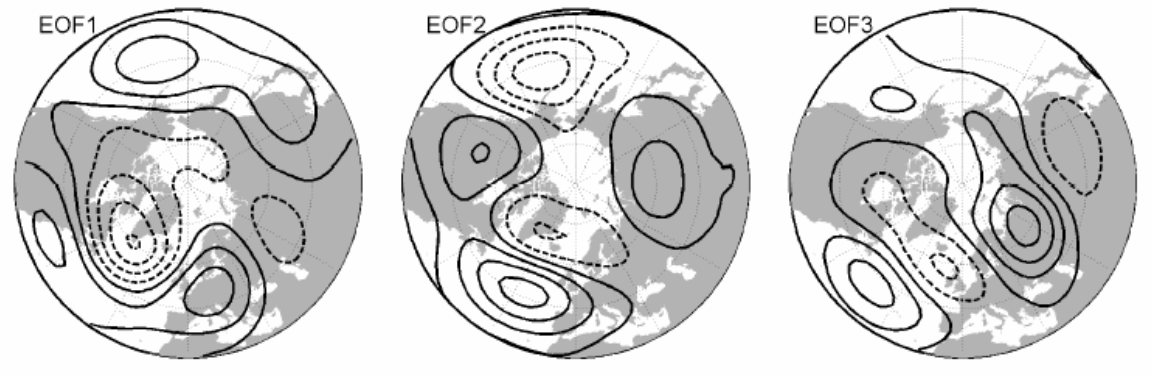

Figure 4.7 – As in Figure 4.6 but for 500-hPa geopotential height field. EOFs 1, 2 and 3 explain 15.1%, 11.2% and 9.8% of the total variability, respectively. Contour interval is 15 gpm.

Table 4.1 shows a strong correlation between the same order PCs of the 500-hPa and 1000-hPa geopotential height fields. Significant correlation is also observed between the first and second PCs and between the second and the third PCs, indicating some dependence on the represented variabilities. The significance levels were calculated by means of 10,000 random permutations of the years preserving the serial autocorrelation, as described in section 3.3.7.

Table 4.1 – Correlations between the first three PCs of the 1000-hPa geopotential height and the first three PCs of the 500-hPa geopotential height (boldface values are above the 99% significance level).

	1000-hPa		
500-hPa	**PC1**	**PC2**	**PC3**
PC1	**0.84**	**-0.41**	0.06
PC2	**0.44**	**0.76**	**0.26**
PC3	-0.08	**-0.20**	**0.67**

4.2.2. Stratospheric-Tropospheric connection

The statistical connection between the tropospheric variability and the stratospheric annular variability is assessed by calculating the lagged correlations of the tropospheric PCs with the 50-hPa zonal mean zonal wind at 65ºN, *i.e.* the U_{50} (65) index. Table 4.2 shows the lagged correlations with maximum absolute value and the lags of occurrence. Positive lags mean that the stratospheric wind is leading. As expected from other works [*e.g.*, Baldwin and Dunkerton 2001], the leading PCs of the tropospheric variability show significant correlations with the stratospheric vortex

strength. The smaller but significant correlation between the stratospheric vortex strength and the second PC of the 500-hPa geopotential height is also worth being noted. This shows that the leading PC of the 500-hPa geopotential height (the NAM index [Baldwin and Dunkerton 2001]) does not represent the full linear connection between the midtroposphere circulation and the stratospheric vortex strength. Christiansen [2002] also argued the importance of the second EOF for the statistical connection with the stratospheric vortex.

Table 4.2 – Lagged correlations between the first three PCs of the 1000-hPa (500-hPa) geopotential height and the 50-hPa zonal mean zonal wind at 65ºN (U_{50} (65)). Shown are the lagged correlations with maximum absolute values, and the numbers in parentheses indicate the lag in days for their occurrence. Positive lags mean that the stratosphere is leading. Boldface values are above the 99% significance level. The last two rows are similar to the first two rows but considering only U_{50} (65) anomalies above or below one standard deviation.

	PC1	PC2	PC3
1000-hPa	**0.53**$_{(2)}$	-0.11$_{(30)}$	-0.20$_{(-30)}$
500-hPa	**0.47**$_{(-2)}$	**0.28**$_{(6)}$	-0.12$_{(-13)}$
$\lvert U_{50}\rvert \geq \sigma$, 1000-hPa	**0.73**$_{(1)}$	0.18$_{(12)}$	0.24$_{(10)}$
$\lvert U_{50}\rvert \geq \sigma$, 500-hPa	**0.67**$_{(-4)}$	**0.51**$_{(6)}$	0.15$_{(-30)}$

To obtain some insight into the origin of the correlations between the U_{50} (65) index and the first two 500-hPa PCs, the annularity of the respective EOF patterns is analyzed. Figure 4.8 shows the meridional profiles of the zonal mean amplitude of the two first 500-hPa EOFs patterns. Using the geostrophic balance, the zonal mean zonal wind anomalies associated with each PC are proportional to the slopes of the meridional profiles of the zonal mean amplitude of the respective EOF patterns. From Figure 4.8, it may be concluded that EOF1 is associated with strong zonal mean zonal

wind variability in the latitudinal belt 45ºN to 65ºN, whereas EOF2 is associated with a zonal mean zonal wind variability at higher latitudes between 55ºN and 70ºN. EOF2 does not explain any variability of the zonal mean zonal wind around 50ºN.

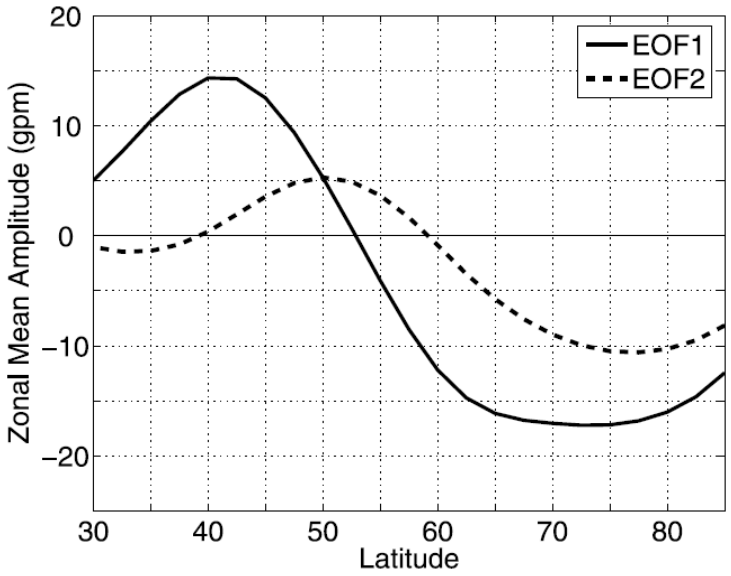

Figure 4.8 – Meridional profiles of the zonal mean amplitude of the first (solid line) and second (dashed line) EOFs of the 500-hPa geopotential height variability. The amplitudes were normalized to one standard deviation of the respective PCs.

To see if the variability of the zonal mean zonal wind around 50ºN is contributing to the higher correlation between the 500-hPa PC1 and the vortex strength, the 500-hPa zonal mean zonal wind anomaly averaged in the latitudinal band 45–55ºN (already designated as U_{500} (45-55) index) is used. The lagged correlations between U_{500} (45-55) and U_{50} (65) are shown in Figure 4.9. The maximum correlation (r = 0.23) between U_{500} (45-55) and U_{50} (65) is statistically significant at the 99% level and occurs when the U_{500} (45-55) index is leading by 14 days. If one considers only vortex anomalies above or below one standard deviation, the maximum correlation is 0.41 with the index U_{500} (45-55) leading by 13 days.

The lagged correlation of the vortex strength with U_{500} (45-55) and PC2 (Figure 4.9)

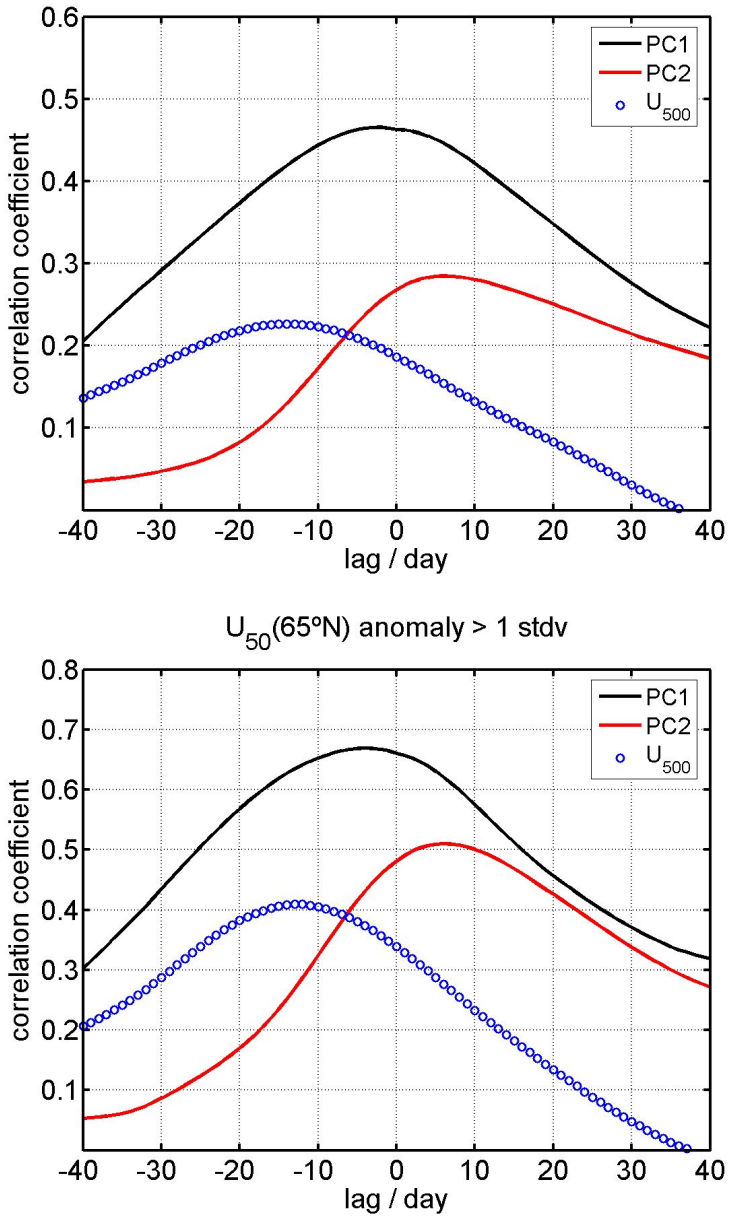

Figure 4.9 – Lagged correlations between the 50-hPa zonal mean zonal wind at 65ºN (U_{50} (65)) and the first two PCs of the 500-hPa geopotential height fields. The curve U_{500} represents the lagged correlation between the U_{50} (65) index and the 500-hPa zonal mean zonal wind in the latitudinal belt 45–55ºN. The bottom plot is similar to the top one but considering only U_{50} (65) anomalies above or below one standard deviation. Positive lags mean that the stratospheric wind is leading.

suggests that there are processes occurring at different times: first, zonal mean wind anomalies in the midlatitude troposphere lead stratospheric polar vortex anomalies of the same sign. Once these are established, the positive correlations with PC2 indicate that stratospheric vortex strength anomalies are leading higher-latitude tropospheric zonal mean wind anomalies of the same sign by few days. The positive correlations between U_{500} (45–55) and U_{50} (65) are consistent with the lagged cross correlation between the 300-hPa NAM and the 300-hPa zonally averaged momentum flux poleward of 20ºN calculated by Baldwin et al. [2003]. As shown by Baldwin et al. [2003, Figure 4a], the correlations are higher when the upper tropospheric momentum flux anomalies lead the NAM anomalies. McDaniel and Black [2005, Figure 4c] also show significant poleward eddy momentum flux anomalies at midlatitude upper troposphere/lower stratosphere, during the maturing stage of strong positive NAM events. Hence our interpretation of the correlations in Figure 4.9, which is presented schematically bellow (Figure 4.10), is that the initial zonal mean momentum anomalies are shifted to the high latitudes by zonal mean-eddy interactions leading to vortex anomalies of the same sign. Then the vortex anomalies will progress downward affecting back the high-latitude troposphere

The correlation between the U_{50} (65) index and the PC1 is higher and shows a maximum at a lag shorter than the ones for the maxima of the correlations with the PC2 and U_{500} (45-55) index. It may be argued that the fact that the maximum correlation between the U_{50} (65) index and the PC1 occurs at negative lags does not support the idea of a downward influence of the stratospheric vortex variability. However, this apparent contradiction may be a consequence of the PCA methodology. The criterion for the identification of the leading EOF/PC is only the maximization of the explained data variability. The more the variability processes are projected onto the leading EOF the greater is the explained variability by the leading PC. The blend of processes may be favoured by the use of 15-days running mean low-pass filtering of the time series. In fact, the 500-hPa PC1 correlates both with U_{50} (65) (r_{max} = 0.47 at lag –2) and with U_{500} (45-55) (r_{max} = 0.64 at lag –1) indices, whereas the 500-hPa

PC2 does not show any correlation with U_{500} (45-55) (r_{max} = 0.07).

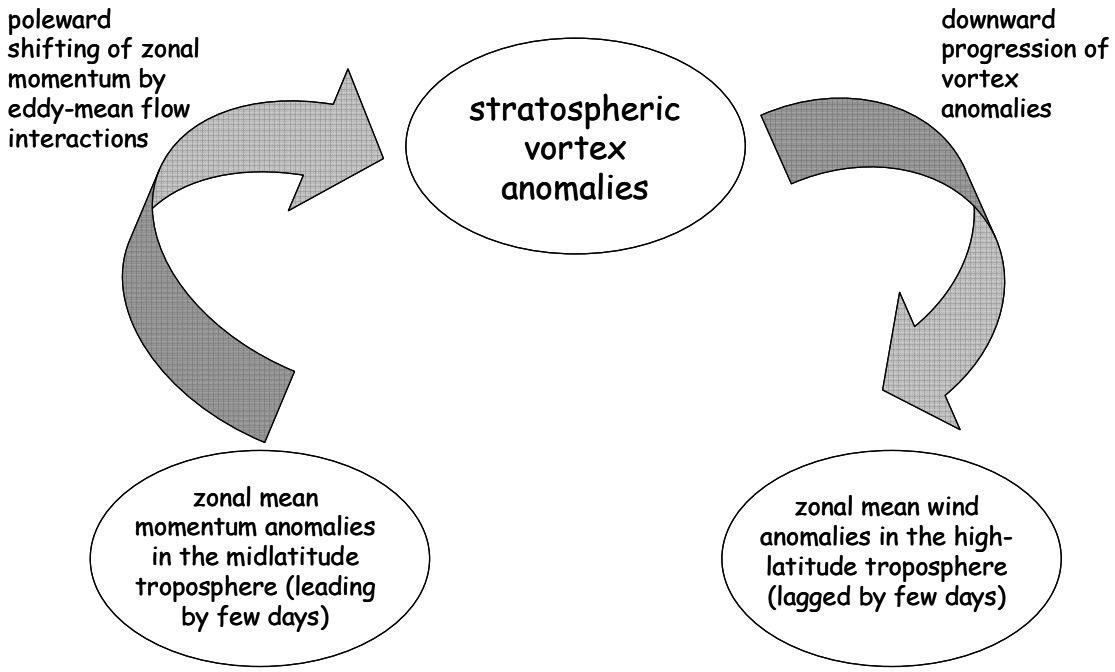

Figure 4.10 – Schematic interpretation of the correlations in Figure 4.9.

4.2.3. Variability linearly decoupled from the midlatitude zonal mean zonal wind

To separate the two processes discussed above, the geopotential height fields were linearly regressed on the U_{500} (45-55) index. Residual geopotential height fields were defined as the geopotential height field minus the variability linearly regressed on the U_{500} (45-55) index. Then a PCA on the residual geopotential fields is performed and the lagged correlation is recalculated, as in the previous subsection.

The first 3 EOFs of the residual geopotential height fields are shown in Figures 4.11 and 4.12, for the 1000- and 500-hPa, respectively. Using the geostrophic balance, it may be deduced from Figure 4.13 that the leading EOF of the 500-hPa residual variability represents anomalies of the zonal mean zonal wind at the same latitudinal band as the second EOF of the total variability, but the anomalies are stronger. The zonal mean geopotential height anomalies show a maximum centred at 50ºN. Hence, as expected, the leading EOF pattern of the residual data does not represent any wind anomaly around 50ºN.

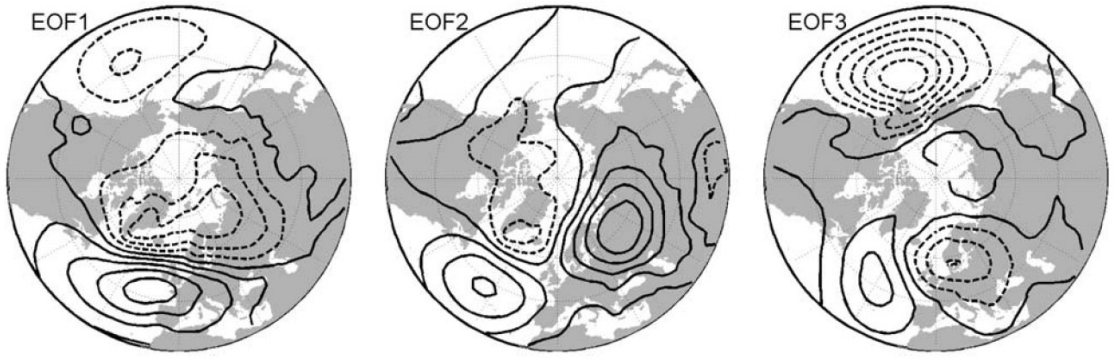

Figure 4.11 – As in Figure 4.6 but for the residual geopotential height variability. EOFs 1, 2 and 3 explain 17.7%, 11.8% and 11.4% of the 1000-hPa residual variability, respectively.

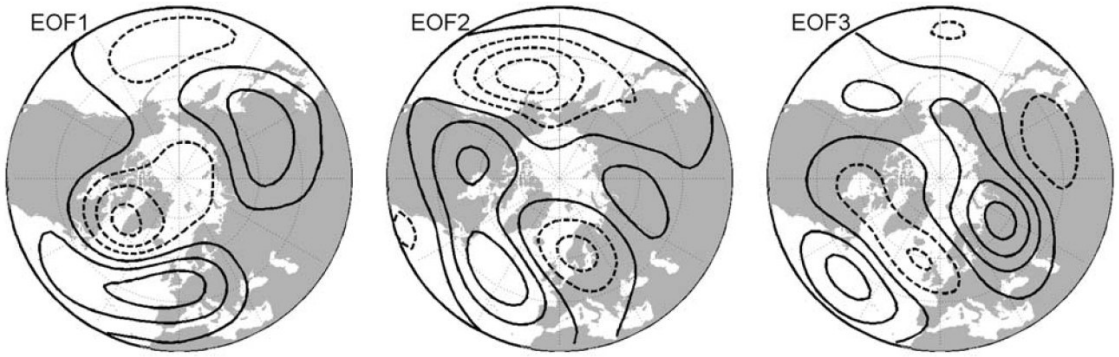

Figure 4.12 – As in Figure 4.7 but for the residual geopotential height variability. EOFs 1, 2 and 3 explain 13.5%, 13.1% and 11.6% of the 500-hPa residual variability, respectively.

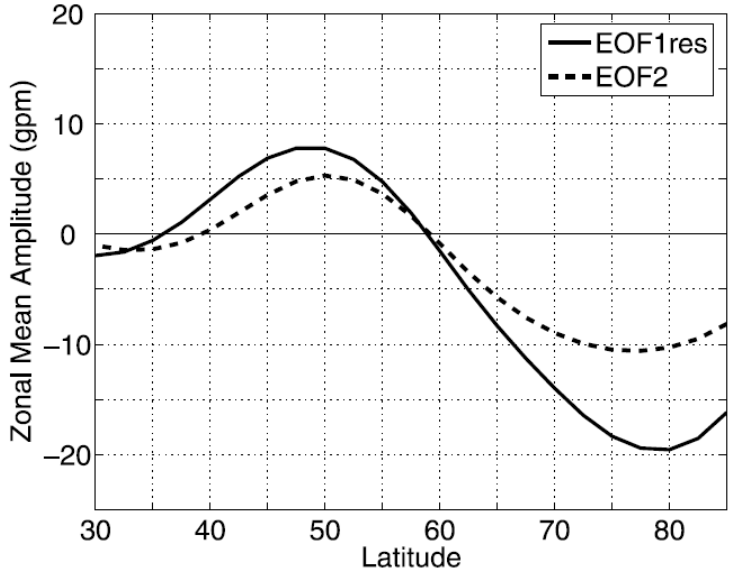

Figure 4.13 – Meridional profiles of the zonal mean amplitude of the first EOF of the residual 500-hPa geopotential height variability (solid line) and second EOF of the total 500-hPa geopotential height variability (dashed line). The amplitudes are normalized to one standard deviation of the respective PCs.

The leading EOFs of the residual variability at 1000- and 500-hPa (Figures 4.11 and 4.12) show midlatitude centres of opposite sign over the North Atlantic and North Pacific, whereas the respective leading EOFs of the total variability (Figures 4.6 and 4.7) have two centres of equal polarity, which are taken as an expression of the annularity. The leading EOFs of the residual variability only show a meridional dipole over the Atlantic basin resembling the NAO, but with the node line shifted northward. Table 4.3 shows the correlation between the PCs of the 500- and 1000-hPa residual geopotential fields. Now, the PCs are paired one to one, and the first two PCs show an increase in correlation when compared to the values obtained for the total variability (Table 4.1). It is worth emphasising that the order of the second and third PCs of the 1000-hPa residual geopotential field is switched in Table 4.3. The variances of PC2 and PC3 are very close and their order may have been changed in the process of computing due to the presence of noise. In fact the EOF patterns associated with PC2 and PC3 of the residual variability (Figure 4.11) are very close to the EOF patterns associated with PC3 and PC2 of the total variability (Figure 4.6), respectively.

Table 4.3 – As in Table 4.1 but for the residual geopotential height variability (Note that the order of the 1000-hPa PC2 and PC3 was changed in the table).

	1000-hPa		
500-hPa	**PC1**	**PC3**	**PC2**
PC1	**0.92**	-0.04	**0.18**
PC2	0.12	**0.81**	0.02
PC3	-0.15	0.15	**0.66**

The correlation between the first 3 PCs of the residual variability and the vortex strength are shown in Table 4.4. Now, only the leading PCs show statistically significant correlation with the vortex strength and the correlation maxima at both

isobaric levels occur at positive lags and have close values. The curves of lagged correlations (Figures 4.14 and 4.15) are consistent with a delayed downward influence of the stratospheric vortex on the residual tropospheric variability.

Nevertheless, when considering the total variability, the maximum of correlation between the leading PC of 500-hPa geopotential height and the vortex strength occurs for negative lags, *i.e.*, with the tropospheric variability leading (Figure 4.9). These results suggest that, after removing the variability linearly dependent on the U_{500} (45-55) index, the leading EOFs/PCs of the residual variability mainly capture the downward influence of the stratospheric vortex variability.

Table 4.4 – As in Table 4.2 but for the residual geopotential height variability.

	PC1	**PC2**	**PC3**
1000-hPa	**0.53**$_{(7)}$	0.16$_{(15)}$	-0.19$_{(8)}$
500-hPa	**0.51**$_{(4)}$	-0.17$_{(-20)}$	-0.10$_{(13)}$
$\lvert U_{50} \rvert \geq \sigma$, 1000-hPa	**0.73**$_{(7)}$	0.28$_{(9)}$	-0.23$_{(-10)}$
$\lvert U_{50} \rvert \geq \sigma$, 500-hPa	**0.73**$_{(5)}$	-0.24$_{(-25)}$	-0.10$_{(-14)}$

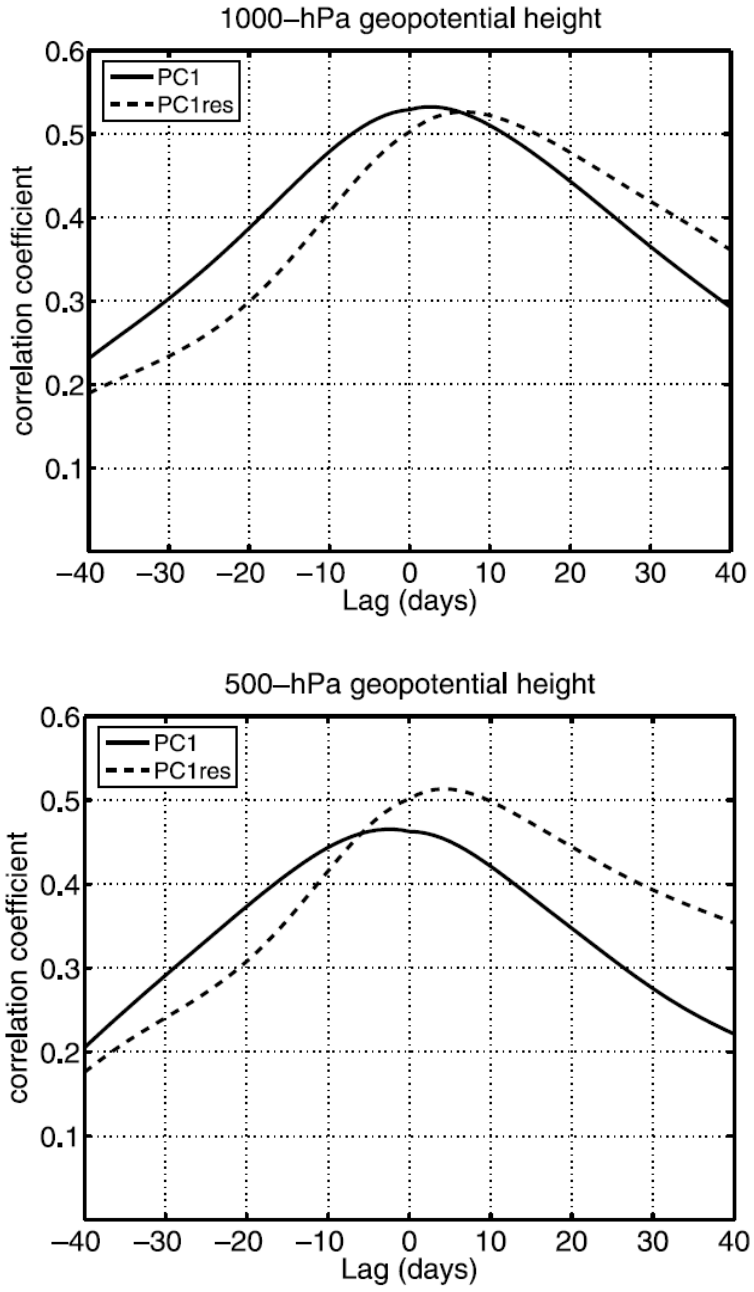

Figure 4.14 – Lagged correlations between the 50-hPa zonal mean zonal wind at 65ºN and the leading PCs of the total (solid line) and residual (dashed line) variabilities of (*top*) 1000-hPa and (*bottom*) 500-hPa geopotential height fields. Positive lags mean that the stratospheric wind is leading.

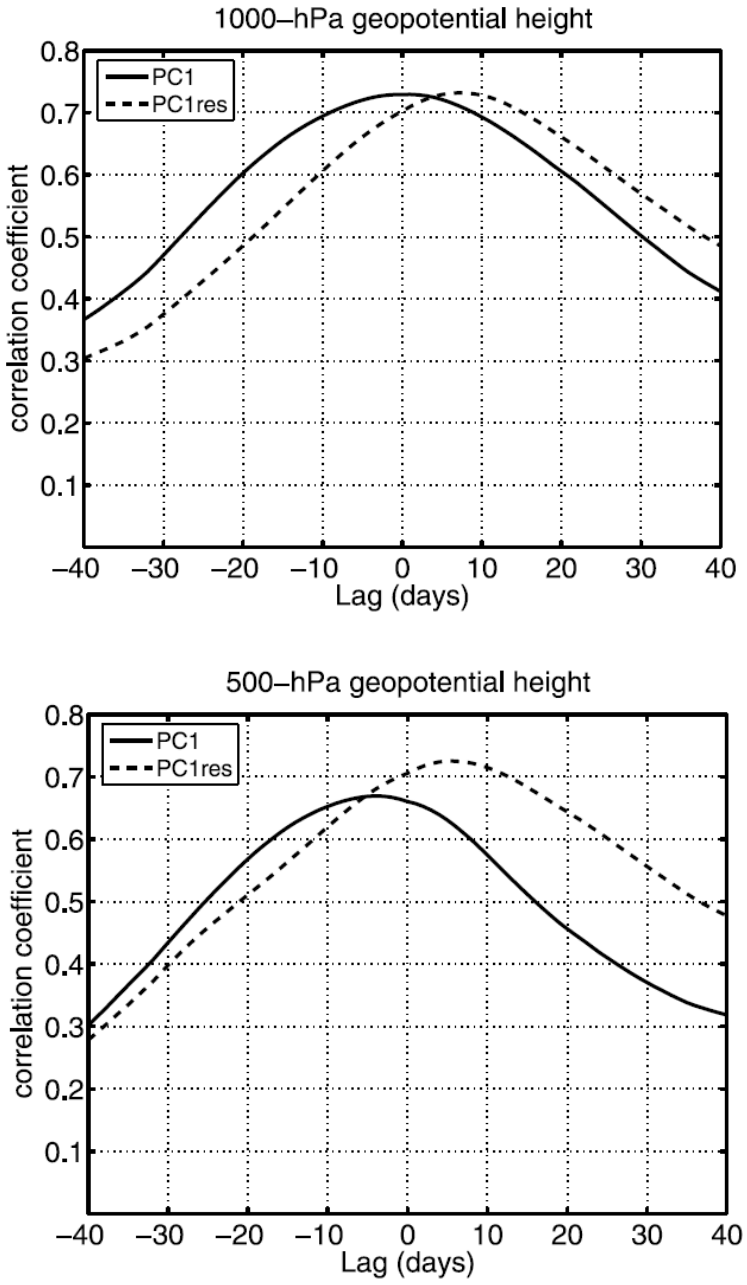

Figure 4.15 – As in Figure 4.14 but considering only 50-hPa zonal mean zonal wind anomalies above or below one standard deviation.

4.2.3.1. The effect of filtering

Until now, all lagged correlations were based on daily time series smoothed by a 15-day running mean. It is of interest to assess the effect of the smoothing on the lags. Lagged correlations as the ones showed in Figure 4.9 were recalculated using unfiltered (*i.e.* not averaged) daily time series (Figure 4.16a). Unfiltered time series for PC1 and PC2 were obtained by projecting the daily unfiltered anomalies onto the EOF1 and EOF2 of the 500-hPa geopotential height field smoothed by the 15-day running mean. Figure 4.16a shows the same lag features as those observed in Figure 4.9. The curve representing the lagged correlations between the unfiltered time series of PC1 and the vortex strength shows a maximum near to zero lag and a shoulder for negative lags. The maximum and the shoulder suggest, now more clearly, that the processes underlying the correlation of the U_{500} (45-55) index and the PC2 with the vortex strength may be associated with circulation variability which projects also onto EOF1.

The time separation between the two signals is also clear if one considers only the intraseasonal variability, *i.e.*, the variability which remains after removing the seasonal (November to March) means. Figure 4.16b summarizes the main findings of this study. The lagged correlations between the intraseasonal anomalies of the U_{50}(65) index and the intraseasonal anomalies of the first two PCs of the 500-hPa total geopotential height variability are shown together with the U_{500} (45-55) index, and the leading PC of the 500-hPa residual geopotential height variability. It may be noted that only U_{50} (65) anomalies above or below one standard deviation of the intraseasonal variability were considered.

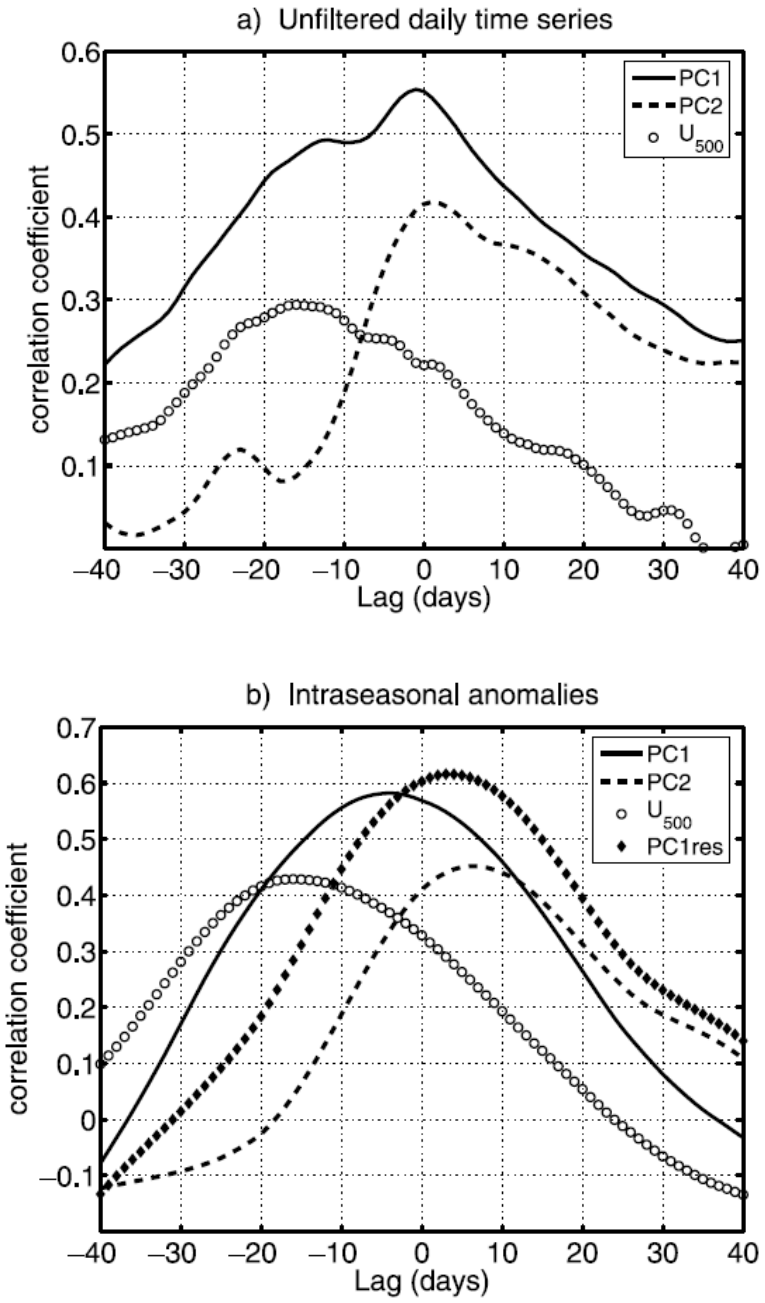

Figure 4.16 – As Figure 4.9 (*bottom*) but (a) considering unfiltered (*i.e.* not averaged) time series and (b) considering only the intraseasonal variability. The curve PC1res represents the lagged correlation between the U_{50} (65) index and the leading PC of the 500-hPa geopotential height residual variability.

4.3. Annular versus non-annular circulation variability

Results presented in the previous section suggest that two processes, occurring at different times, contribute to the NAM spatial structure. It is further suggested that the leading tropospheric variability patterns found in the literature represent variability associated with both processes. The tropospheric variability patterns which appear to respond to the polar vortex variability have a hemispheric scale but show a dipolar structure only over the Atlantic basin. The dipole resembles the NAO pattern, but with the node line shifted northward.

In this section an analysis is presented that clearly shows that much of the tropospheric NAM variability, *i.e.* the variability projected onto the leading EOF of geopotential height at single isobaric levels, is not coupled with the variations of the polar vortex strength. A large fraction of the midlatitude zonal symmetric component of the tropospheric NAM seems to result from two independent dipolar structures over the Pacific and the Atlantic oceans. A zonally symmetric component of the middle and lower tropospheric zonal wind variability seems to only exist at high latitudes.

4.3.1. 3D normal modes dynamical filtering

As shown by Ambaum et al. [2001] hemispheric EOF analyses of different lower-tropospheric parameter fields, that one might expect to be dynamically related, may yield very different results and patterns that are not obviously related. On the other hand Thompson and Wallace [1998; 2000] and Wallace and Thompson [2002] argue that a dynamical coupling between the stratosphere and troposphere is manifest in the annular modes, which characterize deep, zonally symmetric fluctuations of the geopotential height and zonal wind fields. Having these results in mind it seems useful to look for the joint variability of the zonal means of geopotential height and zonal wind at all isobaric levels.

The procedure already described in section 3.2.1 is now applied to the global NCEP-NCAR reanalysis data (section 3.3.1). Because one is interested in the variability of the northern extratropical circulation, the southern hemisphere circulation has been replaced by the specular image of the northern one before the projection onto the normal modes. Since the extratropical circulation is in very close geostrophic balance, in the subsequent analysis only symmetric barotropic Rossby modes (*i.e.*, $m = 0;\ \alpha = 2$) have been retained in the expansion (Equation 3.4), thus obtaining the 3D normal mode projection coefficients ω^2_{00l}.

The barotropic 3D normal modes represent a mass weighted vertical mean of the atmospheric circulation, being therefore very sensitive to the tropospheric circulation. A PCA on the joint variability of the geopotential and the zonal wind fields requires that the two fields are adequately weighted. The U and Z components of the zonally symmetric Rossby modes satisfy the geostrophic balance and the projection onto the normal modes allows for an appropriate weighting of these two fields. On the other hand, an EOF analysis on the projection coefficients will retrieve dynamically consistent patterns for both fields. Hence, the analysis of the joint variability of the zonal means of the geopotential height and zonal wind at all isobaric levels was performed by a PCA of the coefficients of the barotropic zonally symmetric Rossby modes (*i.e.*, $m = 0;\ s = 0;\ \alpha = 2$). Using this procedure, the ageostrophic motions were filtered away and the geopotential height and wind were simultaneously weighted in a dynamical self consistent way. The leading EOF (Figure 4.17) represents one half (50.4%) of the total variability and it is statistically distinct according to North's Rule of Thumb [North et al. 1982] (as discussed in chapter 3). The EOF meridional structures were retrieved by replacing the projection coefficients ω^2_{00l} by the respective EOF loadings (section 3.3.1). The meridional profile of the zonal mean geopotential height associated with the leading EOF of the 500-hPa geopotential height field is also represented in the same figure. Before drawing the

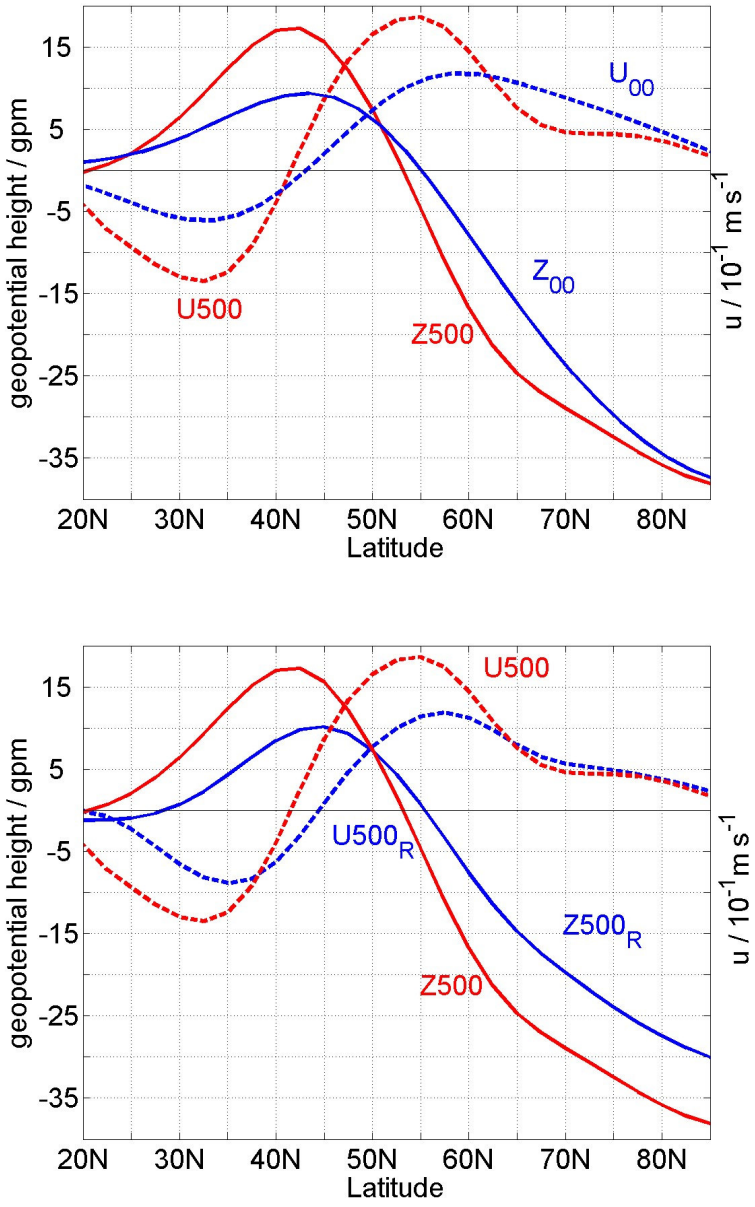

Figure 4.17 – (*Top*) Zonal mean meridional structures of the leading EOFs of the barotropic circulation and of the 500-hPa geopotential height (Z500). (*Bottom*) Zonal mean meridional structures of the leading EOFs of the Z500 variability and of the Z500 variability regressed onto the 70-hPa NAM. U500 and Z500 ($U500_R$ and $Z500_R$) denote the velocity and the 500-hPa geopotential height (regressed on the 70-hPa NAM). U_{00} and Z_{00} denote the velocity and geopotential height of the barotropic circulation. The structures are normalized to one standard deviation of the respective PCs. The geopotential height and the velocity units are respectively gpm and $10^{-1} \times ms^{-1}$.

figure, the zonal mean amplitude of the leading EOF of 500-hPa geopotential height field was divided by the square root of the cosine of the latitude in order to retrieve the zonal mean meridional profile of the geopotential height. The meridional profile of the zonal mean zonal wind (U500) associated with the leading EOF of the 500-hPa geopotential height field was obtained using the geostrophic relationship. The three first EOF patterns of the 500-hPa geopotential height field are shown in the upper row of Figure 4.18 for reference purposes. These figures are basically the same as Figure 4.12 except for the fact that the domain is now north of 20ºN and the filtering is 31-day running means. The results are virtually the same when one uses 15-day running means instead of 31-day running means, but the leading PCs of the 15-day smoothed data represent a smaller fraction of the respective variability.

The fact that the leading EOF of the zonally symmetric barotropic Rossby modes represents annular variability over the whole vertical domain is demonstrated by Figure 4.19. It shows the lagged correlations between the daily NAM indices and the projections of daily anomalies onto the first EOF of the barotropic mode. These projections are highly correlated with the NAM indices over the whole atmosphere, and a signal of delayed correlation with the high levels in the stratosphere may be observed. Comparing the zonal mean geopotential height profiles in Figure 4.17 one observes that the leading EOF of 500-hPa geopotential height field has larger amplitudes at midlatitudes. At high latitudes it shows amplitudes comparable to those of the leading EOF of the barotropic zonally symmetric Rossby modes. The differences of the geopotential height profiles lead to remarkable differences of the respective zonal mean zonal wind profiles. The leading EOF of 500-hPa geopotential height field represents a seesaw of zonal mean zonal wind between the subtropics and midlatitudes, whereas the seesaw is displaced northward in the zonally symmetric barotropic circulation, presenting stronger zonal wind anomalies at high latitudes.

The leading EOF of the 500-hPa geopotential height field captures much more zonally symmetric variability in the midlatitudes than the one represented by the leading EOF of the zonally symmetric barotropic circulation. This suggests that the leading EOF of

the 500-hPa geopotential height field pattern may include variability structures which are not part of the vertically coherent variations of the annular mode. Clearly the correlation of the tropospheric NAMs with the barotropic annular mode (Figure 4.19) is reduced when compared with the stratospheric NAMs. This is especially the case when the tropospheric NAM leads by more than 5 days.

The lagged correlations in Figure 4.19 are based on unfiltered daily time series and a signal of delayed correlation is suggested by the asymmetry of correlation curves for NAM indices at levels above 50-hPa. At stratospheric levels below 50-hPa the correlation curves are very close and nearly symmetric suggesting a rapid progression of the circulation anomalies from the lower stratosphere to the troposphere. Then, for the study of the coupling of the stratospheric and tropospheric circulations, avoiding the necessity of consideration of lagged effects, it is convenient to use a NAM index well inside the stratosphere but close to the tropopause. Considering results of Figure 4.19, on the following one chose to represent the polar vortex strength by the 70-hPa NAM index. However, the results showed to be qualitatively the same if one used the 50-hPa or the 100-hPa NAM indices.

The middle panel in Figure 4.18 shows the regression pattern of the 500-hPa geopotential height field on the 70-hPa NAM. In order to make the regression and the EOF patterns comparable, the 500-hPa geopotential height field was also weighted by the square root of the cosine of the latitude before performing the regression. By visual inspection one might say that the regression pattern shares the main annular features of the leading 500-hPa geopotential height field EOF, but with a weaker Pacific centre. However, comparing the respective meridional structures, shown in the lower panel of Figure 4.17, it becomes clear that they are different. The regression pattern shows a zonal mean meridional structure close to the one of the leading EOF of the barotropic mode (U_{00} and Z_{00} in the upper panel of Figure 4.17).

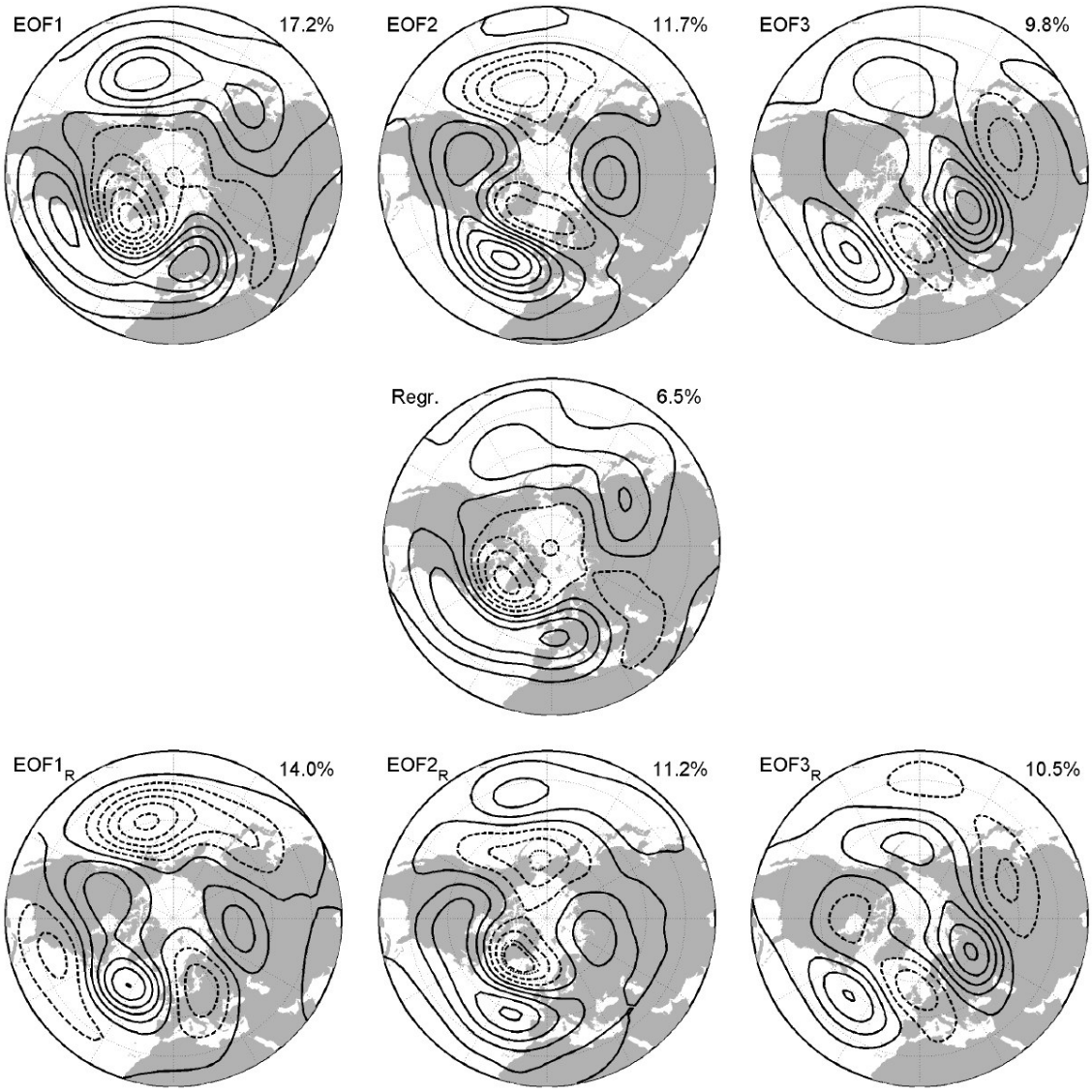

Figure 4.18 – (*Top*) First three EOF patterns of the 500-hPa geopotential height variability. (*Middle*) Regression pattern of the Z500 field onto the 70-hPa NAM. (*Bottom*) As in the top panel, but for the residual variability, *i.e.* the variability that remained after subtraction of Z500 regressed on the 70-hPa NAM. The patterns are normalized to 1 standard deviation of the respective PCs. The values in the right top of each panel are the percentages of variance represented by each (EOF, PC) pair. Contour interval is 10 gpm, except in the regression pattern where the contour interval is 7.5 gpm.

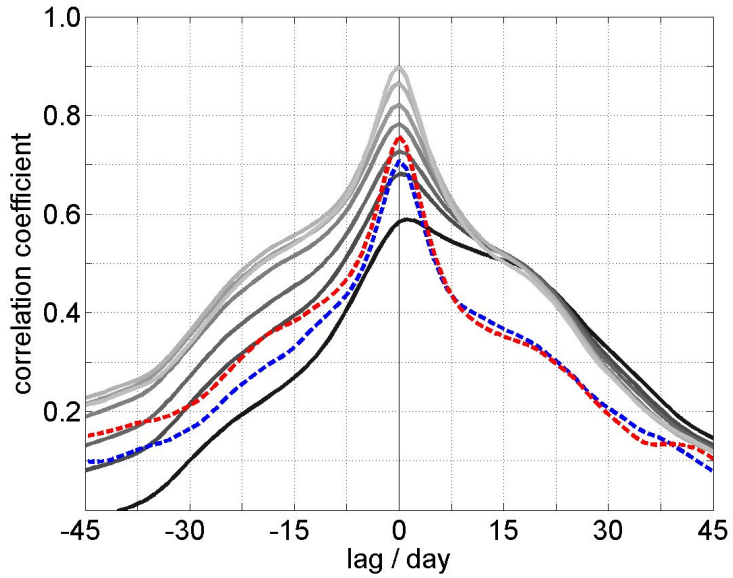

Figure 4.19 – Lagged correlations between the daily data projections onto the first EOF of the barotropic mode and the NAM indices. Solid curves are for stratospheric NAMs from 10-hPa (black) to 150-hPa (light gray). The dashed red curve is for 1000-hPa NAM and the dashed blue curve is for 500-hPa NAM. Positive lags mean that NAM indices are leading.

From the leading EOF and the regression patterns in Figure 4.18, using the geostrophic relationship, one may conclude that the largest zonal wind anomalies must occur in the [90ºW, 30ºE] and the [90ºE, 255ºE] longitude sectors. Figure 4.20 shows the correlations between the zonal means of the 500-hPa zonal winds in each longitude sector.

The correlations are small and negative at midlatitudes and higher and positive at high latitudes. The strong negative correlations near the pole are in agreement with the displacement of the vortex centre over Greenland. This figure shows that positively correlated zonal wind anomalies corresponding to a true annular component occur only at high latitudes. The longitude sector over the Pacific, in which the zonal wind was averaged, is rather broad and its east side is close to the west side of the Atlantic longitude sector. Considering a larger [90ºE, 255ºE] longitude sector does not

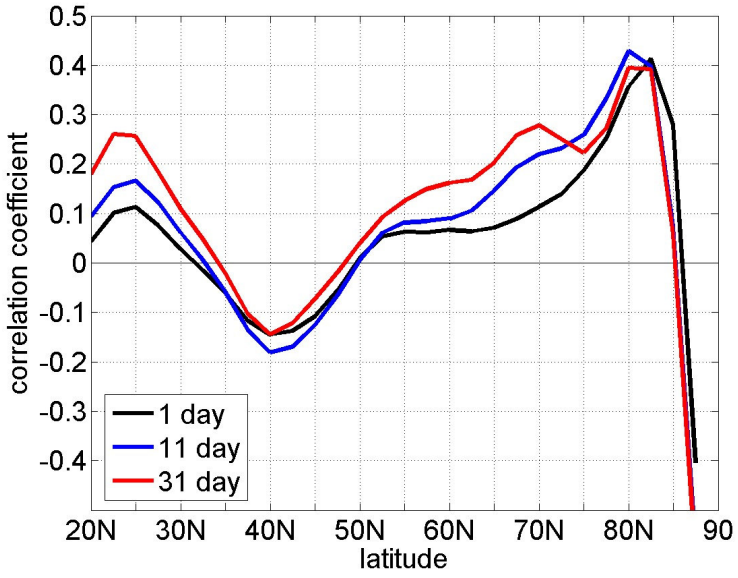

Figure 4.20 – Correlation between the zonal wind means in the longitude sectors of [90ºE, 225ºE] and [90ºW, 30ºE]. The black curve corresponds to daily anomalies. The blue and the red lines correspond to daily anomalies smoothed by 11-day and 31-day running means, respectively.

appreciably change the correlation curves. Since it may also be possible that the zonal winds are shifted in latitude between the two basins, correlations were recomputed considering the zonal mean wind over the Pacific shifted by 2.5º, 5.0º, 7.5º and 10.0º to the north or to the south of the zonal mean wind over the Atlantic sector. Generally the correlations decrease as the latitudinal shift increases. Only for the subtropical (south of 35ºN) latitudes and for the high latitudes (north of 80ºN) the correlation values increase a little for some shifts.

4.3.2. Tropospheric variability decoupled from the stratosphere

By construction both the regression pattern and the leading EOF of the barotropic mode represent tropospheric annular variability coupled with stratospheric annular variability. However, it may be possible that there is an annular component of the tropospheric variability decoupled from the stratosphere. To investigate this possibility a PCA on the residual 500-hPa geopotential height field that remained after subtraction of the 500-hPa geopotential height field data regressed linearly onto the 70-hPa NAM was performed following a similar procedure to the one described in section 4.2.3.

The first 3 EOFs of the residual 500-hPa geopotential height field are shown in the bottom row of Figure 4.18. Comparing these EOFs with the corresponding EOFs of the total variability, in the top of the same figure, one observes that the third EOF is quite insensitive to the stratospheric variability. It is interesting to note that these patterns are also similar to the third EOF obtained after removing the variability linearly dependent on the U_{500} (45-55) index (Figure 4.12), suggesting that this pattern, which represents a wave train over the Atlantic-European sector, may represent a true physical mode, since it is insensitive to both the variability linearly dependent on the U_{500} (45-55) index and stratospheric variability.

The most pronounced differences are seen in the first two EOFs. The first EOF of the residual variability shows the PNA structure and a wave train over the Atlantic and Eurasia like the augmented PNA pattern proposed by Wallace and Thompson [2002]. These results suggest that the first two EOFs of the 500-hPa geopotential height total variability field represent mixed variability associated with both the PNA and the stratospheric vortex variability. The second EOF of the 500-hPa geopotential height residual variability shows two dipoles over the Atlantic and Pacific oceans. As argued by Gerber and Vallis [2005], performing a PCA on a variability field dominated by independent dipolar structures, one may end up falsely with leading EOF patterns

with a high degree of zonal symmetry.

Figure 4.21 shows, again, the meridional structures of the first EOF of the total 500-hPa geopotential height field and the meridional structures of the first two EOFs of the residual 500-hPa geopotential height field. The meridional structure of the leading EOF of the residual variability shows a seesaw shifted equatorwards relatively to the leading EOF of the total variability. On the other hand, the meridional structures of the first EOF of the total field and of the second EOF of the residual field are very similar, except at high latitudes, north of 65ºN, where the residual EOF shows a flattened geopotential profile. The flattening of geopotential at high latitude with a zonal mean zonal wind close to zero must be due to the absence of the annular variability regressed on the stratospheric variability.

These results suggest that, at latitudes south of 65ºN the zonal symmetric component of the first EOF of the total field may largely be the imprint of the two dipolar structures revealed in the second EOF of the residual variability. Here the question remains whether the dipolar structures in the second EOF of the residual variability are independent.

Hence, four anomaly time series of the residual field were defined as follows:

a) Pacific time series (Pac.): the area weighted average of 500-hPa geopotential height anomaly inside the minimum contour of EOF1 of the residual variability, over the Pacific.

b) Iceland time series (Ice.): the area weighted average of 500-hPa geopotential height anomaly inside the minimum contour of EOF2 of the residual variability, over Iceland and Greenland.

c) Bering Strait time series (Ber.): the area weighted average of 500-hPa geopotential height anomaly inside the dotted contour on the EOF2 of the residual variability, over Bering Strait.

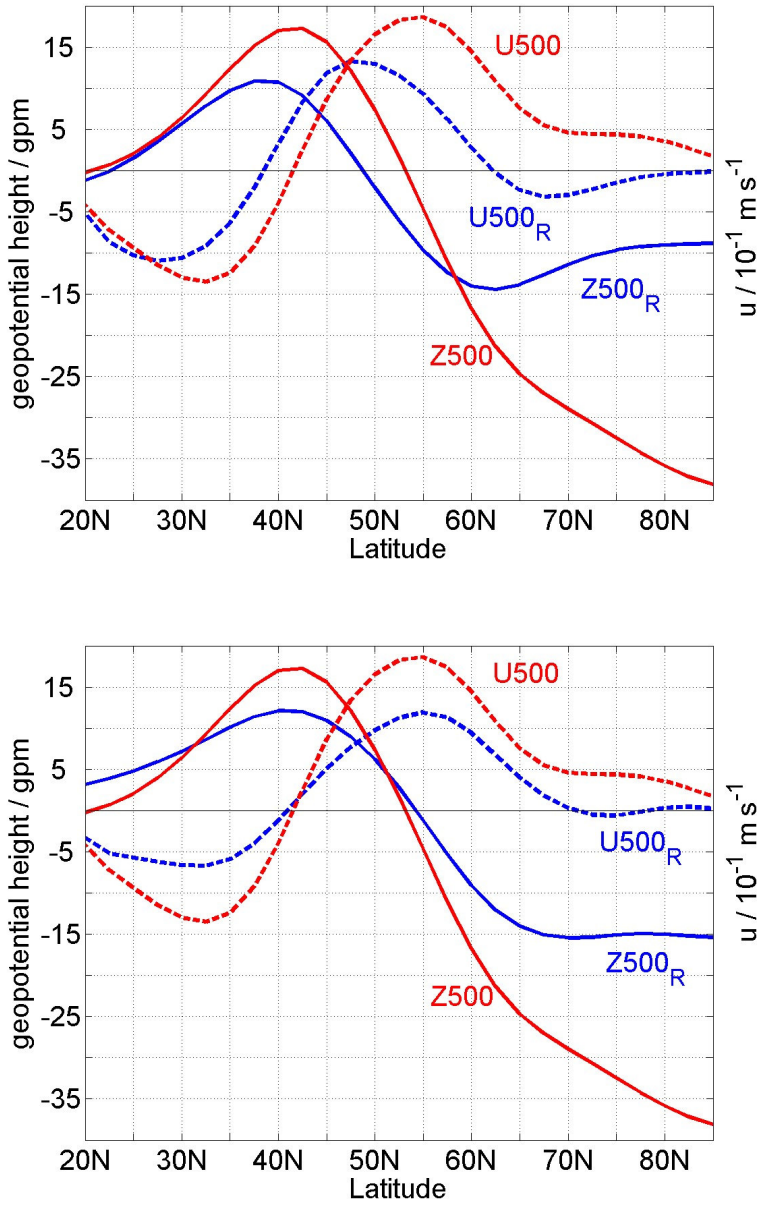

Figure 4.21 – (*Top*) Zonal mean meridional structures of the first EOFs of the total and residual Z500 variabilities. (*Bottom*) Zonal mean meridional structures of the first EOFs of the total and the second EOF of the residual variability. $U500_R$ and $Z500_R$ denote the meridional profiles of the velocity and geopotential height associated with the EOFs of the residual variability, respectively.

d) Siberia time series (Sib.): the area weighted average of 500-hPa geopotential height anomaly inside the maximum contour of EOF3 of the residual variability, over Siberia.

Figure 4.22 shows the correlation maps between the 500-hPa geopotential height residual anomalies at each grid point and the four time series defined above.

The correlation with the Pacific time series shows the characteristic PNA pattern. The secondary wave train over the Atlantic and Eurasia observed in EOF1 of the residual variability is only reminiscent in the correlation pattern. These results suggest a regional (not hemispheric) character of the PNA.

The correlation with the Siberia time series shows a pattern similar to both the third EOFs of the residual and total variabilities, suggesting that both EOFs are capturing true teleconnectivity. These EOFs show a wave train nearly in quadrature with the wave train over the Atlantic and Eurasia observed in the EOF1 of the residual variability. Then it is possible that the PNA, through its Florida centre, may influence the excitation of the Atlantic/Eurasian wave train represented in the third EOFs [Reyers et al. 2006]. In such case, the leading EOF of the residual variability would represent teleconnectivities implied by both the Pacific/North American wave train and an Atlantic/Eurasian wave train.

The most prominent structures in the correlation maps with the Icelandic and the Bering Strait time series are two meridional dipolar structures over the respective ocean basins. The correlations of both time series with grid point anomalies over the opposite ocean basin is very small, explaining less than 4% of their variabilities. The correlation map with the Icelandic time series depicts the NAO pattern. It is worth remarking that similar correlation maps are obtained if one considers the total 500-hPa geopotential height variability or if 15-day running means are used instead of 31-day running means.

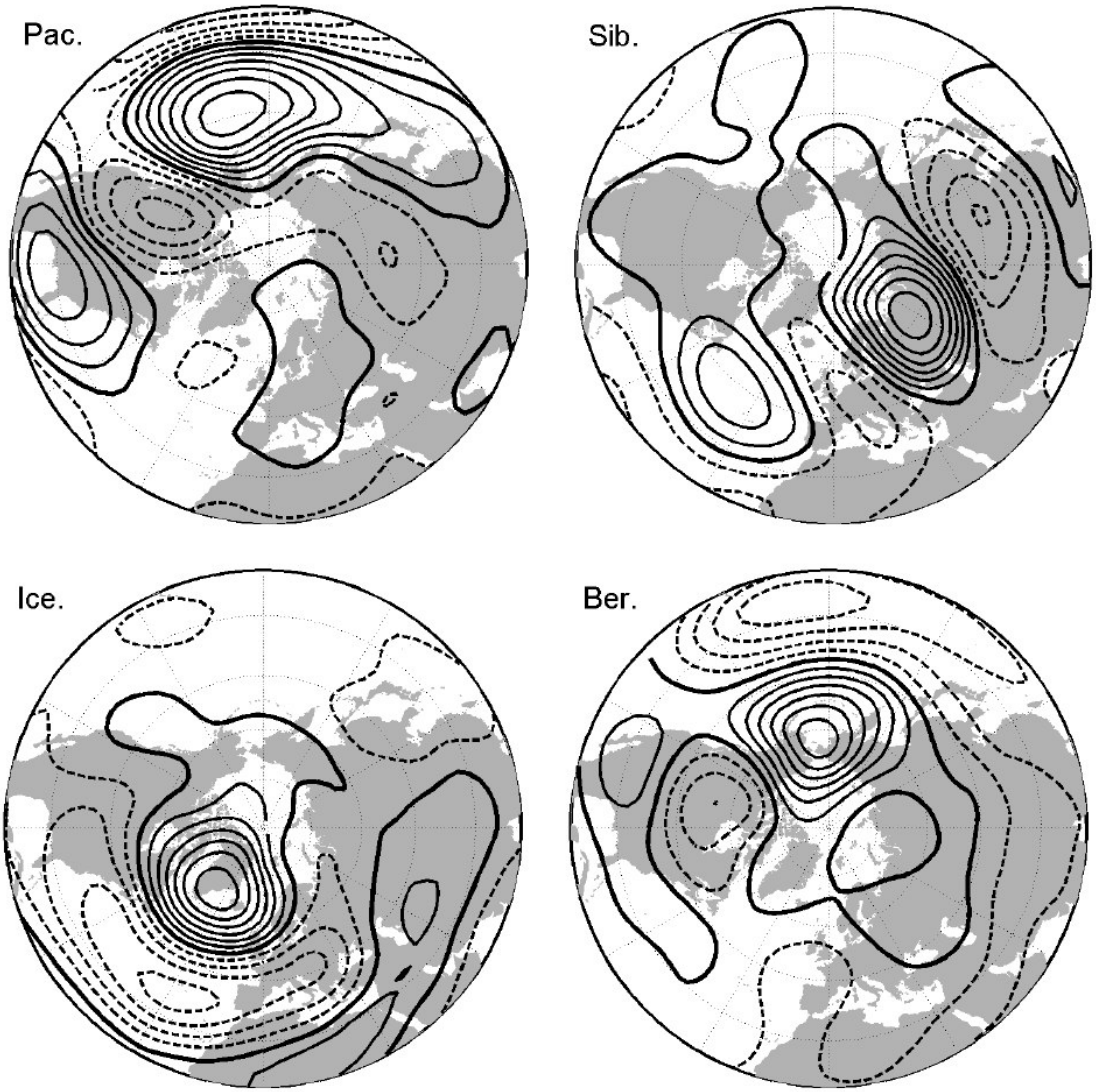

Figure 4.22 – Correlation maps between Z500 residual anomalies and the four time series defined over the Pacific (Pac.), Siberia (Sib.), Iceland (Ice.) and over the Bering Strait (Ber.) centres (see the text for the definition of these centres). Contour interval is 0.15. The solid thick lines represent the zero contours.

Table 4.5 shows the correlations between the four time series defined above. The statistical significance of the correlation values was assessed performing 10,000 random permutations of the years. By permuting only the years one conserves the serial autocorrelation of the smoothed daily time series. Using one-sided statistical test at the level p=0.15, the weak correlation between the Icelandic and Bering indices (r=0.07) does not reject the null hypothesis that they are uncorrelated. The results of Figure 4.22 and Table 4.5 together show that, at least, a very large fraction of the zonally symmetric component of the leading EOF of the 500-hPa geopotential height total variability is due to independent variability of dipolar structures over the Pacific and Atlantic basins. This result is completely consistent with the theoretical findings of Gerber and Vallis [2005].

Table 4.5 – Correlations between the time series of the area weighted averages of the Z500 residual anomalies over the Pacific (Pac.), the Siberia (Sib.), the Icelandic (Ice.) and the Bering Strait (Ber.) centres. The time series were smoothed by a 31-days running mean. The asterisk denotes values statistically different from 0 at the level p=0.05, using one-sided test.

	Sib.	**Ice.**	**Ber.**
Pac.	0.00	-0.10	0.19*
Sib.		-0.15*	0.01
Ice.			0.07

4.3.2.1. 1000-hPa geopotential height field

Much of the discussion about the teleconnectivity represented in the NAM/AO structure in the literature was based on the analysis of the variability of the mean SLP field and the 1000-hPa geopotential height field (Z1000) [*e.g.*, Thompson and Wallace 1998; Deser 2000; Ambaum et al. 2001; Wallace and Thompson 2002]. Figure 4.23 shows an analysis similar to the one in Figure 4.18 but for the 1000-hPa geopotential height field. The regression of the 1000-hPa geopotential height field anomalies on the 70-hPa NAM reveals a pattern very close to the first EOF of 1000-hPa geopotential height field (the AO). The spatial correlation between the two patterns is r = 0.97. The bottom panels of Figure 4.23 show the first three EOFs of the residual 1000-hPa geopotential height field that remained after regressing out the 70-hPa NAM. The second and third EOFs seem to be very insensitive to the stratospheric variability. The first EOF of the residual field is similar to the first EOF of the total field (their spatial correlation is r = 0.94) but with the relative magnitudes of the Atlantic and Pacific centres changed. This is because of the regression of 1000-hPa geopotential height field on the 70-hPa NAM is stronger over the Atlantic area than over the Pacific.

Since the leading EOFs of the total and residual 1000-hPa geopotential height fields are similar, one may, again, question if there is a tropospheric annular component independent from the stratospheric annular variability. To check this possibility in the 1000-hPa geopotential height residual field, the three following time series were defined:

a) Pacific time series (Pac.): the area weighted average of 1000-hPa geopotential height anomaly field inside the maximum contour of the EOF1 of the residual variability, over the Pacific.

b) Iceland time series (Ice.): the area weighted average of 1000-hPa geopotential height anomaly field inside the minimum contour of EOF1 of the residual variability, over Iceland and Greenland.

c) Atlantic time series (Atl.): the area weighted average of 1000-hPa geopotential height anomaly field inside the maximum contour of the EOF1 of the residual variability, over the Atlantic.

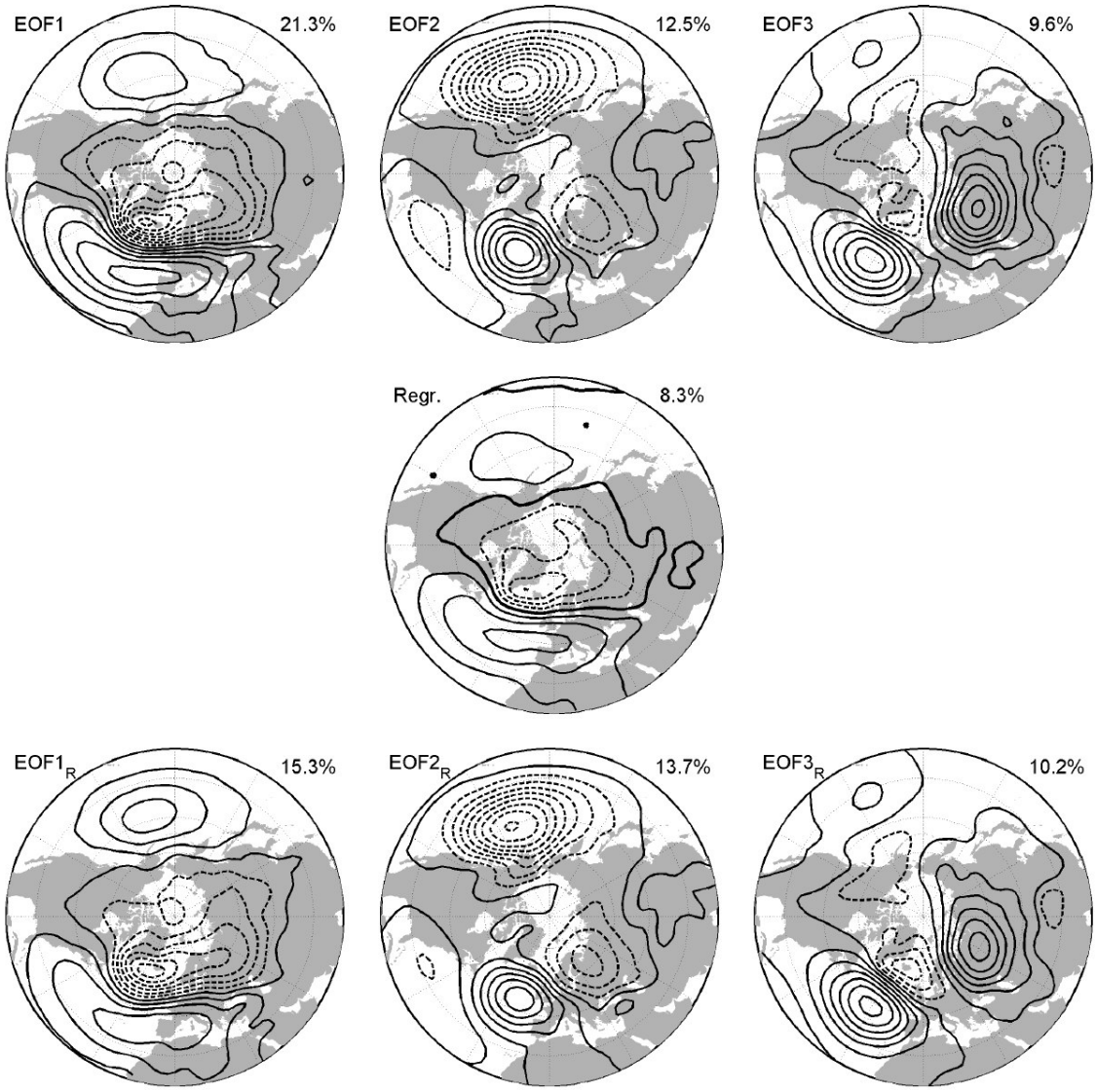

Figure 4.23 – As in Figure 4.18 but for the 1000-hPa geopotential height field (Z1000). Contour interval is 5 gpm.

Figure 4.24 shows the correlation maps between the 1000-hPa geopotential height residual time series anomalies at each grid point and the three time series defined above.

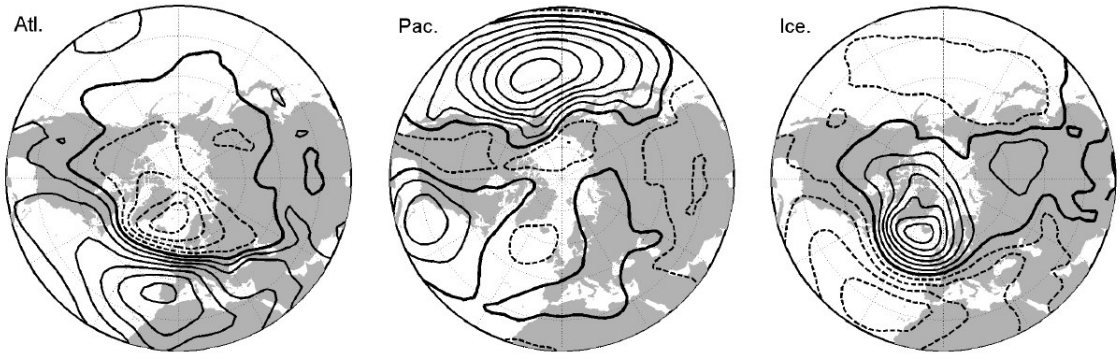

Figure 4.24 – Correlation maps between Z1000 residual anomalies and the three 1000-hPa anomaly time series defined over the Atlantic (Atl.), Pacific (Pac.) and Iceland (Ice.) centres (see the text for the definition of these centres). Contour interval is 0.15. The solid thick lines represent the zero contours.

The correlation maps reproduce the NAO dipole and a surface imprint of the PNA pattern. However, the correlations between the Atlantic centre and the 1000-hPa geopotential height field anomalies over the Pacific are near zero and even negative over the northern Pacific. It may be argued, as in Wallace and Thompson [2002], that the positive correlation between the Atlantic and Pacific centres is "destroyed" by the anticorrelation associated with the EOF2 pattern. They suggested that the structure of the EOF2 represents an augmented-PNA teleconnection pattern. By the same argument they used one must expect that such teleconnection pattern would reinforce the anticorrelations between the Icelandic centre and the 1000-hPa geopotential height field anomalies over the Pacific. Nevertheless the anticorrelation between the Icelandic centre and the 1000-hPa geopotential height field anomalies over the Pacific

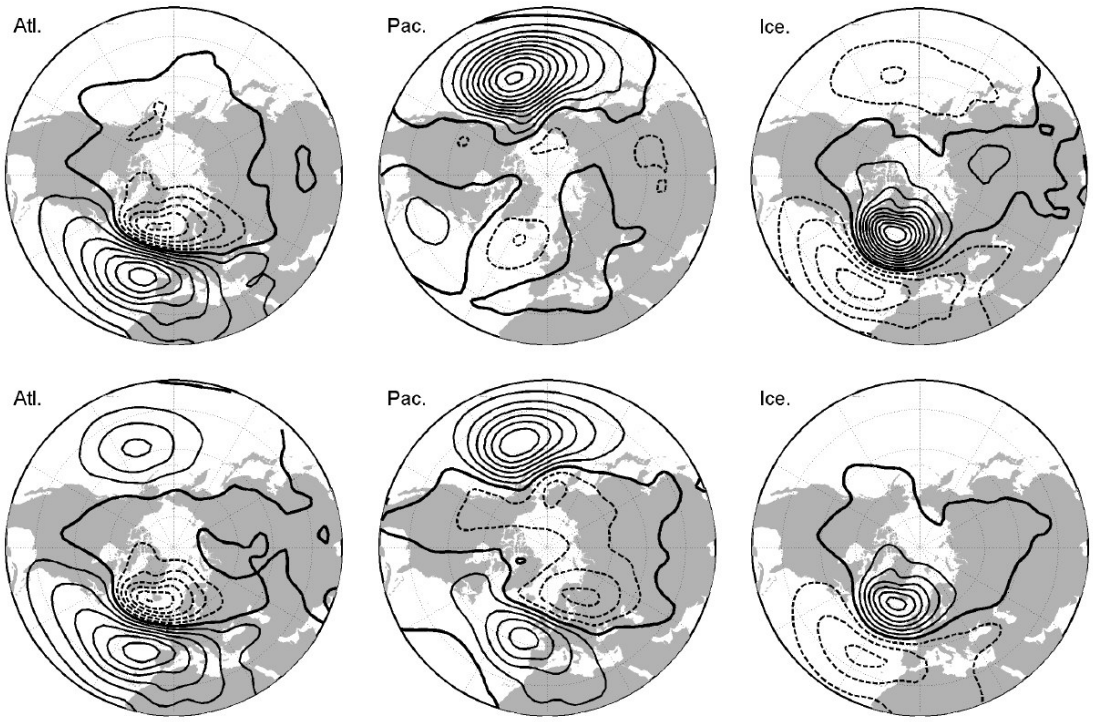

Figure 4.25 – (*Top*) Regression maps of the Z1000 residual anomalies on the three normalized 1000-hPa anomaly time series defined over the Atlantic (Atl.), Pacific (Pac.) and Iceland (Ice.) centres (see the text for the definition of these centres). (*Bottom*) As in the top but regressing out also the variability associated with the PC2. Contour interval is 5 gpm. The solid thick lines represent the zero contours.

is small and it seems not to be different from the anticorrelation implied by EOF2 itself. In fact, following the procedure of Wallace and Thompson [2002] one obtains contradicting results. The top row in Figure 4.25 shows the regression maps of the 1000-hPa geopotential height field residual anomalies on the three normalized 1000-hPa anomaly time series defined above. The regression map on the Atlantic time series depicts the NAO pattern. On the other hand, the regression map on the Icelandic time series is similar to the leading EOF. Their spatial correlation is r=-0.83. The bottom maps in Figure 4.25 also show the same regression maps but after

removing the variability represented by PC2. Now the regression map with the Atlantic centre shows a centre with equal polarity over the Pacific. However, the regression on the Icelandic time series lost its centre over the Pacific and depicts the NAO pattern. Very similar results were obtained when the same analysis is performed on the total variability instead of the residual variability. Therefore, the above correlation and regression maps suggest that the Pacific centre of the leading 1000-hPa geopotential height field EOF does not belong to the teleconnection pattern represented by the NAO dipole.

5. WAVE ENERGY ASSOCIATED WITH THE VARIABILITY OF THE STRATOSPHERIC POLAR VORTEX

In this chapter a study is performed on the energetics of planetary wave forcing associated with the variability of the wintertime stratospheric polar vortex. The analysis relies on the 3D normal mode expansion and mainly departs from the traditional ones in respect to the wave forcing, which is here assessed in terms of total energy amounts associated with Rossby waves. In the first section of the chapter both the energy associated with climatological circulation and wave transience are defined and spectra are presented.

Within the context of the wave-mean flow interaction, we investigate how the polar night jet oscillates with total energy of Rossby waves through lagged correlations between the vortex strength and the wave energy. We also pay attention to the way both the zonal and the meridional scales of Rossby modes interact with the vortex strength. Obtained results indicate that an increase of the total energy will be accompanied by an increased wavenumber one propagation into the stratosphere, decelerating the jet. The analysis of the correlations between individual Rossby modes and the vortex strength further confirm the result from linear theory that the waves that force the vortex are those associated with the largest zonal and meridional scales.

Finally, we present results of two separate composite analyses of displacement- and split-type stratospheric sudden warming (SSW) events, which have revealed different dynamics. We show that displacement-type SSWs are forced by positive anomalies of the energy associated with the first two baroclinic modes of planetary Rossby waves with zonal wavenumber 1; split-type SSWs are in turn forced by positive anomalies of the energy associated with the planetary Rossby wave with zonal wavenumber 2, and the barotropic mode appears as the most important component. As far as SFW events are concerned, obtained results suggest that the wave dynamics is similar to the one in

displacement-type SSW events. Results presented in this chapter have been published in Liberato et al. [2007].

5.1. Energy spectra associated with climatological circulation and wave transience

Although comprehensive studies of normal mode energy spectra may be found in the literature [*e.g.*, Tanaka and Ji 1995 and references therein], we present in this section, for reference purposes, the meridional mean energy spectra for the Rossby modes of wavenumbers *s = 1* and *2* associated with the first five vertical structures *m*.

The spectral characteristics of the synoptic to planetary waves are described by Tanaka [1985] and Tanaka and Kung [1988] by means of the 3D normal mode decomposition, including the vertical spectrum. The scheme is referred to as normal mode energetics. According to the results of their normal mode energetics analysis, the energy spectrum of the barotropic component of the atmosphere obeys to a characteristic slope of 2 to 3 power of the eigenfrequency of Laplace's tidal equation σ. Tanaka and Kasahara [1992] also found that the energy spectrum is uniquely determined as a function of the phase speed of the Rossby mode *c*. Tanaka et al. [2004] have also shown that the barotropic energy spectrum, *E*, of the general circulation may be represented as $E = mc^2$, *i.e.*, the energy spectrum is proportional to the squared phase speed of Rossby modes in the general circulation of the atmosphere (the proportional constant *m* describes a factored total mass of the atmosphere per unit area).

Here the analysis of circulation variability was performed by computing the variance of each coefficient w_{msl}^{α}, since it is proportional to the transient total energy. It may be noted that by transient total energy associated with the respective mode we mean the total energy associated with the deviation of the daily circulation field from the climatological mean. Assessing the amount of transient energy is a very effective way

of achieving a physically based filtering of the data.

5.1.1. Energy associated with wave transience

Let $w^{\alpha}_{msl}(\tau, j)$ denote the complex wave amplitudes at day τ of year *j*. Decomposing the wave amplitudes in their climatological and anomaly parts and using Equation 3.7, we may compute the contributions to the climatological (mean) energy associated with the climatological circulation and the wave transience,

$$\left\langle E^{\alpha}_{msl}(\tau,\cdot)\right\rangle = \frac{p_s h_m}{c_s}\left(\left|\left\langle w^{\alpha}_{msl}(\tau,\cdot)\right\rangle\right|^2 + \left\langle\left|w^{:\alpha}_{msl}(\tau,\cdot)\right|^2\right\rangle\right) \tag{5.1}$$

where $\langle x(\tau,\cdot)\rangle$ represents the mean over all years for a given day τ, with the summation index replaced by a dot, and $w^{:\alpha}_{msl}(\tau, j)$ are the amplitude anomalies for a given day τ of a given year *j*. Here, the term transience refers to the deviations of the actual values from their climatological means [Andrews et al. 1987, section 5.1].

In order to reduce the statistical fluctuations of the averaged circulation, the daily means for all years were smoothed by a 31-day running mean, and the amplitude anomalies were redefined as

$$w^{'\alpha}_{msl}(\tau, j) = w^{\alpha}_{msl}(\tau, j) - \tilde{w}^{\alpha}_{msl}(\tau,\cdot) \tag{5.2}$$

where $\tilde{w}^{\alpha}_{msl}(\tau,\cdot)$ represents the smoothed average, which is assumed to negligibly differ from the expected values of $\langle w^{\alpha}_{msl}(\tau,\cdot)\rangle$, *i.e.*, the true climatology.

The spectra of the parcel of the mean energy associated with the wave transience,

$$\overline{E^{'}_{msl}} = \frac{p_s h_m}{c_s}\left(\overline{\left|w^{'}_{msl}\right|^2}\right) \tag{5.3}$$

are shown in Figure 5.1, for the wavenumber one and two of the first five vertical components. This parcel of the mean energy is a measure of the variability of the circulation. As expected a large amount of energy appears associated with the

barotropic spectrum which peaks in meridional indices $l = 4,5$ The maxima of the baroclinic energy spectra show a clear tendency to appear in higher meridional index as m (=1,2,3,4) increases. This may be understood as a consequence of an equatorward confinement of the meridional structures as m increases. In fact, the equivalent height, h_m, decreases with the order m of the mode. As the equivalent height decreases, the meridional structures become more concentrated towards the equator. For a given equivalent height, the meridional structures extend more poleward as the meridional index increases [Longuet-Higgins 1968, Figure 10]. Hence, the higher baroclinic components of extratropical circulation will be projected onto higher meridional modes. Finally it may be noted that for $m = 3$ and $m = 4$ the peaks in the meridional index $l = 1$ must be associated with tropical variability [Castanheira 2000].

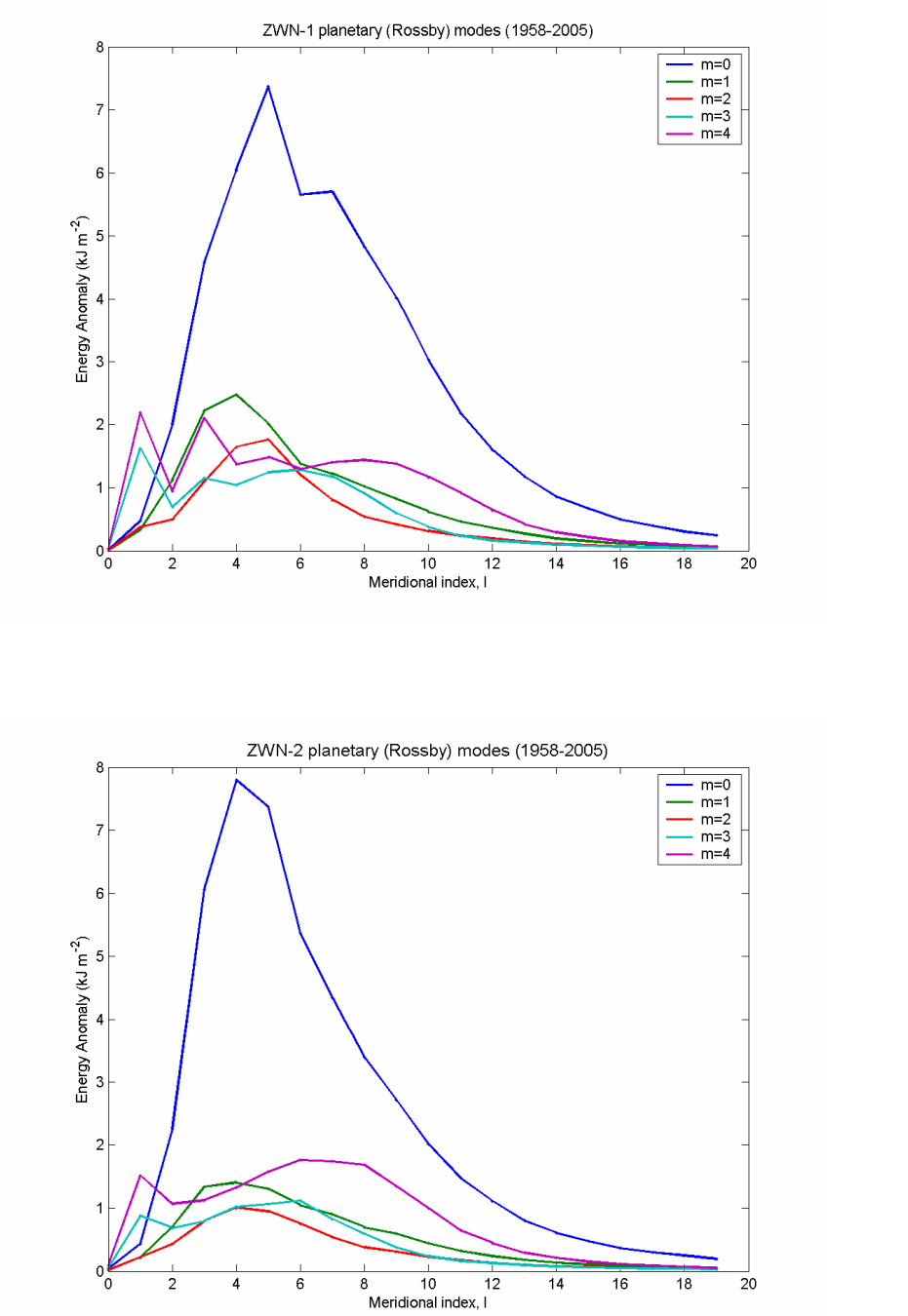

Figure 5.1 – Spectra of transient energy of wavenumber one (*top*) and two (*bottom*) Rossby modes associated with the barotropic (*m=0*) and the first four baroclinic components (*m=1,2,3,4*).

5.1.2. Variability of wave energy

Energy has been calculated for each wave, using Equation 3.7, without filtering the coefficients and then restricting to low frequency waves, *i.e.* the coefficients were filtered by a 15-day running mean that was applied before computing the energy. Energy anomalies were computed following the method described on section 3.3.6.

Figure 5.2 represents the extended winter mean energy spectra of the Rossby modes with wavenumbers $s = 1$ and 2, for the barotropic (Figure 5.2a) and first two baroclinic modes $m = 1, 2$ (Figures 5.2b and 5.2c). Both the complete spectra and the spectra for low frequency waves are presented and it may be observed that the patterns of the spectra are similar, even though values are lower, as expected, in the case of the filtered spetra.

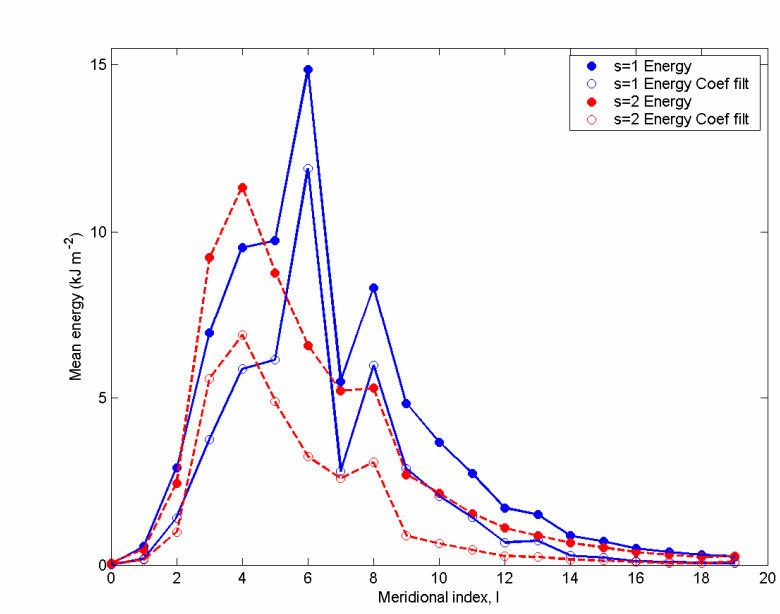

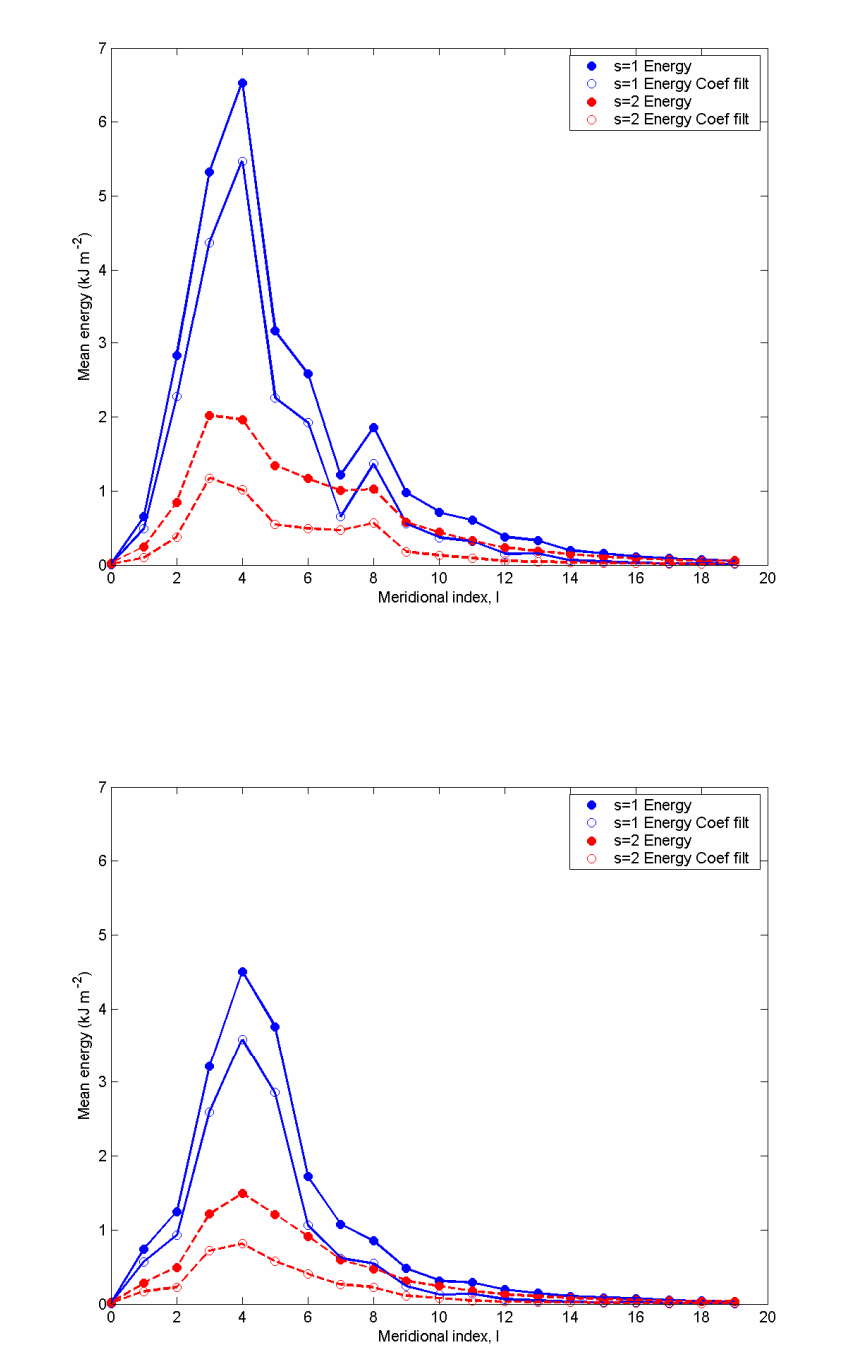

Figure 5.2 – Extended winter mean energy (1958 – 2005) of the Rossby modes with wavenumbers *s = 1* and *2* associated with: (*left page*) barotropic (*m = 0*); and the first two baroclinic (*top*) *m = 1* and (*bottom*) *m = 2* structures. Both the complete spectra (solid blue) and the spectra for low frequency waves (dashed red) are represented for each wavenumber.

The variability spectra, *i.e.* the spectra of the standard deviation of intraseasonal or interannual anomalies (Figure 5.3) are similar to the respective spectra of the mean energy. The barotropic modes represent the largest amount of energy, in agreement with the fact that they are sensitive to the circulation of the largest fraction of the atmospheric mass, the troposphere. The baroclinic modes $m = 1, 2$ are more sensitive to the lighter layer of atmospheric mass, the stratosphere, and represent smaller amounts of energy. A remarkable feature in the spectra of baroclinic ($m = 1, 2$) modes is the large difference between the energy of wavenumbers $s = 1$ and $s = 2$, which is to be attributed to the wavenumber filtering by the stratosphere.

Since we aim to relate time changes in the energy associated with planetary Rossby waves with the observed vortex variability, we have projected the atmospheric circulation onto the first 20 Rossby modes. Results shown in Figures 5.1 to 5.3 clearly point out that the most important modes were indeed retained in our analysis.

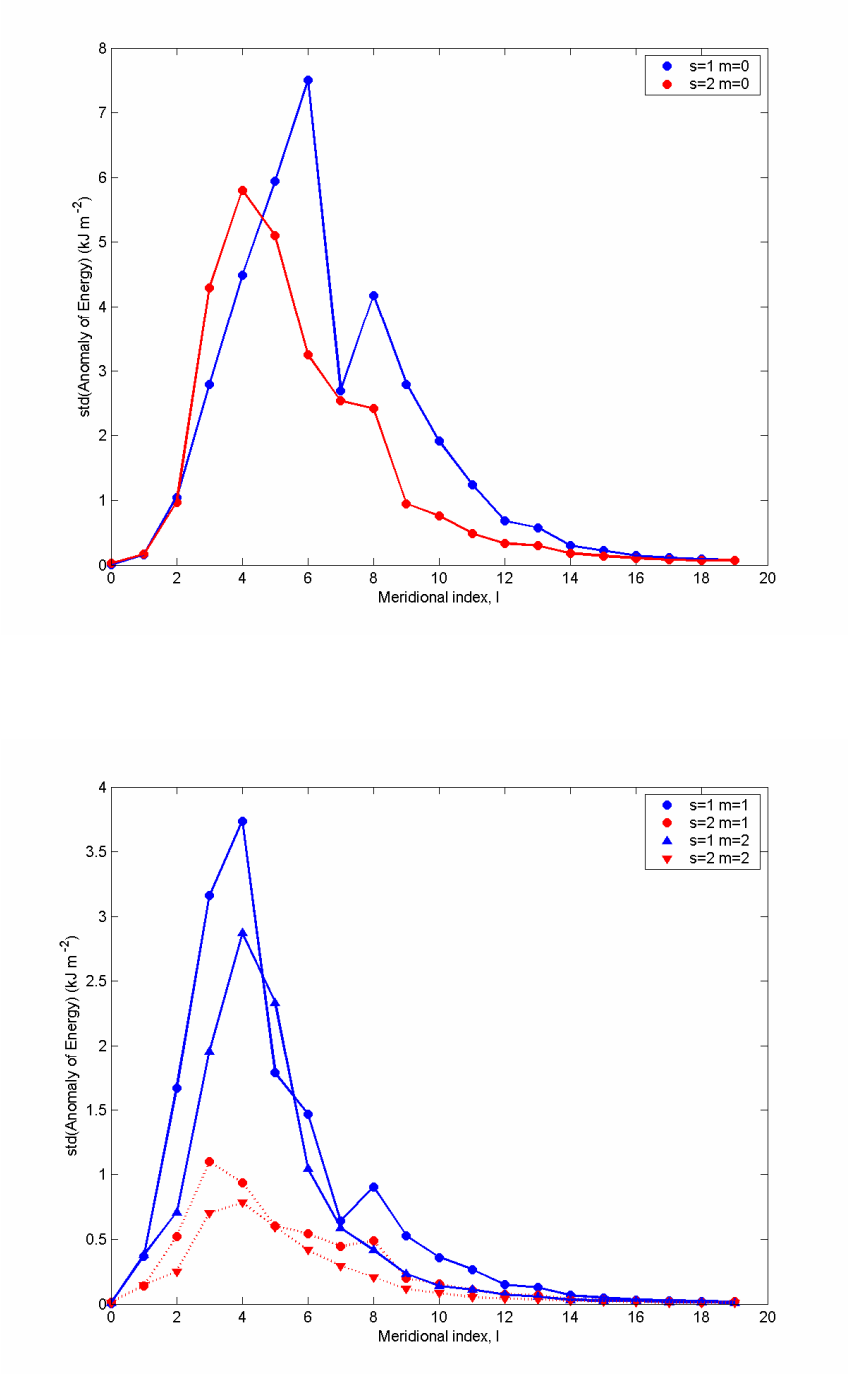

Figure 5.3– Extended winter variability spectra of the Rossby modes with wavenumbers *s = 1* and *2* associated with: (*top*) barotropic (*m = 0*); and (*bottom*) the first two baroclinic (*m = 1, 2*) structures.

5.2. Study of Vortex Variability – the classical approach

Recently, a set of observational studies has focused on the daily evolution of strong vortex anomalies [McDaniel and Black 2005], polar vortex intensification (VI) [Limpasuvan et al. 2005], the life cycle of SSW events [Limpasuvan et al. 2004; Nakagawa and Yamazaki 2006; Charlton and Polvani 2007] and the evolution of SFW events [Black et al. 2006].

During boreal winter tropospheric NAM events are often preceded by variations in the strength of the stratospheric polar vortex [Baldwin et al. 2003]. However, not all NAM cases follow the statistical prototype of stratospheric initiation followed by downward signal movement (hereafter referred to as downward "propagation") into the troposphere, as certain robust stratospheric NAM events are not associated with corresponding succeeding tropospheric NAM events [Baldwin and Dunkerton 1999; Zhou et al. 2002]. Accounting for such case to case variability represents an important test of any theory regarding stratospheric influences upon tropospheric climate.

Black and McDaniel [2004] focused their study in identifying dynamical reasons why some strong stratospheric NAM events do not extend downward to tropospheric levels. Black and McDaniel's [2004] results indicate important roles for both direct and indirect forcing mechanisms in performing stratospheric influences upon tropospheric climate. These authors conclude that whether or not a tropospheric NAM signal emerges from a given stratospheric NAM event is largely dependent upon (1) whether stratospheric PV anomalies descend to sufficiently low altitudes within the stratosphere and (2) the detailed nature of any pre-existing zonally-symmetric (annular) modes in the troposphere.

The statistical relation between the stratosphere and tropospheric circulation anomaly patterns associated with the NAM on intraseasonal time scales has been studied [Baldwin and Dunkerton 1999; Baldwin et al. 2003] but detailed diagnoses of the dynamical processes leading to daily variability in the NAM are needed to fully understand the mechanisms governing stratosphere-troposphere interaction. McDaniel

and Black [2005] provide an observational study of the zonal wind tendency budget for both the growth and decay stages of large amplitude positive and negative NAM events. McDaniel and Black [2005] deduce the proximate forcings of the zonal mean wind tendency during maturing and declining NAM stages employing transformed eulerian mean, piecewise potential vorticity inversions, and regional Plumb flux diagnoses. A remarkable degree of reverse symmetry is observed between the zonal-mean dynamical evolution of positive and negative NAM events. Anomalous equatorward and downward (poleward and upward) Eliassen-Palm fluxes are observed during the maturation of positive (negative) NAM events, consistent with index of refraction considerations and an indirect downward stratospheric influence. The associated patterns of anomalous wave driving provide the primary forcing of the zonal wind tendency field. Spectral analyses reveal that both the stratospheric and tropospheric patterns of wave driving are primarily due to low frequency planetary scale eddies.

Regional wave activity flux diagnoses further illustrate that this wave driving pattern represents the zonal mean manifestation of planetary scale anomalies over the North Atlantic that are linked to local anomalies in stationary wave forcing. The decay of NAM events coincides with the collapse in the pattern of anomalous stationary wave forcing over the North Atlantic region. McDaniel and Black's [2005] diagnostic results indicate that both (a) synoptic eddies and (b) direct downward stratospheric forcing provide second order reinforcing contributions to the intraseasonal dynamical evolution of NAM events.

Similar to past studies McDaniel and Black [2005] find that stratospheric variations in the NAM are strongly driven by variations in upward propagating tropospheric planetary scale waves [*e.g.*, Hartmann et al. 2000; Limpasuvan et al. 2004].

McDaniel and Black [2005] reviewed several mechanisms that have been proposed to explain stratosphere-troposphere coupling observed during the NAM. In one of the mechanisms the stratosphere provides an indirect influence upon the troposphere.

Specifically, changes in the vertical wind shear near the tropopause alter the index of refraction which in turn alters the propagation of tropospheric Rossby waves [Chen and Robinson 1992; Hartman et al. 2000]. During the positive (negative) phase of the NAM, strong positive (negative) zonal-wind anomalies are observed in the stratosphere at high latitudes (~65ºN) while negative (positive) zonal-wind anomalies are observed in the mid-latitude (~35ºN) stratosphere. The associated vertical wind shear is such that during the positive phase vertically propagating tropospheric Rossby waves are deflected equatorward with less wave activity reaching the stratospheric polar vortex. The reduction of wave breaking in the polar vortex results in an anomalously strong polar jet, providing a positive feedback that tends to keep the NAM in the positive phase. Meanwhile, the redirection of wave activity within the troposphere provides anomalous wave driving signatures within the middle and upper troposphere. Thus this mechanism provides an indirect stratospheric influence in which tropospheric waves act to alter the tropospheric zonal wind field. This indirect mechanism may affect the forcing and propagation characteristics of synoptic [Polvani and Kushner 2002; Song and Robinson 2004] and planetary scale tropospheric waves [DeWeaver and Nigam 2000; Hartmann et al. 2000].

Limpasuvan et al. [2004; 2005] have studied polar VI showing that the gross behavior of VI events is similar in shape but opposite in sign to the one associated with SSW events. A strong relationship exists between these midwinter weakenings in the polar vortex, known as SSW events, and intraseasonal NAM variability [Limpasuvan et al. 2004].

In the NH, the linkage between the stratosphere and troposphere appears most obvious when the stratospheric polar vortex undergoes unusually strong variation in wind strength and temperature. Conditions of anomalously weak stratospheric polar vortex are associated with SSW events in which the polar stratospheric temperature rises dramatically over a short time period [*e.g.*, McIntyre 1982; Andrews et al. 1987].

Quiroz [1977], O'Neill and Taylor [1979], and O'Neill [1980] first presented

evidence for the appearance of near-surface temperature anomalies in conjunction with the major NH SSW event of 1976–1977.

Kodera et al. [2000] have studied the relationship between SSW events and slowly propagating zonal wind anomalies during the NH cold season (November to March) using two leading EOF of 15-day mean zonal-mean zonal wind. They showed that major SSW events occur in phase with the slowly propagating zonal wind anomalies, which implies a "conditioning" of the atmosphere by the slowly varying state. These authors also stress that changes in the tropospheric planetary waves associated with the slowly propagating zonal wind anomalies coincide with changes in the AO. On their figure 2 (here reproduced as Figure 5.4) they describe the anomaly progression by the trajectory in the phase space of the first two EOF around the plane, at intervals of 45º. The first EOF has large amplitude in the polar region of the upper stratosphere, while the second EOF describes an inclined, dipole-type pattern: the positive pole is located at the midlatitude stratopause, while the negative pole is located at high latitudes in the middle stratosphere. According to the authors, Figure 5.4 illustrates how movement around the phase angle ϕ describes the structure of downward and poleward propagating wind anomalies in the stratosphere, which progress at a rate proportional to the change in phase angle.

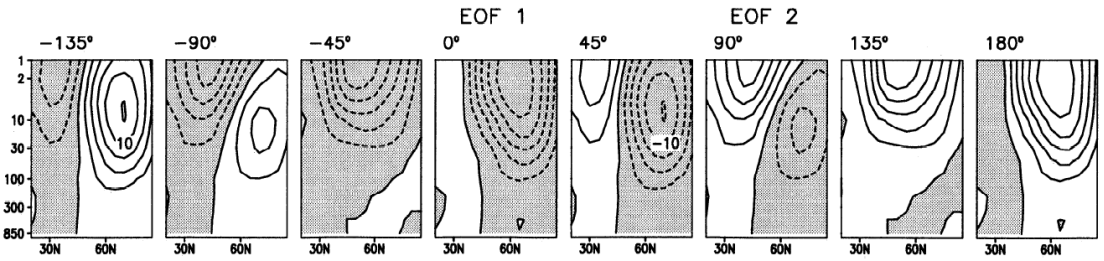

Figure 5.4 – Spatial structure of zonal winds corresponding to a different direction of a unit vector in a plane constructed by EOF 1 and EOF 2. Panels show patterns corresponding to one rotation from -135º to 180º. Number on each panel indicates an angle of rotation ϕ in equation $P(\phi) = A(\cos\phi \cdot EOF1 + \mathrm{s}en\phi \cdot EOF2)$. EOF 1 and EOF 2 correspond to phases ϕ = 0º and 90º (as marked). Contour interval is 2.5 ms^{-1}, and negative values are shaded (Figure 2 from Kodera et al. [2000]).

Limpasuvan et al. [2004] noted that the composite SSW life cycle is preceded by preconditioning of the upper stratospheric circulation and by anomalous planetary-scale wave forcing at stratospheric and near-surface levels. As the SSW matures (and the vortex becomes weaker), the largest stratospheric zonal flow and temperature anomalies and the region of largest wave driving descend throughout the depth of the stratosphere, as a result of wave mean flow interactions. When the anomalous wave driving reaches the lowermost stratosphere, the associated flow anomalies appear to penetrate the tropopause, drawing substantial anomalous responses in both wave propagation and the mean meridional circulation at tropospheric levels [Haynes et al. 1991; Kuroda and Kodera 1999; Shindell et al. 1999a]. In contrast to the waves that initiate the stratospheric warming, the anomalous tropospheric wave forcing during the mature phase of the SSW is associated primarily with waves smaller than planetary-scale.

Limpasuvan et al. [2004] also show (on their Figure 10) that strong heat flux anomalies are observed in the preconditioned upper stratosphere several weeks before the weakest state of the polar vortex. The heat fluxes are associated mainly with quasi-stationary wavenumber 1 disturbances that are evident at both tropospheric and stratospheric levels.

On a subsequent work, Limpasuvan et al. [2005] examined stratosphere-troposphere evolution associated with polar VI events in the NH winter. These authors show that incipient stage of a VI event is marked by anomalously low wave activity and descending westerly anomalies over the depth of the polar stratosphere. Reduced poleward planetary wave heat flux occurs as the circumpolar wind becomes stronger and geopotential height anomalies penetrate toward the surface. The downward progressing geopotential height anomaly patterns project strongly onto the positive state of the NAM. Concurrently, anomalous poleward momentum flux develops in the upper troposphere, and the related tropospheric mean meridional circulation provides an easterly torque which maintains the wind anomalies reaching lower-troposphere against surface drag. These authors argue that the gross behaviour of the composite VI

event is similar in shape but opposite in sign to that associated with SSW events. However, the descent of the wind and temperature anomalies over the VI life cycle is generally weaker and slower than its SSW counterpart preceding the maximum vortex anomaly. Similarly, after the maximum wind event, the weakening of the winds is faster than the strengthening of the winds after a SSW. According to Limpasuvan et al. [2005] this is because stratospheric wind reduction anomalies are produced by wave driving, which can be rapid, and increases in wind speed are associated with the radiative cooling of the polar cap, which happens more gradually. While the contributions of the anomalous momentum fluxes by the quasi-stationary and synoptic eddies are similar to SSWs, the much stronger anomalous momentum flux observed during VI can be attributed to the larger role of eddies with timescales between 15 and 40 days and of wavenumber 2 scale. Notable differences between VI and SSW appear in the tropical region. In particular, anomalous VI tends to occur more frequently during La Niña conditions while most El Niño winters tend to be associated with SSW events.

The factors affecting the downward propagation of SSW events to the troposphere have also been studied by Nakagawa and Yamazaki [2006] through composite analysis of 45-year reanalysis data from the ECMWF. The study distinguished two types of SSW events: a wave-2 type SSW event and a wave-1 type SSW event. During the growth stage of SSW, events that propagate into the troposphere exhibit enhanced upward flux of the wavenumber two wave, while events that do not propagate downward display reduced wavenumber two flux. In both events, upward flux of the wavenumber one wave is enhanced, but the enhancement is stronger in the non-propagating event. Nakagawa and Yamazaki's [2006] composite for propagating events reveals a negative Eurasian pattern of horizontal geopotential anomalies in the troposphere during the growth stage, and a negative AO pattern following the event, while non-propagating events are preceded by a positive Eurasian pattern. In both types of events, the tropospheric anomalies are generated mainly by tropospheric planetary wave forcing prior to the emergence of SSW.

Since the discovery of SSW events by Scherhag [1952], many studies have examined the dynamics of individual major warming events. However, only a few studies, including those by Labitzke [1977] and Manney et al. [2005] have attempted to establish a climatology of major, midwinter, SSW events. According to Charlton and Polvani [2007] their study builds on those earlier works and is novel and distinctive in three important respects. First, they provide full dating information for SSW events, including the day of occurrence, and tabulate all events from the late 1950s to the present. Second, their climatology is established based on two widely used reanalysis datasets, which had not been previously examined for SSW activity. Third, these authors use a new analysis technique that, for the first time, classifies the SSW events into vortex displacement and splitting events.

Charlton and Polvani's [2007] study is closely related to the one of Limpasuvan et al. [2004]. However, while the latter used the 50-hPa annular mode to define SSW events and considered only the NCEP–NCAR reanalysis dataset, Charlton and Polvani [2007], using the WMO definition of SSW events (easterly winds at 10-hPa and 60°N), developed a more sophisticated algorithm and examined both the NCEP–NCAR and the 40-yr ECMWF ReAnalysis (ERA-40) datasets in the extended winter (November–March).

Using this new tool, they attempted to answer several key questions, in particular the following ones:

- Are vortex displacements and vortex splits dynamically different? If so how?
- Do vortex displacements and vortex splits differ in their impacts on the tropospheric flow?

They conclude that:

1) Vortex displacements and splits should be considered dynamically distinct. Prior to vortex displacements and vortex splits, the vertical and horizontal structure of the stratosphere and troposphere is different. In particular,

anomalously strong zonal flow in the troposphere appears essential for the occurrence of vortex splits. Vortex splits are accompanied by a significantly anomalous flow in the Pacific sector. There is also clear evidence of early, precursor wave activity for the vortex splits but not for vortex displacements.

2) While there are some differences in the spatial structures of the tropospheric impact of vortex displacements and vortex splits, there is little difference in the averaged tropospheric impact. This suggests that the mechanism for the impact of the stratosphere on the tropospheric flow following major stratospheric disturbances might have little dependence upon the precise structure of anomalies in the lower stratosphere.

This work of Charlton and Polvani [2007] and their conclusions are relevant to this study as we will be using their climatology in our analysis (Table 3.1 in section 3.3.4). Moreover, we anticipate that our results will contribute to elucidate the problems posed by the above-mentioned questions.

Black et al. [2006] studied the evolution of SFW events focusing on the relationship between SFW events and the observed Northern extratropical circulation. Specifically, SFW events are associated with a vertically coherent north-south dipole pattern in the zonal wind anomaly field at mid to high latitudes. However, this pattern is distinct from the canonical NAM structure as the primary centers in the north-south anomaly dipole are retracted northward compared to the NAM. Results of Black et al. [2006] indicate that SFW events may be associated with a distinct and previously unrecognized intraseasonal annular mode of variability that strongly couples the stratosphere and troposphere on submonthly time scales at mid to high latitudes (the Polar Annular Mode – PAM). Black and McDaniel [2006] also found that the evolution of SSW events is dominated by NAM variability whereas NAM and PAM play approximately equal roles in SFW events.

The tropospheric anomaly patterns obtained by Black and McDaniel [2006] are more strongly annular with relatively weak amplitudes over the North Atlantic. This

suggests that, during periods of stratosphere-troposphere NAM coupling, the tropospheric patterns have a substantial component that represents an internal tropospheric response to stratospheric NAM variability [*e.g.*, the indirect tropospheric response discussed by McDaniel and Black 2005]. As such, Black and McDaniel's [2006] analysis provides a useful dynamical framework for delineating stratospheric and tropospheric NAM variability. This separation also serves to isolate the direct impact of the polar vortex variability upon the troposphere. Since stratospheric the NAM and PAM events studied by these authors induce large-scale tropospheric circulation anomaly patterns with similar amplitudes, Black and McDaniel [2006] suggest that variations in the strength and position of the stratospheric polar vortex each provide comparable direct effect to the tropospheric circulation. However, these impacts have different spatial patterns and time scales.

The dynamical nature of wave driving field was explored by Black and McDaniel [2006] by performing temporal and spatial decompositions of the input wave fields. These analyses indicate that the anomalous wave driving signatures in both the stratosphere and troposphere are mainly due to low frequency (intraseasonal periods greater than 10 days) planetary scale (wavenumbers 1-3) eddies. The role of smaller scale (wavenumbers 4 and higher) eddies is to provide secondary enhancements to the upper tropospheric wave driving pattern near 60ºN. Further, zonal-mean analyses of the regional wave activity flux field indicate that the composite anomaly field, itself, is able to account for most of the low frequency planetary scale wave driving. This suggests that the composite anomaly field contains the fundamental essence of the intraseasonal dynamical evolution of the NAM.

5.3. Study of Vortex Variability – the energy perspective

In the above-mentioned studies as well as in many others, the analysis of the wave forcing of the stratospheric polar vortex was performed within the traditional framework of EP flux. However, the use of the EP flux as a diagnostic tool of wave

propagation is strictly valid only in the case of small-amplitude waves. Frequent usage is also made of other concepts associated with EP flux diagnostics, such as refractive indices and critical lines, even though neither the Wentzel–Kramers–Brillouin–Jeffries (WKBJ) approximation relating refractive indices and critical lines to wave propagation nor the relation between wave propagation and EP flux are valid in the case of strongly nonlinear flows like those that take place during SSW events [Thuburn and Lagneau 1999].

To our knowledge no studies have considered the wave forcing of the stratospheric polar vortex from the point of view of the energy associated with the forcing waves. The main goal of this chapter is therefore to perform a diagnostic study of the total (*i.e.* kinetic + available potential) energy associated with the planetary waves that force the vortex dynamics. The analysis is based on a 3D normal mode decomposition of the atmospheric global circulation, which is partitioned into planetary Rossby waves and inertio–gravity waves, both types of waves possessing barotropic and baroclinic vertical structures. Time changes in the energy associated with each wave component may then be related with the observed vortex variability. It is worth emphasizing that instead of being restricted to the extratropical region, the analysis is here applied to the global atmosphere, and the circulation components are selected based on 3D global functions. In this respect the connection between the polar stratospheric variability and the QBO is worth being emphasized [Holton and Tan 1980; Labitzke 1982], together with the model results of Naito et al. [2003] that have revealed a short-time cooling response to SSW events extending to the summer hemisphere, a feature that suggests the global character of SSW events.

Another important feature of the method used here is that the energy is computed for the total circulation (*i.e.* climatology + anomaly) and therefore energy anomalies, associated with vortex variability, also include the contribution from the climatological waves, which should be taken into account when performing composite analysis.

The fact that the 3D normal modes are eigensolutions of a set of primitive equations, linearized with respect to a basic state at rest, may be pointed out as a shortcoming of their use. However, the normal modes form a complete basis to expand the global circulation, and the divergent or rotational character as well as the horizontal and vertical structures of the circulation projected onto them do not depend on the magnitude of the anomalies. On the other hand, as the normal mode approach allows decomposing the circulation both into zonal and meridional scales, we may assess the sensitivity of vortex wave forcing to both spatial scales. In this respect it is worth recalling that the linear wave theory shows that the vertical wave propagation depends both on zonal and meridional wavenumbers [Andrews et al. 1987]. However, EP flux diagnostic studies found in the literature only show the dependence on the zonal scale by means of Fourier decompositions.

5.3.1. Lagged correlations between the vortex strength and the wave energy

As previously mentioned, Limpasuvan et al. [2004; 2005] have shown that the gross behavior of VI events is similar in shape but opposite in sign to the one associated with SSW events. It is therefore natural to analyze vortex forcing by means of lagged correlations between stratospheric NAM indices and wave energy anomalies. A 15-day running mean was applied to the NAM indices as well as to the total (*i.e.* climatological + anomaly) atmospheric fields before computing the energy. This procedure was motivated by the known fact that the stratospheric vortex is mainly forced by stationary waves, but similar results were obtained when the 15-day running average was applied after computing the energy, an indication of the negligible role played by high-frequency waves in the process of vortex deceleration.

5.3.1.1. Zonal dependence

Results obtained for planetary Rossby waves of wavenumber $s = 1$ are shown in

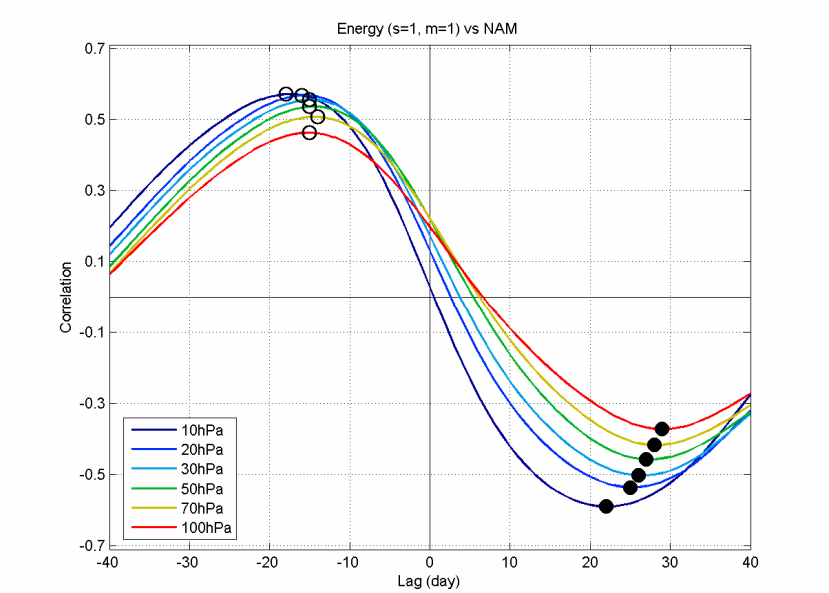

Figure 5.5 – Lagged correlations at six levels in the stratosphere between NAM indices and wave energy associated with wavenumber *s=1 m=1*. Solid (open) circles identify lags of maximum anticorrelation (correlation). Positive lags mean that energy is leading.

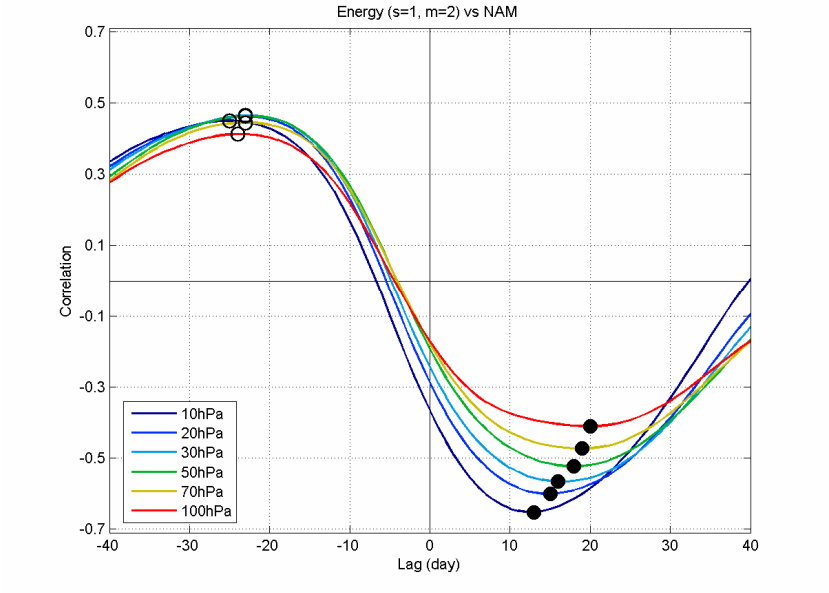

Figure 5.6 – As in Figure 5.5 but for wave energy associated with wavenumber *s=1 m=2*.

Figures 5.5 and 5.6, where positive lags mean that the energy is leading. For both baroclinic modes $m = 1$ and $m = 2$ correlation curves indicate that the total energy oscillates out of phase with the polar night jet. For positive lags, one may also observe that an increase (decrease) of the total energy of Rossby waves is followed by a weakening (strengthening) of the polar vortex. It is worth stressing that within the context of the wave–mean flow interaction, obtained results are an indication that an increase of the total energy will be accompanied by an increased wave-1 propagation into the stratosphere, decelerating the jet (as mentioned before in section 5.2).

A downward progression of vortex anomalies is also apparent, since the maximum anticorrelation with the NAM index at the 100-hPa level occurs about one week later than the corresponding maximum at the 10-hPa level. Furthermore, such downward progression is consistent with the observed lag differences between $m = 1$ and $m = 2$. In fact, as shown in Figure 3.1, the vertical structure function $m = 1$ represents wind speeds increasing upward in the stratosphere, a vertical profile consistent with the atmospheric state before a warming event. In turn, vertical structure function $m = 2$ represents wind speeds decreasing in the upper stratosphere, and such a profile is consistent with the developing phase of a warming event [as discussed before in our Figure 5.4, from Kodera et al. 2000].

On the other hand, if vertical structure functions are multiplied by −1, then the same reasoning may be valid when applied to VI events. Finally, it is worth noting that the observed oscillatory behavior in the correlation curves for $s = 1$ and $m = 1$ and 2 closely agrees with the findings by Limpasuvan et al. [2004], and further suggests a stratospheric vacillation cycle [Kodera et al. 2000].

5.3.1.2. Meridional dependence

As previously noted, the linear wave theory suggests that the vertical wave propagation depends on both the zonal and the meridional wavenumbers [Andrews et al. 1987]. However the lagged correlations that are depicted in Figures 5.5 and 5.6 refer to the sum of the energy of all meridional modes. To assess the effects due to the meridional scales we computed the lagged correlations between the energy of each Rossby mode and the vortex strength at the same stratospheric levels. Figures 5.7 and 5.8 show the obtained largest correlations or anticorrelations as a function of the meridional index of the Rossby modes. It should be noted that the considered positive (negative) lags lie inside the time intervals where the maximum anticorrelations (correlations) in Figures 5.5 and 5.6 were found [*i.e.*, the considered positive (negative) lags are contained by the interval where curves in Figures 5.5 and 5.6 are marked by solid (open) circles]. It is well apparent that the larger meridional scales (*i.e.* the smaller meridional indices) are the only ones that significantly interact with the vortex strength. As negative correlations were obtained when the energy was leading the vortex strength (*i.e.* with positive lags) and therefore represent a forcing of the vortex strength, it may seem awkward that the magnitude of the anticorrelations is smaller for meridional indices $l = 0, 1,$ and 2. However, such behavior is readily understood if we take into account that the largest values (weights) of the first meridional structures do appear at lower latitudes than those associated with high meridional indices. In fact, since the weights of the meridional structures at high latitudes increase as the meridional index increases [Longuet-Higgins 1968], meridional modes $l = 0, 1,$ and 2 ($l = 3,\ldots,6$) are more sensitive to the atmospheric circulation at lower (higher) latitudes. The meridional Rossby mode $l = 8$ of the second baroclinic structure (Figure 5.8) also presents a conspicuous positive correlation for positive lags, but positive energy anomalies in this mode may be also associated with an upscale energy transfer to the modes that forces the vortex.

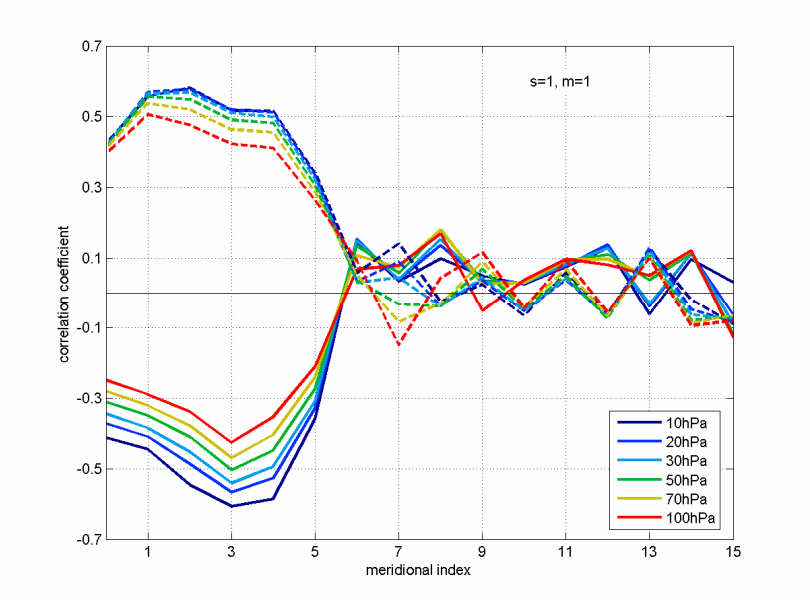

Figure 5.7 – Lagged correlations between the energy associated to Rossby modes with wavenumber *s=1* and baroclinic structure *m=1* and the NAM indices at the same six levels in the stratosphere. Solid (dashed) curves show the largest anticorrelations or correlations for positive (negative) lags.

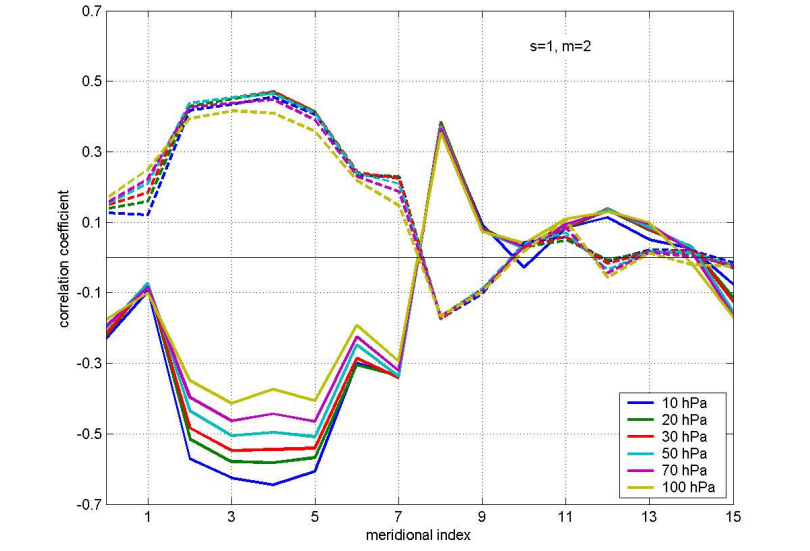

Figure 5.8 – As in Figure 5.7 but for wave energy associated with wavenumber *s=1 m=2*.

As pointed out above, positive correlations in Figures 5.5 and 5.6 may reflect a stratospheric vacillation (see also Figure 5.9), but since the vortex strength is leading, such positive values may also be due to some other effect of the vortex. In this respect, we note that the obtained maximum correlation for $s = 1$ and $m = 1$ (Figure 5.7) occurs for meridional indices $l = 1$ and 2, a feature that may be the result of equatorward wave refraction during the strong vortex period.

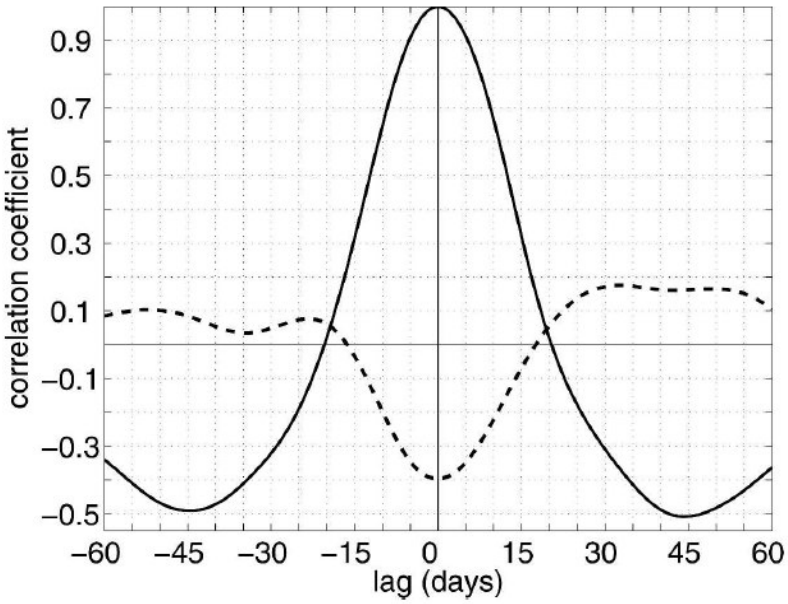

Figure 5.9 – Time change in energy associated to Rossby modes with wavenumber $s = 1$ and baroclinic structure $m = 2$. Solid line represents the autocorrelation of the sum of energy associated with meridional indices $l = 2, 3, 4$ and 5. Dashed line represents the lagged correlations between the sum of energy of the same meridional indices and the energy of the Rossby mode with meridional index $l = 8$.

5.3.1.3. SSW events

As specified in Table 3.1, we have separately analyzed the energy composites for displacement- and split-type SSW events and it is worth noting that both composites correspond to daily intraseasonal anomalies without any smoothing. Figure 5.10 shows the composite for displacement-type SSW events and it is apparent that such events are preceded by a period of about one month of statistically significant (at the 5% level) positive anomalies of the energy associated with the baroclinic modes $m = 1$ and $m = 2$ of zonal wavenumber 1. Circa one week after the event's central date, the baroclinic component $m = 1$ presents statistically significant (at the 5% level) negative anomalies that remain until the end of the study period. A general positive trend may be observed in the barotropic component ($m = 0$) of wavenumber 2, and a general negative trend is apparent in the barotropic component of zonal wavenumber 1. These results are consistent with the findings by Charlton and Polvani [2007] for the composites of meridional heat flux.

Statistical significance was determined using the method described in section 3.3.7. Statistical significance of anomalies in the energy composites was assessed by means of 1,000 random composites. Each composite was built up by randomly choosing n central dates (day 0) from the winter period between the earliest observed SSW event and the latest one. For each composite day the 2.5, 5, 95, and 97.5 percentiles were determined from the 1,000 random samples.

Data multiplicity was taken into account by building up a new set of 1,000 random composites and then evaluating the percentage of composites with a statistically significant (at the 5% level) number of days larger than the observed ones. Table 5.1 shows the obtained percentages that are given separately for the positive and the negative anomalies. Cases where the percentage of random composites is smaller than 5% are shown in boldface.

Table 5.1 – Percentages of random composites that have a number of statistically significant (at 5% level) positive (negative) anomalies greater than the obtained number of statistically significant positive (negative) anomalies in the observed composite of displacement-type SSW events. Cases where the percentage of random composites is smaller than 5% are shown in boldface.

	Positive Anomalies			**Negative Anomalies**		
	m=0	*m=1*	*m=2*	*m=0*	*m=1*	*m=2*
s=1	100	**0.0**	**0.0**	100	**0.7**	6.0
s=2	100	100	100	38.3	100	100

As shown in Figure 5.11, composites for split-type SSW events suggest a different dynamics from the ones of displacement-type SSW events. In this case both wavenumbers 1 and 2 seem to play an important role and a precursor of such events, associated with positive (negative) energy anomalies of the baroclinic $m = 1$ (barotropic $m = 0$) components of zonal wavenumber 1, seems to take place during the period from about 30 to 15 days before the central date. It may be possible that early wavenumber 1 energy anomalies are associated with a deceleration of the stratospheric jet, setting the conditions for wavenumber 2 propagation into the polar region. However, the present analysis cannot rule out the possibility of a downscale energy transfer due to nonlinear wave interactions. Following such preconditioning, split-type SSW events evolve with an increase of energy associated with the barotropic and the baroclinic components of wavenumber 2, during a period of about 15 days before the event central's date. Afterward, the baroclinic components of both wavenumbers 1 and 2 present statistically significant (at the 5% confidence level) negative anomalies. Finally, the observed drastic change in the sign of anomalies of the barotropic component of wavenumber 2, from negative to positive lags, is particularly worth noting since it gives an indication of drastic changes in the energetics of the tropospheric circulation before and after the central dates of split-

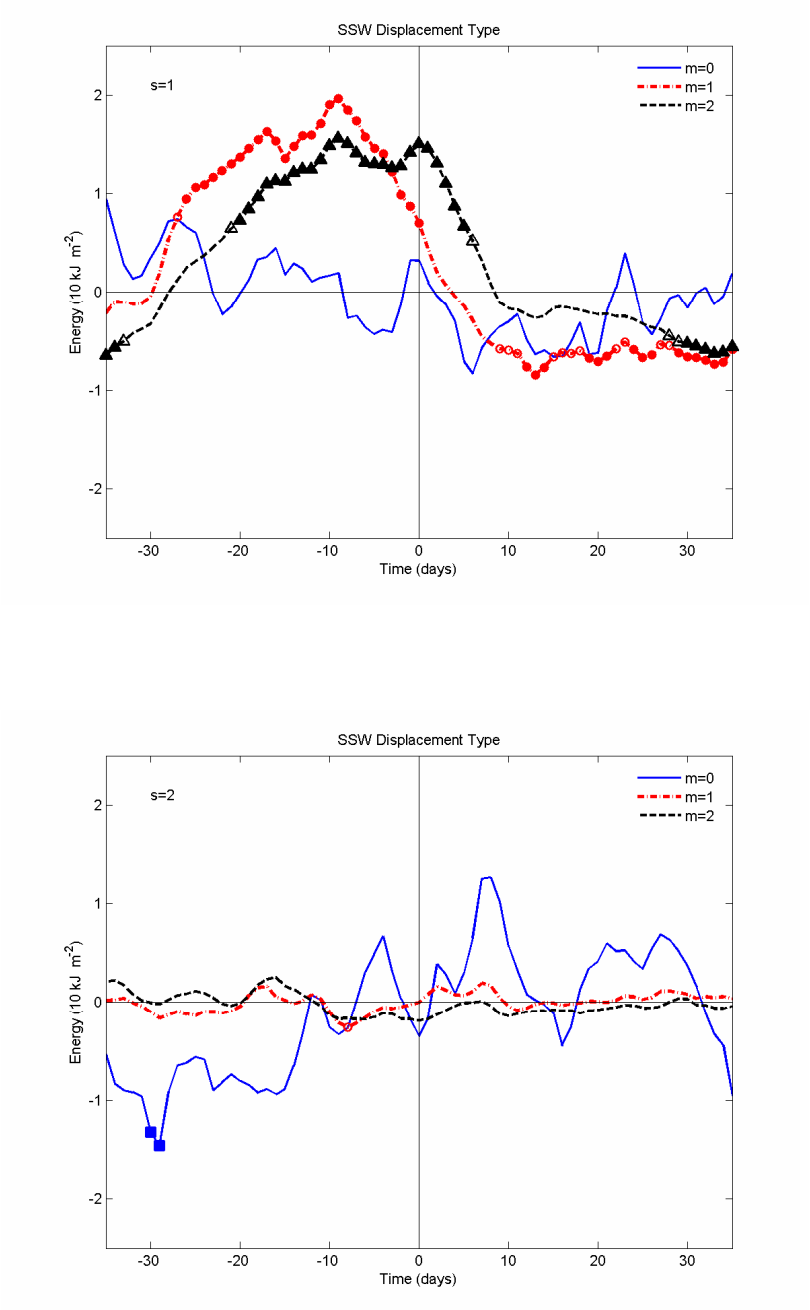

Figure 5.10 – Daily composites of intraseasonal anomalies of wave energy for SSW events of the displacement type (*top s = 1*; and *bottom s = 2*). Day 0 refers to the central date of the event. Solid (open) symbols identify mean values of intraseasonal anomalies that statistically differ from zero at the 5% (10%) significance level.

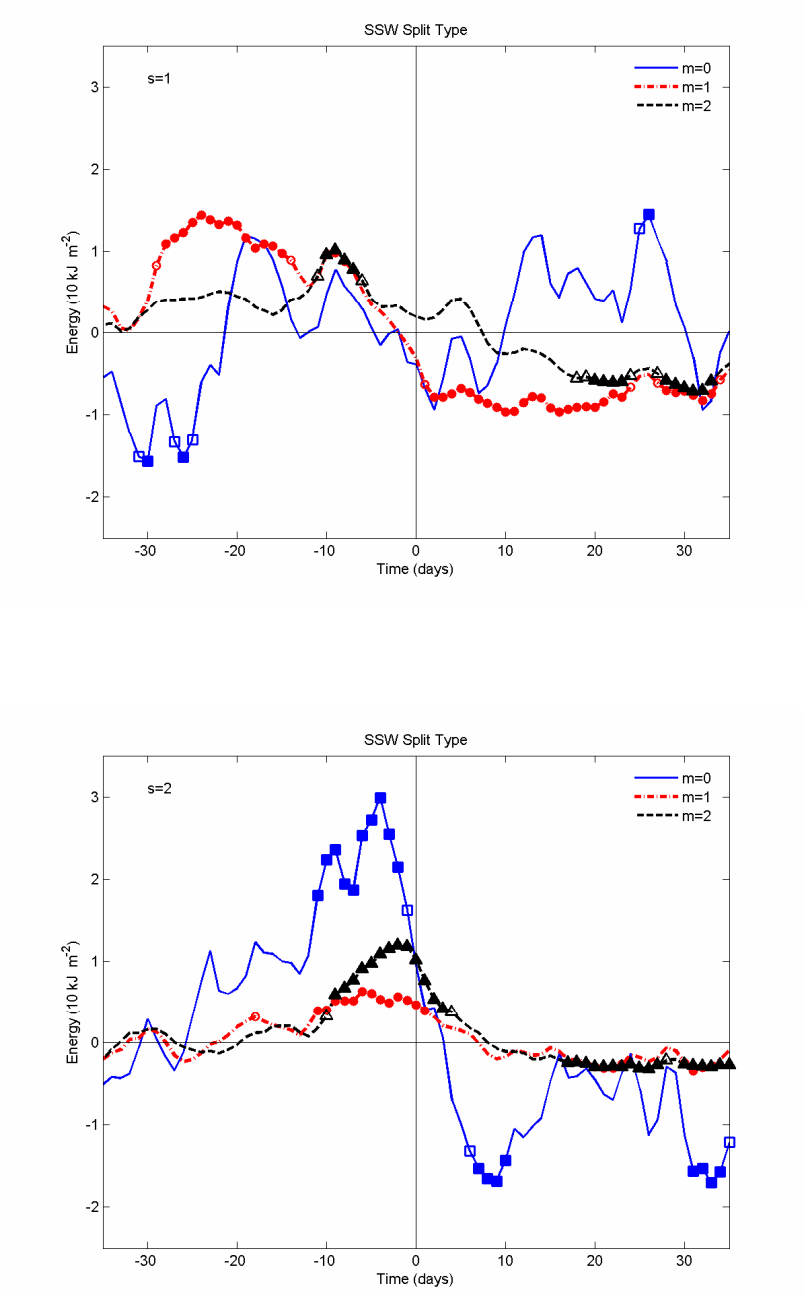

Figure 5.11 – Daily composites of intraseasonal anomalies of wave energy for SSW events of the split type (*top s = 1*; and *bottom s = 2*). Day 0 refers to the central date of the event. Solid (open) symbols identify mean values of intraseasonal anomalies that statistically differ from zero at the 5% (10%) significance level.

type SSW events. This result agrees with those of Nakagawa and Yamazaki [2006] already described, who have shown that during the growth stage of SSW events that propagate into the troposphere, there is an enhanced upward flux of energy associated with wavenumber 2. Obtained results also support the findings of Charlton and Polvani [2007] (see their conclusions – points 1 and 2 in section 5.2), but it is worth stressing that our analysis points to the possible different nature of the tropospheric impacts by displacement- and split-type SSW events.

Table 5.2 shows the statistical significance of the composites of split-type SSWs taking into account data multiplicity.

Table 5.2 – Same as in Table 5.1, but for the split-type SSW events.

	Positive Anomalies			**Negative Anomalies**		
	m=0	*m=1*	*m=2*	*m=0*	*m=1*	*m=2*
s=1	53.7	**1.3**	20.9	38.0	**0.0**	**4.1**
s=2	**2.1**	**0.8**	**1.0**	**2.7**	9.9	**0.1**

5.3.2. SFW events

Figure 5.12 presents the energy composites that were obtained for the considered set of the 19 earliest SFW events having occurred before 11 April. In case of zonal wavenumber 1, it is well apparent that SFW events are preceded by statistically significant (at the 5% level) positive energy anomalies of the first two baroclinic components (*m = 1* and *2*), which concentrate into two distinct periods of time. This feature is in strong agreement with the findings of Black et al. [2006] who have

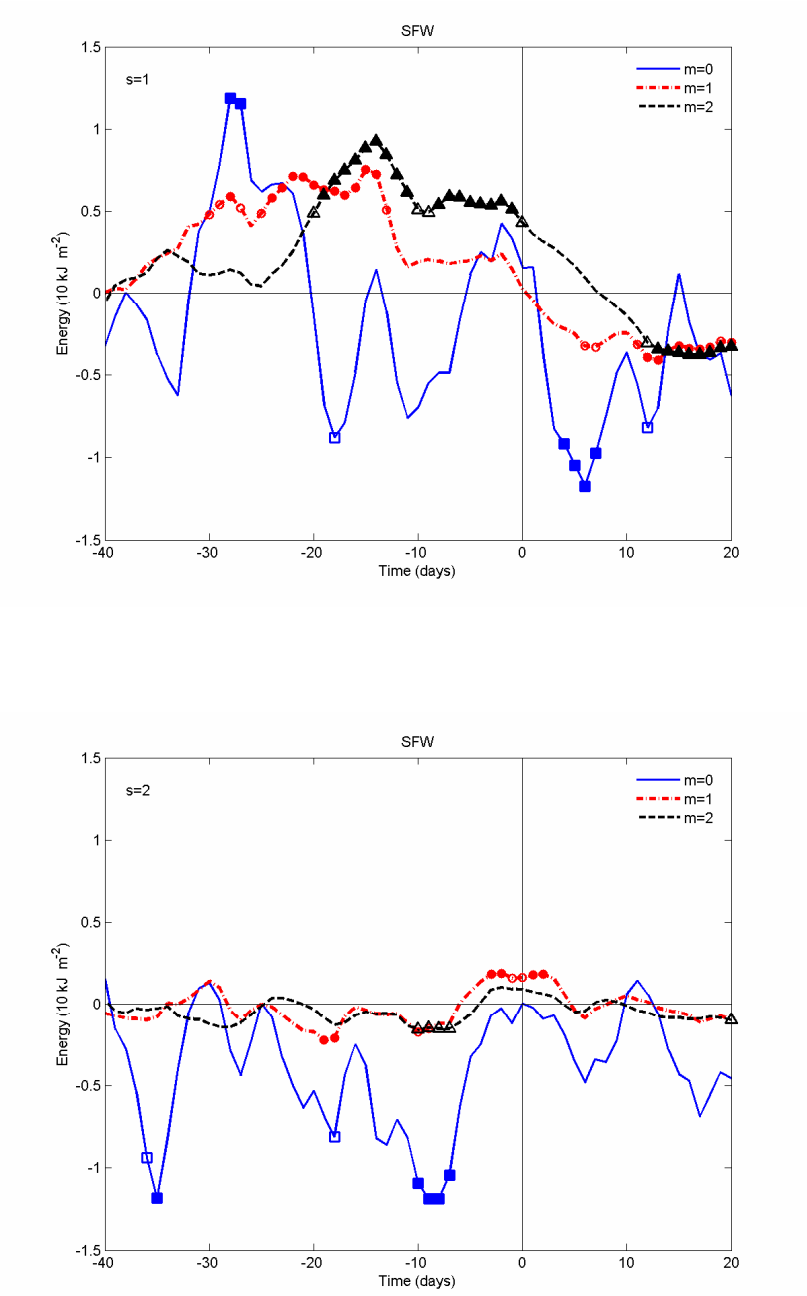

Figure 5.12 – Daily composites of intraseasonal anomalies of wave energy for SFW events (*top s = 1*; and *bottom s = 2*). Day 0 refers to the central date of the event. Solid (open) symbols identify mean values of intraseasonal anomalies that statistically differ from zero at the 5% (10%) significance level.

identified two periods of strong vortex deceleration (see their Figure 2) that coincide with two distinct bursts of upward EP flux (see their Figure 3). In particular it is worth noting that the observed positive anomaly of the second baroclinic Rossby mode during the second deceleration period (*i.e.* the time interval where the anomalies of *m= 2* are the only statistically significant ones) is also in agreement with the results of Black et al. [2006]. Indeed, the second deceleration period in their Figure 2 is characterized by easterly zonal mean zonal wind in the upper stratosphere and westerly zonal wind in the lower stratosphere, a vertical structure that is well captured by the baroclinic component *m = 2*. The statistical significance of the SFW composites is shown in Table 5.3.

Table 5.3 – Same as in Table 5.1, but corresponding to SFW events.

	Positive Anomalies			**Negative Anomalies**		
	m=0	*m=1*	*m=2*	*m=0*	*m=1*	*m=2*
s=1	35.2	**1.5**	**0.2**	18.0	**5.0**	5.8
s=2	100	17.8	100	10.2	40.5	100

Finally, a comparison of Figures 5.10 and 5.12 suggests that the wave dynamics of SFW events presents some similarities to the displacement-type SSW events. Both events seem to be forced by means of an increase of energies associated with the baroclinic Rossby modes (*m = 1* and *2*) of planetary wavenumber 1. Positive anomalies of the energy are observed during the 30 days before the events, and there is a trend of the energy associated with the barotropic Rossby mode of wavenumber 1 to decrease during the evolution of the events.

6. CONCLUSIONS

The annular nature of the leading patterns of the NH winter extratropical circulation variability is revisited, and evidence is presented of the separation of both components of annular and non-annular variability. The analysis relies on a PCA of tropospheric geopotential height fields followed by lagged correlations of leading Principal Components with the stratospheric polar vortex strength as well as with a *proxy* of midlatitude tropospheric zonal mean zonal momentum anomalies.

Obtained results suggest that processes, occurring at two different times, may contribute to the NAM spatial structure. Polar vortex anomalies appear positively correlated with midlatitude tropospheric zonal mean zonal wind anomalies that occur before the stratospheric anomalies. Following the polar vortex anomalies, zonal mean zonal wind anomalies of the same sign are observed in the troposphere at high latitudes. The time scale separation of the two signals is of about two weeks. As it is well known, the PCA criterion for the identification of the leading PC is the maximization of the represented data variability. Then, our results suggest that, in the case of tropospheric circulation, that maximization is achieved with the variability associated with the two above processes projecting on the leading EOF pattern. The ‘‘accumulation’’ or ‘‘deficit’’ of zonal mean zonal momentum at midlatitudes confers the annular character to the leading patterns in those latitudes, and the ‘‘response’’ to vortex variability confers the annularity at high latitudes.

To separate the processes discussed above, the geopotential height fields were linearly regressed on the 500-hPa zonal mean zonal wind anomaly averaged in the latitudinal band 45º–55ºN (U_{500} (45–55) index). Residual geopotential height fields were defined as the geopotential height field minus the variability linearly regressed on the U_{500} (45–55) index. Then, a PCA of the residual geopotential fields was performed, and the lagged correlations with the polar night jet were recalculated. It is worth noting that subtracting the variability linearly dependent on the U_{500} (45-55) index does not necessarily mean removing a dynamical zonally symmetric component. In fact, the

correlation between the time series of the midlatitude (45º–55º N) zonal wind strengths over the East Asia/Pacific sector (120ºE, 240º E) and over the Atlantic sector (90ºW, 40ºE) is very close to zero (r = 0.02).

The leading EOF patterns of the residual variability, which seem to respond to the vortex variability have a hemispheric scale but only show a dipolar structure over the Atlantic basin like the NAO. The annularity of this pattern is clearly an imprint of the Arctic center as referred by Deser [2000]. These findings agree with the results of Feldstein and Franzke [2006] which suggest that neither the NAO events are confined to the North Atlantic, nor NAM events are annular.

It is worth noting that the leading EOF patterns of the residual variability, which seem to respond to the vortex variability, have a hemispheric scale showing only a dipolar structure over the Atlantic basin that resembles NAO. These findings agree with the results of Feldstein and Franzke [2006] which suggest that neither NAO events are confined to the North Atlantic, nor NAM events are annular.

It is worth stressing that the separation of the two processes that contribute for tropospheric NAM is especially relevant in studies of the tropospheric response to changes originated in the stratosphere, *e.g.* changes in stratospheric chemical composition and related global climate change. NAM indices represent zonally symmetric zonal wind anomalies which spread from mid to high latitudes, whereas the annularity of tropospheric response to stratospheric anomalies is confined to high latitudes.

PCA was also applied to data that were previously filtered by means of a 3D normal mode decomposition scheme of the atmospheric circulation, a procedure that allows selecting both the most important zonal wavenumbers and meridional scales. For instance Castanheira et al. [2002] have uncovered horizontal patterns of atmospheric circulation variability by means of a PCA performed on the time series of the projection coefficients.

Accordingly, a PCA was performed on the variability of the 31-day running averages

of the barotropic zonally symmetric circulation of the NH for the cold season (November-March). Leading EOF represents one half (50.4%) of the total variance, which is statistically distinct from the remaining variability. The second EOF represents 23.3% of the total variance. The daily time series of circulation anomalies projected onto the leading EOF is highly correlated ($r \geq 0.7$) with the lower stratosphere annular mode indices, showing that the annular variability extends from the stratosphere deep into the troposphere. However, the analysis also reveals differences between the zonally symmetric components of the annular modes defined at single isobaric tropospheric levels (EOF1) and the meridional profile of EOF1 of the barotropic zonally symmetric circulation. It is shown that the annular modes defined at single isobaric tropospheric levels (EOF1) represent a much larger fraction of zonally symmetric variability at midlatitudes than the one represented by the EOF1 of barotropic zonally symmetric circulation. The zonally symmetric component of the 500-hPa geopotential height regressed onto the lower stratosphere (70-hPa) NAM also reveals the same differences with the zonally symmetric components of the annular modes defined at single isobaric tropospheric levels (EOF1). Therefore it may be concluded that a large fraction of midlatitude zonally symmetric variability, as represented by the leading EOF at single isobaric tropospheric levels, is not linearly associated with the stratospheric variability.

A PCA was also performed on the residual variability of 500-hPa geopotential that remained after regressing out the 70-hPa NAM index. The leading EOF of such variability reveals the PNA teleconnection pattern associated with a secondary wave train over the Atlantic and Eurasia. The second EOF has a zonally symmetric component similar to the one of the leading EOF of the total variability and is the imprint of two meridional dipoles over the Pacific and the Atlantic oceans. Only a very small fraction (less than 4%, $|r| < 0.2$) of the variability over each ocean basin is correlated with the variability of the northern centre of the meridional dipole in the opposite ocean basin. Results from the analysis of the 1000-hPa geopotential height field are consistent with those from the analysis of the 500-hPa geopotential height

field. The Pacific and Atlantic centres of the leading EOF of the 1000-hPa geopotential height residual field do not belong to a common three-centre teleconnection pattern. These results show that the midlatitude annular imprint on the leading EOFs of the 500- and 1000-hPa geopotential height total fields is strongly exaggerated by the PCA method, based on a criterion of maximizing the represented variance integrated over the analyzed domain. In fact, the zonal mean zonal wind anomalies over each northern ocean are positively correlated only at high latitudes.

No zonally symmetric coherent variability was found in the residual tropospheric circulation. Hence the zonally symmetric coherent variability of the extratropical tropospheric circulation appears to be always coupled with the stratospheric annular variability. By construction, the leading EOF of the barotropic zonally symmetric circulation explicitly takes this coupling into account. However, because the barotropic component is approximately given by a vertical mass-weighted average of the atmospheric circulation, it is much more sensitive to tropospheric variability. On the other hand, the leading EOFs of total geopotential fields at single isobaric levels show midlatitude zonally symmetric components which are strongly exaggerated by variability due to local dynamics. This does not seem to be the case of the leading EOF of the barotropic zonally symmetric circulation which represents a weaker annular component in midlatitudes. Taken together, these results suggest that projections onto the leading EOF of the barotropic zonally symmetric circulation may provide a better index for the annular behaviour in the troposphere than projections onto the leading EOFs of geopotential fields at single isobaric levels (NAM indices).

It is worth remarking again that tropospheric NAM indices do not seem to be appropriate to represent the zonally symmetric circulation response to climate changes. In fact, as already stressed, the zonally symmetric component of the leading EOF of the isobaric geopotential height field in the troposphere is, at least to a great extent, the imprint of independent dipolar structures over the ocean basins. These results are particularly important for studies of the tropospheric response to changes originating in the stratosphere, *e.g.* changes in stratospheric chemical composition.

Use of indices based on the leading EOF of tropospheric geopotential height field may in turn imply some artificial impact at midlatitudes.

We have also looked at the problem of the variability of the stratospheric polar vortex from the point of view of planetary wave energetics. Our analysis differs from traditional methods in that we have concentrated on a diagnosis of the energy associated with the forcing waves instead of analyzing Eliassen–Palm fluxes. Another difference from previous studies relates to the fact that instead of being restricted to the extratropical subdomain, our analysis is applied to the whole atmosphere, and the relevant circulation components are selected by means of projections onto 3D global functions that allow partitioning the atmospheric (global) circulation into planetary Rossby waves and inertio–gravity waves with barotropic and baroclinic vertical structures.

We have found that positive (negative) anomalies of the energy associated with the first two baroclinic Rossby modes $m = 1$ and $m = 2$ of planetary wave $s = 1$ are followed by the downward progression of negative (positive) anomalies of the vortex strength. A signature of the vortex vacillation is also well apparent in the lagged correlation curves between the wave energy and the vortex strength. The analysis of the correlations between individual Rossby modes and the vortex strength further confirmed the result from linear theory that the waves that force the vortex are those associated with the largest zonal and meridional scales.

Composites of SSW events of both displacement- and split-types were finally analysed, revealing different dynamics. Displacement-type SSW events are forced by positive anomalies of the energy associated with the first two baroclinic Rossby modes $m = 1$ and $m = 2$ of planetary zonal wavenumber $s = 1$. On the other hand, split-type SSW events are forced by positive anomalies of the energy associated with planetary zonal wavenumber $s = 2$. Besides, the barotropic Rossby component of wavenumber $s = 2$ has revealed a strong anomaly signal of opposite sign before and after the central date of the event, suggesting that the tropospheric circulation plays an

important role in the activation of split-type SSW events, and that, after the events, anomalies propagate down to the troposphere [Nakagawa and Yamazaki 2006]. In the case of split-type SSW events, a preconditioning of the stratospheric circulation seems to take place three weeks before the event as suggested by the observed behaviour of the anomalies of the baroclinic Rossby modes of zonal wavenumber $s = 1$. In the case of SFW events, obtained results closely agree with the findings of Black et al. [2006] and there is evidence that composites of SFW events exhibit an overall similar behaviour to the ones observed in composites of the displacement-type SSW events.

REFERENCES

Ambaum, M. H. P., and B. J. Hoskins, 2002: The NAO Troposphere-Stratosphere Connection. J. Climate, 15, 1969–1978.

Ambaum, M. H. P., B. J. Hoskins, and D. B. Stephenson, 2001: Arctic Oscillation or North Atlantic Oscillation? J. Climate, 14, 3495–3507.

Andrews, D. G., J. R. Holton, and C. B. Leovy, 1987: Middle Atmosphere Dynamics. Academic Press, 489 pp.

Baldwin, M. P., and T. J. Dunkerton, 2001: Stratospheric harbingers of anomalous weather regimes. Science, 294, 581–584.

Baldwin, M. P., D. B. Stephenson, D. W. J. Thompson, T. J. Dunkerton, A. J. Charlton, and A. O'Neill, 2003: Stratospheric Memory and Skill of Extended-Range Weather Forecasts. Science, 301, 636–640.

Baldwin, M. P., X. Cheng and T. J. Dunkerton, 1994: Observed correlations between winter-mean tropospheric and stratospheric circulation anomalies, Geophys. Res. Lett., 21, 1141–1144.

Baldwin, M. P., and T.J. Dunkerton, 1999: Propagation of the Arctic Oscillation from the stratosphere to the troposphere. J. Geophys. Res., 104, 30937–30946.

Barnett, T. P., 1985: Variations in near-global sea level pressure. J. Atmos. Sci., 42, 478–501.

Barnston, A. G., and R. E. Livezey, 1987: Classification, seasonality, and persistence of the low-frequency atmospheric circulation patterns. Mon. Wea. Rev., 115, 1083–1126.

Bjerknes, J. , 1969: Atmospheric teleconnections from the equatorial Pacific, Mon. Wea. Rev., 97, 163–172.

Black, R. X., 2002: Stratospheric forcing of surface climate in the Arctic Oscillation. J. Climate, 15, 268–277.

Black, R. X., B. A. McDaniel, and W. A. Robinson, 2006: Stratosphere–troposphere coupling during spring onset. J. Climate, 19, 4891–4901.

Black, R. X., and B.A. McDaniel, 2004: Diagnostic case studies of the Northern Annular Mode. J. Climate, 17, 3990-4004.

Black, R. X., and B. A. McDaniel, 2006: The Polar Annular Mode: Submonthly Stratosphere-Troposphere coupling in the Arctic. Geophys. Res. Lett. (submitted).

Bretherton, C. S., C. Smith, and J. M. Wallace, 1992: An intercomparison of methods for finding coupled patterns in climate data. J. Climate, 5, 541–560.

Castanheira J. M., M. L. R. Liberato, L. de la Torre, H.-F. Graf, and A. Rocha, 2008: Annular versus non-annular variability of the Northern Hemisphere atmospheric circulation. J. Climate (in press, accepted on 07/12/2007).

Castanheira, J. M., 2000: Climatic variability of the atmospheric circulation at the global scale. Ph. D. Thesis, University of Aveiro, Portugal, 186 pp.

Castanheira, J. M., and H.-F. Graf, 2003: North Pacific–North Atlantic relationships under stratospheric control? J. Geophys. Res., 108, 4036–4045, doi:10.1029/2002JD002754.

Castanheira, J. M., C. C. DaCamara, and A. Rocha, 1999: Numerical solutions of the vertical structure equation and associated energetics. Tellus, 51A, 337–348.

Castanheira, J. M., H.-F. Graf, C. DaCamara, and A. Rocha, 2002: Using a physical reference frame to study global circulation variability. J. Atmos. Sci., 59, 1490–1501.

Castanheira, J. M., M. L. R. Liberato, C. A. F. Marques, and H.-F. Graf, 2007: Bridging the Annular Mode and North Atlantic Oscillation paradigms. J. Geophys. Res., 112, D19103, doi:10.1029/2007JD008477.

Charlton, A. J., and L. M. Polvani, 2007: A new look at stratospheric sudden warmings. Part I: Climatology and modelling benchmarks. J. Climate, 20, 449–469.

Charney, J. G., and P. G. Drazin, 1961: Propagation of planetary-scale disturbances

from the lower into the upper atmosphere. J. Geophys. Res., 66, 83–109.

Chen, P., and W. A. Robinson, 1992: Propagation of planetary waves between the troposphere and stratosphere. J. Atmos. Sci., 49, 2533–2545.

Cheng, X., and T. J. Dunkerton, 1995: Orthogonal rotation of spatial patterns derived from singular value decomposition analysis. J. Climate, 8, 2631–2643.

Christiansen, B., 2001: Downward propagation of zonal mean zonal wind anomalies from the stratosphere to the troposphere: Model and reanalysis. J. Geophys. Res., 106, 27307–27322.

Christiansen, B., 2002: On the physical nature of the Arctic Oscillation. Geophys. Res. Lett., 29 (16), 10.1029/2002GL015208.

Daley, R., 1991: Atmospheric Data Analysis. Cambridge University Press, 457 pp.

Deser, C., 2000: On the teleconnectivity of the "Arctic Oscillation". Geophys. Res. Lett., 27, 779–782.

DeWeaver E., and S. Nigam, 2000: Do stationary waves drive the zonal-mean jet anomalies of the northern winter? J. Climate, 13, 2160–2176.

Dickinson, R. E., 1968: Planetary Rossby Waves Propagating Vertically Through Weak Westerly Wind Wave Guides. J. Atmos. Sci., 25, 984–1002.

Dole, R. M., 1986: Persistent anomalies of the extratropical Northern Hemisphere wintertime circulation: Structure. Mon. Wea. Rev., 114, 178–207.

Dommenget, D. and M. Latif, 2002: A Cautionary Note on the Interpretation of EOF. J. Climate, 15, 216–225.

Eichelberger, S. J., and J. R. Holton, 2002:, A mechanistic model of the northern annular mode, J. Geophys. Res., 107(D19), 4388, doi:10.1029/2001JD001092

Feldstein, S. B., 2000: Is interannual zonal mean flow variability simply climate noise? J. Climate, 13, 2356–2362.

Feldstein, S. B., 2000: The timescale, power spectra, and climate noise properties of

teleconnection patterns. J. Climate, 13, 4430–4440.

Feldstein, S. B., and C. Franzke, 2006: Are the North Atlantic Oscillation and the Northern Annular Mode Distinguishable? J. Atmos. Sci., 63, 2915–2930.

Feldstein, S. B., and W. A. Robinson, 1994: Comments on 'Spatial structure of ultra-low frequency variability of the flow in a simple atmospheric circulation model.' Quart. J. Roy. Meteor. Soc., 120, 739–745.

Geller, M.A., and J.C. Alpert, 1980: Planetary wave coupling between the Troposphere and the Middle Atmosphere as a possible sun-weather mechanism. J. Atmos. Sci., 37, 1197–1215.

Gerber, E. P., and G. K. Vallis, 2005: A stochastic model for the spatial structure of annular pattern of variability and the North Atlantic Oscillation. J. Climate, 18, 2102–2118.

Glowienka-Hense, R., 1990: The North Atlantic Oscillation in the Atlantic-European SLP. Tellus, 42A, 497–507.

Gong, D., and S. Wang, 1999: Definition of the Antarctic oscillation index. Geophys. Res. Lett., 26, 459–462.

Graf, H.-F., J. Perlwitz, and I. Kirchner, 1994: Northern Hemisphere tropospheric mid-latitude circulation after violent volcanic eruptions, Contr. Atm. Phys., 67, 3–13.

Graf, H.-F., J. Perlwitz, I. Kirchner, and I. Schult, 1995: Recent northern winter climate trends, ozone changes, and increased greenhouse forcing. Contrib. Atmos. Phys., 68, 233–248.

Hartmann, D. L., J. M. Wallace, V. Limpasuvan, D. W. J. Thompson, and J. R. Holton, 2000: Can ozone depletion and global warming interact to produce rapid climate change? Proc. Natl. Acad. Sci. USA, 97, 1412–1417.

Haynes, P. H., 2005: Stratospheric dynamics. Ann. Rev. Fluid Mech., 37,263–293.

Haynes, P. H., C. J. Marks, M. E. McIntyre, T. G. Shepherd, and K. P. Shine, 1991:

On the ‘‘downward control’’ of extratropical diabatic circulations by eddy-induced mean zonal forces. J. Atmos. Sci., 48, 651–679.

Hines, C. O., 1974: A possible mechanism for the production of sun-weather correlations. J. Atmos. Sci., 31, 589–591.

Holton J. R., P. H. Haynes, M. E. McIntyre, A. R. Douglass, R. B. Rood, L. Pfister, 1995: Stratosphere–troposphere exchange. Rev. Geophys., 33, 403–39.

Holton, J. R., 1976: Semi-spectral numerical-model for wave-mean flow interactions in stratosphere – application to sudden stratospheric warmings. J. Atmos. Sci., 33, 1639–1649.

Holton, J. R., and C. Mass, 1976: Stratospheric vacillation cycles. J. Atmos. Sci., 33, 2218–2225.

Holton, J. R., and H.-C. Tan, 1980: The influence of the equatorial quasi-biennal oscillation on the global circulation at 50 mb. J. Atmos. Sci., 37, 2200–2208.

Honda, M., and H. Nakamura, 2001: Interannual Seesaw between the Aleutian and Icelandic Lows. Part II: Its Significance in the Interannual Variability over the Wintertime Northern Hemisphere. J. Climate, 14, 4512–4529.

Horel, J. D., and J. M. Wallace, 1981: Planetary-scale atmospheric phenomena associated with the Southern Oscillation. Mon. Wea. Rev., 109, 813–829.

Hoskins, B. J., and D. Karoly, 1981: The steady linear response of a spherical atmosphere to thermal and orographic forcing. J. Atmos. Sci., 38, 1179–1196.

Hurrell, J. W., 1995: Decadal trends in the North Atlantic Oscillation: Regional temperatures and precipitation, Science, 269, 676-679.

Hurrell, J. W., 1996: Influence of variations in extratropical wintertime teleconnections on Northern Hemisphere temperature, Geophys. Res. Lett., 83, 665-668.

Jolliffe, I. T., 1986: Principal Component Analysis. Springer-Verlag, 290 pp.

Juckes M. N. , and M. E. McIntyre, 1987: A high resolution, one-layer model of breaking planetary waves in the stratosphere. Nature, 328, 590–596.

Kalnay, E., and Coauthors, 1996: The NCEP/NCAR 40-Year Reanalysis Project. Bull. Amer. Meteor. Soc., 77, 437–471.

Kasahara, A., and K. Puri, 1981: Spectral representation of three-dimensional global data by expansion in normal mode functions. Mon. Wea. Rev. 109, 37–51.

Kistler R., and Coauthors, 2001: The NCEP–NCAR 50-Year Reanalysis: Monthly means CD-ROM documentation. Bull. Amer. Meteor. Soc., 82, 247–267.

Kitoh, A., H. Koide, K. Kodera, S. Yukimoto and A. Noda, 1996: Interannual variability in the stratospheric-tropospheric circulation in a coupled ocean-atmosphere GCM, Geophys. Res. Lett., 23, 543-546.

Kodera, K., 1993: Quasi-Decadal Modulation of the Influence of the Equatorial Quasi-Biennial Oscillation on the North Polar Stratospheric Temperatures, J. Geophys. Res., 98(D4), 7245–7250.

Kodera, K., 1994: Influence of volcanic eruptions on the troposphere through stratospheric dynamical processes in the Northern Hemisphere winter. J. Geophys. Res., 99, 1273–1282.

Kodera, K., and H. Koide, 1997: Spatial and seasonal characteristics of recent decadal trends in the northern hemisphere troposphere and stratosphere. J. Geophys. Res., 102, 19433–19447.

Kodera, K., and K. Yamazaki, 1994: A possible influence of recent polar stratospheric coolings on the troposphere in the Northern Hemisphere winter, Geophys. Res. Lett., 21, 809–812.

Kodera, K., H. Koide, and H. Yoshimura, 1999: Northern Hemisphere winter circulation associated with the North Atlantic Circulation and the stratospheric polar-night jet, Geophys. Res. Lett., 26, 443–446.

Kodera, K., M. Chiba, H. Koide, A. Kitoh, and Y. Nikaidou, 1996: Interannual variability of the winter stratosphere and troposphere in the Northern Hemisphere. J. Met. Soc. Japan, 74, 365–382.

Kodera, K., Y. Kuroda, and S. Pawson, 2000: Stratospheric sudden warmings and slowly propagating zonal mean zonal wind anomalies. J. Geophys. Res., 105, 12 351–12 359.

Kuroda Y., and K. Kodera, 1999: Role of planetary waves in the stratosphere–troposphere coupled variability in the Northern Hemisphere winter. Geophys. Res. Lett, 26, 2375–2378.

Kushnir, Y., and J. M. Wallace, 1989: Low-frequency variability in the Northern Hemisphere winter: Geographical distribution, structure and time-scale dependence. J. Atmos. Sci., 46, 3122–3142.

Kutzbach, J. E., 1970: Large-scale features of monthly mean Northern Hemisphere anomaly maps of sea-level pressure, Mon. Wea. Rev., 98, 708–716.

Kutzbach, J., 1967: Empirical eigenvectors of sea level pressure, surface temperature, and precipitation complexes over North America. J. Appl. Meteor., 6, 791–802.

Labitzke, K., 1977: Interannual Variability of the Winter Stratosphere in the Northern Hemisphere. Mon. Wea. Rev., 105, 762–770.

Labitzke, K., 1982: On the interannual variability of the middle stratosphere during the northern winters. J. Meteor. Soc. Japan, 60, 124–139.

Leith, C. E., 1973: The standard error of time-average estimates of climatic means. J. Appl. Meteor., 12, 1066–1069.

Liberato, M.L.R., J.M. Castanheira, L. de la Torre, C.C. DaCamara, and L. Gimeno, 2007: Wave Energy Associated with the Variability of the Stratospheric Polar Vortex. J. Atmos. Sci., 64, 2683–2694.

Limpasuvan, V., D. L. Hartmann, D. W. J. Thompson, K. Jeev, and Y. L. Yung, 2005:

Stratosphere-troposphere evolution during polar vortex intensification. J. Geophys. Res., 110, D24101, doi:10.1029/2005JD006302.

Limpasuvan, V., D. W. J. Thompson, and D. L. Hartmann, 2004: The life cycle of the Northern Hemisphere sudden stratospheric warmings. J. Climate, 17, 2584–2596.

Livezey, R. E., and W. Chen, 1983: Statistical Field Significance and its Determination by Monte Carlo Techniques. Mon. Wea. Rev., 111, 46–59.

Longuet-Higgins, M. S., 1968: The eigenfunctions of Laplace's tidal equations over a sphere. Philos. Trans. Roy. Soc. London, A262, 511–607.

Lorenz, E. N., 1951: Seasonal and irregular variations of the Northern Hemisphere sea-level pressure profile. J. Atmos. Sci., 8, 52–59.

Lorenz, E. N., 1956: Empirical orthogonal functions and statistical weather prediction, Rep. 1, Statist. Forecasting Project, MIT, 49pp.

Madden, R. A., 1976: Estimates of the natural variability of time averaged sea level pressure. Mon. Wea. Rev., 104, 942–952.

Manney, G. L., K. Kruger, J. L. Sabutis, S. A. Sena, and S. Pawson, 2005: The remarkable 2003–2004 winter and other recent warm winters in the Arctic stratosphere since the late 1990s. J. Geophys. Res., 110, D04107, doi:10.1029/2004JD005367.

Nakamura, H., M. Tanaka, and J. M. Wallace, 1987: Horizontal structure and energetics of Northern Hemisphere winter teleconnection patterns. J. Atmos. Sci., 44, 3377–3391.

Mantua, N., S. Hare, Y. Zhang, J. Wallace, and R. C. Francis, 1997: A Pacific interdecadal climate oscillation with impacts on salmon production. Bull. Amer. Meteor. Soc., 78, 1069–1079.

Matsuno, T., 1970: Vertical Propagation of Stationary Planetary Waves in the Winter Northern Hemisphere. J. Atmos. Sci., 27, 871–883.

Matsuno, T., 1971: A dynamical model of the stratospheric sudden warming. J. Atmos. Sci., 28, 1479–1494.

McDaniel, B. A., and R. X. Black, 2005: Intraseasonal dynamical evolution of the Northern Annular Mode. J. Climate, 18, 3820–3839.

McIntyre M. E., 1982: How well do we understand the dynamics of stratospheric warmings? J. Meteorol. Soc. Japan, 60, 37–65.

McIntyre M. E., 2003a: Balanced flow. In Encyclopedia of Atmospheric Sciences, vol. 2, ed. JR Holton, JA Pyle, JA Curry. London: Academic/Elsevier.

McIntyre M. E., 2003b: Potential vorticity. In Encyclopedia of Atmospheric Sciences, vol. 2, ed. JR Holton, JA Pyle, JA Curry. London: Academic/Elsevier.

McIntyre M. E., and T. N. Palmer, 1983: Breaking planetary waves in the stratosphere. Nature, 305, 593–600.

McIntyre M. E., and T. N. Palmer, 1984: The "surf zone" in the stratosphere. J. Atmos. Terr. Phys., 46, 825–849.

Mo, K. C., and M. Ghil, 1987: Statistics and Dynamics of Persistent Anomalies. J. Atmos. Sci., 44, 877–902.

Mo, K. C., and R. E. Livezey, 1986: Tropical–extratropical geopotential height teleconnections during the Northern Hemisphere winter. Mon. Wea. Rev., 114, 2488–2515.

Monahan, A. H., and J. C. Fyfe, 2006: On the Nature of Zonal Jet EOFs. J. Climate, 19, 6409–6424.

Monahan, A. H., L. Pandolfo, and J. C. Fyfe, 2001: The preferred structure of variability of the Northern Hemisphere atmospheric circulation, Geophys. Res. Lett., 28, 1019–1022.

Naito, Y., M. Taguchi, and S. Yoden, 2003: A parameter sweep experiment on the effects of the equatorial QBO on stratospheric sudden warmings events. J. Atmos.

Sci., 60, 1380–1394.

Nakagawa, K. I., and K. Yamazaki, 2006: What kind of stratospheric sudden warming propagates to the troposphere? Geophys. Res. Lett., 33, L04801, doi:1029/2005GL024784.

North, G. R., 1984: Empirical orthogonal functions and normal modes. J. Atmos. Sci., 41, 879–887.

North, G. R., T. L. Bell, R. F. Cahalan, and F. J. Moeng, 1982: Sampling errors in the estimation of empirical orthogonal functions, Mon. Wea. Rev., 110, 699–706.

O'Neill, A., 1980: The dynamics of stratospheric warmings generated by a general circulation model of the troposphere and stratosphere. Quart. J. Roy. Meteor. Soc., 106, 659–690.

O'Neill, A., 2003: Stratospheric sudden warmings. Encyclopedia of Atmospheric Sciences, J. R. Holton, J. A. Pyle, and J. A. Curry, Eds., Elsevier, 1342–1353.

Obukhov, A. M., 1947: Statistically homogeneous fields on a sphere. Ups. Mat. Navk., 2, 196–198.

Perlwitz J., and N. Harnik, 2003: Observational evidence of a stratospheric influence on the troposphere by planetary wave reflection. J. Climate, 16, 3011–3026.

Perlwitz, J., and H.-F. Graf, 1995: The statistical connection between tropospheric and stratospheric circulation of the Northern Hemisphere in winter. J. Climate, 8, 2281–2295.

Perlwitz, J., and H.-F. Graf, 2001a: Troposphere-stratosphere dynamic coupling under strong and weak polar vortex conditions. Geophys. Res. Lett., 28, 271–274.

Perlwitz, J., and H.-F. Graf, 2001b: The variability of the horizontal circulation in the troposphere and stratosphere: A comparison. Theor. Appl. Clim., 69, 149–161.

Perlwitz, J., and N. Harnik, 2004: Downward coupling between the stratosphere and troposphere: The relative roles of wave and zonal mean processes. J. Climate, 17,

4902–4909.

Plumb, R. A., and K. Semeniuk, 2003: Downward migration of extratropical zonal wind anomalies. J. Geophys. Res., 108, 4223, (doi:10.1029/2002JD002773).

Polvani, L. M., and D. W. Waugh, 2004: Upward wave activity flux as a precursor to extreme stratospheric events and subsequent anomalous surface weather regimes. J. Climate, 17, 3548–3554.

Polvani, L. M., and P. J. Kushner, 2002: Tropospheric response to stratospheric perturbations in a relatively simple general circulation model. Geophys. Res. Lett., 29, 1114, doi:10.1029/2001GL014284.

Preisendorfer, R. W., 1988: Principal Component Analysis in Meteorology and Oceanography. Elsevier, 425 pp.

Quadrelli, R., and J. M. Wallace, 2004a: A simplified linear framework for interpreting patterns of Northern Hemisphere wintertime climate variability. J. Climate, 17, 3728–3742.

Quadrelli, R., and J. M. Wallace, 2004b: Varied expressions of the hemispheric circulation observed in association with contrasting polarities of prescribed patterns of variability. J. Climate, 17, 4245–4253.

Quiroz, R. S., 1977: Tropospheric-stratospheric polar vortex breakdown of January 1977, Geophys. Res. Lett., 4, 151–154.

Reyers, M., U. Ulbrich, M. Christoph, J. Pinto, and M. Kerschgens, 2006: A mechanism of PNA influence on NAO. Geophysical Research Abstracts, Vol. 8, 10703, 2006, SRef-ID: 1607-7962/gra/EGU06-A-10703.

Richman, M. B., 1986: Rotation of principal components. J. Climatol., 6, 293–335.

Robock A., 2000: Volcanic eruptions and climate. Rev. Geophys., 38, 191–219.

Robock, A., and J. Mao, 1992: Winter warming from large volcanic eruptions, Geophys. Res. Lett., 12, 2405–2408.

Rogers, J. C., and E.-M. Thompson, 1995: Atlantic Arctic cyclones and the mild Siberian winters of the 1980s, Geophys. Res. Lett., 22, 799–802.

Rossby, C.-G. 1939: Relations between variations in the intensity of the zonal circulation of the atmosphere and displacements of the semipermanent centers of action. J. Mar. Res., 2, 38–55.

Schmitz, G., and N. Grieger, 1980: Model calculations on the structure of planetary waves in the upper troposphere and lower stratosphere as a function of the wind field in the upper stratosphere. Tellus, 32, 207–214.

Scott, R. K., P. H. Haynes, 1998: Internal interannual variability of the extratropical stratospheric circulation: The low-latitude flywheel. Q. J. Roy. Meteor. Soc., 124, 2149–2173.

Scherhag, R., 1952: Die explosionsartigen Stratosphärenerwärmungen des Spätwinters 1951–52. Ber. Dtsch. Wetterdienst (USZone), 6, 51–63.

Schubert, S. D., 1986: The structure, energetics and evolution of the dominant frequency-dependent three-dimensional atmospheric modes. J. Atmos. Sci., 43, 1210–1237.

Shindell, D. T., R. L. Miller, G. A. Schmidt, and L. Pandolfo, 1999a: Simulation of recent northern winter climate trends by greenhouse-gas forcing, Nature, 399, 452–455.

Shindell, D. T., D. Rind, N. Balachandran, J. Lean, and P. Lonergan, 1999b: Solar cycle variability, ozone and climate. Science, 284, 305–308 , doi:10.1126/science.284.5412.305.

Simmons, A. J., J. M. Wallace and G. W. Branstator, 1983: Barotropic wave propagation and instability, and atmospheric teleconnection patterns. J. Atmos. Sci., 40, 1363–1392.

Song, Y., and W. A. Robinson, 2004: Dynamical mechanisms for stratospheric influences on the troposphere. J. Atmos. Sci., 61, 1711–1725.

Tanaka H. L., Y. Watarai, and T. Kanda, 2004: Energy spectrum proportional to the squared phase speed of Rossby modes in the general circulation of the atmosphere, Geophys. Res. Lett., 31 (13), L13109, doi:10.1029/2004GL019826.

Tanaka, H. L., 1985: Global energetics analysis by expansion into three dimensional normal mode functions during the FGGE winter. J. Meteor. Soc. Japan, 63, 180–200.

Tanaka, H. L., 2003: Analysis and modeling of the Arctic Oscillation using a simple barotropic model with baroclinic eddy forcing. J. Atmos. Sci., 60, 1359–1379.

Tanaka, H. L., and Q. Ji, 1995: Comparative energetics of FGGE Reanalyses using the normal mode expansion. J. Meteor. Soc. Japan, 73, 1–12.

Tanaka, H., and E. C. Kung, 1988: Normal mode energetics of the general circulation during the FGGE Year. J. Atmos. Sci., 45, 3723–3736.

Tanaka, H. L., and A. Kasahara, 1992: On the normal modes of Laplace's tidal equation for zonal wavenumber zero. Tellus, 44A, 18–32.

Tanaka, H. L., and H. Tokinaga, 2002: Baroclinic instability in high latitudes induced by polar vortex: A connection to the Arctic Oscillation. J. Atmos. Sci., 59, 69–82.

Thompson, D. W. J., M. P. Baldwin, and J. M. Wallace, 2002: Stratospheric connection to Northern Hemisphere wintertime weather: Implications for predictions. J. Climate, 15, 1421–1428.

Thompson, D. W., and J. M. Wallace, 1998: The Arctic Oscillation signature in the wintertime geopotential height and temperature fields. Geophys. Res. Lett., 25, 1297–1300.

Thompson, D. W., and J. M. Wallace, 2000: Annular modes in the extratropical circulation. Part I: Month-to-month variability. J. Climate, 13, 1000–1016.

Thompson, D. W., J. M. Wallace and G. C. Hegerl, 2000: Annular modes in the extratropical circulation. Part II: Trends. J. Climate, 13, 1018–1036.

Thompson, D. W. J., M. P. Baldwin, and S. Solomon, 2005: Stratosphere-troposphere

coupling in the Southern Hemisphere. J. Atmos. Sci., 62, 708–715.

Thuburn, J., and V. Lagneau, 1999: Eulerian mean, contour integral, and finite-amplitude wave activity diagnostics applied to a single-layer model of the winter stratosphere. J. Atmos. Sci., 56, 689–710.

Ting, M., M. P. Hoerling, T. Xu, and A. Kumar, 1996: Northern Hemisphere teleconnection patterns during extreme phases of the zonal-mean circulation. J. Climate, 9, 2615–2633.

Ting, M., M. P. Hoerling, T. Xu, and A. Kumar, 2000: Reply. J. Climate, 13, 1040–1043.

Trenberth, K. E., and J. Hurrell, 1994: Decadal atmosphere–ocean variations in the Pacific. Climate Dyn., 9, 303–319.

Uppala, S.M., Kållberg, P.W., Simmons, A.J., Andrae, U., da Costa Bechtold, V., Fiorino, M., Gibson, J.K., Haseler, J., Hernandez, A., Kelly, G.A., Li, X., Onogi, K., Saarinen, S., Sokka, N., Allan, R.P., Andersson, E., Arpe, K., Balmaseda, M.A., Beljaars, A.C.M., van de Berg, L., Bidlot, J., Bormann, N., Caires, S., Chevallier, F., Dethof, A., Dragosavac, M., Fisher, M., Fuentes, M., Hagemann, S., Hólm, E., Hoskins, B.J., Isaksen, L., Janssen, P.A.E.M., Jenne, R., McNally, A.P., Mahfouf, J.-F., Morcrette, J.-J., Rayner, N.A., Saunders, R.W., Simon, P., Sterl, A., Trenberth, K.E., Untch, A., Vasiljevic, D., Viterbo, P., and Woollen, J. 2005: The ERA-40 re-analysis. Quart. J. R. Meteorol. Soc., 131, 2961–3012.doi:10.1256/qj.04.176

Van Loon, H., and J. C. Rogers, 1978: The seesaw in winter temperatures between Greenlandand northern Europe. Part I: General Description. Mon.Wea.Rev., 106, 296–310.

Volodin, E. M., and V. Ya. Galin, 1998: The nature of the Northern Hemisphere winter troposphere circulation response to observed ozone depletion in low stratosphere, Quart. J. Roy. Met. Soc., 124, 1–30.

Von Storch, H., and F. W. Zwiers, 1999: Statistical Analysis in Climate Research, 484

pp., Cambridge Univ. Press, New York.

Walker, G. T., and E. W. Bliss, 1932: World weather V. Mem. Roy. Meteor. Soc., 4, 53–83.

Wallace J. M., C. Smith, C. S. Bretherton, 1992: Singular value decomposition of wintertime sea surface temperature and 500-mb height anomalies. J Climate, 5, 561–576.

Wallace J. M., Y. Zhang, and J. Renwick, 1995: Dynamic contribution to hemispheric mean temperature trends. Science, 270, 780–783.

Wallace, J. M., 2000: North Atlantic Oscillation/Annular Mode: Two paradigms—One phenomenon. Quart. J. Roy. Meteor. Soc., 126, 791–805.

Wallace, J. M., and D. S. Gutzler, 1981: Teleconnections in the geopotential height field during the Northern Hemisphere winter. Mon. Wea. Rev., 109, 784–812.

Wallace, J. M., and D. W. J. Thompson, 2002: The Pacific Center of Action of the Northern Hemisphere Annular Mode: Real or Artifact? J. Climate, 15, 1987–1991.

Waugh, D. W., 1997: Elliptical diagnostics of stratospheric polar vortices. Quart. J. Roy. Meteor. Soc., 123, 1725–1748.

Wilks, D. S., 1995: Statistical Methods in the Atmospheric Sciences. Academic Press, 467pp.

Wilks, D. S., 2005: Statistical Methods in the Atmospheric Sciences. Elsevier, 592pp.

Wittman, M. A. H., L. M. Polvani, and A. J. Charlton, 2005: On the meridional structure of annular modes. J. Climate, 18, 2119–2122.

Yoden, S., 1990: An illustrative model of seasonal and interannual variations of the stratospheric circulation. J. Atmos. Sci., 47, 1845–1853.

Zhou, S., A. J. Miller, J. Wang, and J. K. Angell, 2002: Downward-propagating temperature anomalies in the preconditioned polar stratosphere. J. Climate, 15, 781–792.